UNIVERSITY OF CRETE
DEPARTMENT OF PHYSICS

Postgraduate Program
Microelectronics - Optoelectronics

Thesis

"Processing of Biomaterials Surfaces for Gene Delivery Applications"

Stella Aslanoglou

Supervisors: C. Fotakis & E. Stratakis

Heraklion, Crete, April 2016

ΠΑΝΕΠΙΣΤΗΜΙΟ ΚΡΗΤΗΣ
ΤΜΗΜΑ ΦΥΣΙΚΗΣ

Μεταπτυχιακό Πρόγραμμα
Μικροηλεκτρονικής - Οπτοηλεκτρονικής

Διπλωματική Εργασία

"Κατεργασία επιφανειών βιοϋλικών για εφαρμογές στην μεταφορά γονιδίων"

Στέλλα Ασλάνογλου

Επιβλέποντες: Κ. Φωτάκης & Ε. Στρατάκης

Ηράκλειο, Κρήτη, Απρίλιος 2016

Preface

This Master Thesis was performed within the collaboration of the Institute of Electronic Structure and Laser (IESL) of the Foundation for Research and Technology-Hellas (FORTH) with the Future Industries Institute of University of South Australia.

Part of the work was performed at the South Australian node of the Australian National Fabrication Facility (ANFF) under the National Collaborative Research Infrastructure Strategy to provide nano- and microfabrication facilities for Australia's researchers.

It was partially funded by the European Union Program " COST " and its " NEWGEN " Action, whose research is focused in " New Generation Biomimetic and Customized Implants for Bone Engineering ".

Η διατριβή αυτή αφιερώνεται στις αγαπημένες μου φίλες Κέλλη, Σάντυ και Φρύνη που είναι παρούσες σε κάθε βήμα της ζωής μου με ουσιαστικό τρόπο κι ας μας χωρίζουν ήπειροι, χώρες και ωκεανοί. Τις ευχαριστώ για την αγάπη και την αφοσίωσή τους λέγοντάς τους πως οι αποστάσεις στη ζωή υπάρχουν για να τις διασχίζουμε…και για να δοκιμάζουμε τα όρια της θέλησής μας.

This Master Thesis is dedicated to my beloved friends Kelly, Sandy and Fryni, who are always present in every step of my life in a meaningful way even if continents, countries and oceans are keeping us apart. I would like to thank them for their love and loyalty telling them that the distances in our life exist for us to cross them…and for testing the limits of our will.

Acknowledgments

I would like to thank some people who contributed to the successful completion of this Master Thesis. First of all, I would like to thank Prof Costas Fotakis, who honored me with being the main supervisor of my Thesis. I am grateful to Dr Emmanuel Stratakis for the continuous guidance and support that already offered and still offers me, as well as for his understanding and compassion, facing me like his spiritual child. I could not exclude from my acknowledgments Dr Anthi Ranella for her valuable comments during the analysis of the results. Moreover, I owe my gratitude to my beloved friend and outstanding scientist Dr Chara Simitzi, who is always around, in every difficulty, as "deux es machima", offering generously her valuable knowledge and advice.

In addition, I would like to thank the rest members of my committee, Prof Spiros Anastasiadis and Dr Panagiotis Loukakos for their remarks and comments to the point during the reading of this Thesis.

I owe my sincere thanks to Prof Nico Voelcker, for welcoming me in his lab at the Future Industries Institute of the University of South Australia as well as for the fruitful discussions that we had during my stay there. I would also like to thank Dr Roey Elnathan for his daily supervision and guidance but especially for his faith in my abilities from the first day of our collaboration. Moreover, I would like to express my gratitude to Dr Bahman Delalat for his valuable assistance in the cell culture part as well as fluorescent microscope imaging. Also, my sincere thanks to Dr Maria Alba-Martin for the nice collaboration that we had.

I owe my gratitude to Mr Dipankar Chugh for the assistance that he offered me in understanding the operation of the Deep Reactive Ion Etcher (DRIE).

I could not exclude from my acknowledgments all the staff members of the clean room and especially Mr Simon Doe and Dr Donghoon Chang for their assistance, knowledge and the excellent collaboration that they offered me.

As any successful effort does not come by itself, I have to thank at first my parents Leonidas and Maria for their wholehearted love, understanding and support and then my friends in every longitude and latitude of the world, who are present in every step of mine. Finally, I thank George for his real feelings, which remind me of the beauties of life in a daily basis.

Ευχαριστίες

Θα ήθελα να ευχαριστήσω ορισμένους ανθρώπους που συνέβαλλαν στην επιτυχή ολοκλήρωση της παρούσας εργασίας. Αρχικά, θέλω να ευχαριστήσω τον καθηγητή κ. Κώστα Φωτάκη που με τίμησε ως κύριος επιβλέπων της μεταπτυχιακής μου εργασίας. Είμαι ευγνώμων στον Δρ. κ. Μανώλη Στρατάκη για την συνεχή καθοδήγηση και υποστήριξη που μου προσέφερε αλλά και που συνεχίζει να μου προσφέρει, καθώς και για την κατανόηση και ανθρωπιά που δείχνει, αντιμετωπίζοντάς με σαν πνευματικό του παιδί. Δεν θα μπορούσα να παραλείψω από τις ευχαριστίες μου την Δρ. κ. Ανθή Ρανέλλα για τα πολύτιμα σχόλιά της κατά την ανάλυση των αποτελεσμάτων. Επίσης οφείλω ένα μεγάλο ευχαριστώ στην αγαπημένη μου φίλη και εξαίρετη επιστήμονα Δρ. κ. Χαρά Σιμιτζή που βρίσκεται πάντα κάπου εκεί, σε κάθε δυσκολία, ως απομηχανής θεός, προσφέροντας απλόχερα τις πολύτιμες γνώσεις και συμβουλές της.

Ακόμα θα ήθελα να ευχαριστήσω τα υπόλοιπα μέλη της τριμελούς επιτροπής, τον καθηγητή κ. Σπυρίδων Αναστασιάδη καθώς και τον Δρ. κ. Παναγιώτη Λουκάκο για τις επισημάνσεις και τα εύστοχα σχόλιά τους κατά την ανάγνωση της παρούσας εργασίας.

Τις θερμές μου ευχαριστίες οφείλω στον Prof Nico Voelcker που με καλωσόρισε στο εργαστήριό του στο Future Industries Institute του Πανεπιστημίου της Νότιας Αυστραλίας καθώς και για τις επικοδομητικές συζητήσεις που είχαμε κατά τη διάρκεια της παραμονής μου εκεί. Θα ήθελα επίσης να ευχαριστήσω τον Dr Roey Elnathan για την καθημερινή του επίβλεψη και καθοδήγηση αλλά κυρίως για την πίστη που έδειξε στις δυνατότητές μου από τις πρώτες κιόλας μέρες της συνεργασίας μας. Επιπλέον θα ήθελα να εκφράσω τις ευχαριστίες μου στον Dr Bahman Delalat για την πολύτιμη βοήθειά του στο κομμάτι των κυτταρικών καλλιεργειών καθώς και στην απεικόνιση με τη χρήση μικροσκοπίου φθορισμού. Επίσης πολλές θερμές ευχαριστίες στην Dr Maria Alba-Martin για την όμορφη συνεργασία που είχαμε.

Ένα μεγάλο ευχαριστώ οφείλω ακόμα στον κ. Dipankar Chugh για την βοήθεια που μου προσέφερε στην κατανόηση της λειτουργίας του Deep Reactive Ion Etcher (DRIE).

Δεν θα μπορούσα να μην ευχαριστήσω, όλους τους εργαζομένους του καθαρού χώρου και ιδιαίτερα τον Simon Doe και τον κ. Dr Donghoon Chang για την βοήθεια, τις γνώσεις και την άριστη συνεργασία που μου προσέφεραν.

Καθώς όμως κάθε επιτυχημένη προσπάθεια δεν έρχεται από μόνη της, οφείλω να ευχαριστήσω αρχικά τους γονείς μου Λεωνίδα και Μαρία για την αμέριστη αγάπη, κατανόηση και υποστήριξή τους και ύστερα τις φίλες και τους φίλους μου σε όλα τα μήκη και πλάτη του κόσμου που δηλώνουν παρών σε κάθε μου βήμα. Τέλος, ευχαριστώ τον Γιώργο για τα αληθινά του αισθήματα που μου υπενθυμίζουν καθημερινά την ομορφιά της ζωής.

Abstract

Around 4000 human diseases have been traced to gene disorders so far (1). Most of them are life-threatening and affect all aspects of patient's life in a daily basis. The only way to eliminate a genetic disease is to treat it at its roots. Gene therapy is an experimental technique that works in this direction by using different approaches including the replacement or the "silencing" of a mutated gene and the introduction of a new gene. The intracellular delivery of genetic material is well known as "transfection" and it is either viral or non-viral.

The delivery of genes to mammalian cells using non-viral methods has become a very promising approach for gene therapy in the last few years (2). One of the current impediments of successful gene therapy is the inefficient delivery of the corrective nucleic acid code into target cells. New methods are required to deliver nucleic acid reagents into diverse cell types effectively and with high yields.

In this study, we report on the development of a novel delivery platform for cell transfection studies in vitro, comprising of vertically aligned silicon nanowire (VA-SiN) arrays with a tapered profile, termed as "silicon micro-conical tips (Si MC tips)". Fabrication starts with self-assembly of a hexagonal close-packed (hcp) 2D array of polystyrene nanospheres (PSNS) over a large area of a Si wafer via convective assembly. The resulting hcp monolayer array is then converted into non-close-packed monolayer arrays using O_2 plasma etching. The etched PSNS then serve as a mask for the Deep Reactive Ion Etching (DRIE) of silicon using the "Bosch" process. The final step in the fabrication of the micro-conical arrays is the formation of a smoother and sharper morphology using a combination of thermal oxidation and wet etching.

These arrays were classified in three different categories, regarding the height of the tips, exhibiting a range of architectures (Table 4.2) and together with flat Si wafers have been applied to in vitro cell cultures using HEK293 cells as a model cell line. After the functionalization of the Si MC tip arrays' surface with Green Fluorescent Protein (GFP)-plasmid, the delivery was performed by mechanical penetration using centrifugation force, with the Si MC tips facing towards the cells (Delivery Method 1). A delivery system like this can offer us two main advantages: fast delivery and parallel delivery of the plasmid to a huge amount of cells. Before proceeding to cell transfection studies, we examined the viability of the cells during their contact with the Si MC tips as well as the existence or not of penetration through the cell membrane into the cytoplasm by FIB-SEM.

The viability studies performed demonstrated that a prolonged incubation (for a couple of hours) of the aforementioned setup leads progressively to the death of the cells in both cases. At the footprint that the Si MC tips leave, after their removal, on the well plate and at the Si MC tips themselves. This is probably attributed to the lack of oxygen and nutrition available to the cells during the contact. However, a short incubation of maximum 30 m time leaves all the cells alive. In addition, there are still remaining cells attached on the well plate, fact that gives us the potential of achieving transfection on the well plate as well.

As far as the FIB-SEM imaging is concerned, the fluorescent images taken revealed the successful cytoplasm penetration of the Si MC tips of all different characteristics within 15 m and 30 m incubation time respectively. This is a good but not an adequate indicator that we will have transfection as well.

Finally, we proceeded to transfection studies in order to test the efficacy of our plasmid DNA delivery system. For comparative reasons, cell transfection studies were performed employing an additional strategy (cells on top of the Si MC tips – Delivery Method 2) and following a similar protocol. Our results showed that cell transfection was achieved using both delivery methods. Transfected cells were detected on the surface of the Si MC tip arrays and especially on those comprising of higher and pointed tips in the same time. However, no transfected cells were detected on the well plate using Delivery Method 1 (Si MC tips on top of the cells) within 20 m of incubation.

To sum up, in this study we presented at first a novel method for the fabrication of vertically aligned silicon NW arrays with a tapered profile using a combination of nanosphere lithography and deep reactive ion etching. At a second step, we used these SiNW arrays as a cell transfection platform in vitro in order to deliver plasmid DNA into HEK293 cells. The delivery of the plasmid is achieved by mechanical penetration of the NWs into the cytoplasm with the aid of centrifugation force using a very short experimental protocol. We suggest that a delivery system like this could be a future tool in facilitating gene therapy practices.

Περίληψη

Περίπου 4000 ανθρώπινες ασθένειες έχουν σχετιστεί με γενετικές ανωμαλίες μέχρι στιγμής (1). Οι περισσότερες από αυτές είναι απειλητικές για την ζωή των ασθενών και επηρεάζουν όλες τις πτυχές της ζωής τους σε καθημερινή βάση. Ο μόνος τρόπος να εξαλείψει κανείς μια γενετική ασθένεια είναι να την θεραπεύσει στη ρίζα της. Η γονιδιακή θεραπεία είναι μια πειραματική τεχνική, η οποία λειτουργεί σε αυτή την κατεύθυνση χρησιμοποιώντας διαφορετικές προσεγγίσεις, οι οποίες περιλαμβάνουν την αντικατάσταση ή την "σίγαση" ενός μεταλλαγμένου γονιδίου και την εισαγωγή ενός καινούργιου. Η ενδοκυτταρική μεταφορά γεννετικού υλικού είναι ευρέως γνωστή ως "διαμόλυνση" (transfection) και πραγματοποιείται με την χρήση ιών και μη.

Η μεταφορά γονιδίων σε ανθρώπινα κύτταρα χρησιμοποιώντας μεθόδους που δεν περιλαμβάνουν τη χρήση ιών έχει γίνει μια πολλά υποσχόμενη προσέγγιση στη γονιδιακή θεραπεία τα τελευταία χρόνια (2). Ένα από τα τρέχοντα εμπόδια στην επιτυχή γονιδιακή θεραπεία είναι η ανεπαρκής μεταφορά του διορθωτικού γονιδίου στα στοχευμένα κύτταρα. Νέες μέθοδοι απαιτούνται για την μεταφορά νουκλεϊκών οξέων σε διαφορετικούς τύπους κυττάρων αποτελεσματικά και με υψηλές αποδόσεις.

Σε αυτή την εργασία, παρουσιάζουμε την ανάπτυξη μιας καινοτόμας πλατφόρμας μεταφοράς για διαμόλυνση κυττάρων in vitro, αποτελούμενη από συστοιχίες κάθετα προσανατολισμένων νανοσυρμάτων πυριτίου (VA-SiNWs) κωνικού προφίλ, τα οποία ονομάστηκαν "μικρο-κωνικές ακίδες πυριτίου". Η κατασκευή ξεκινά με την αυτοδιάταξη (self-assembly) μιας εξαγωνικής συμπυκνωμένης δυσδιάστατης συστοιχίας νανοσφαιρών πολυστυρενίου πάνω σε μια μεγάλη επιφάνεια πυριτίου μέσω επαγωγικής διάταξης (convective assembly). Η προκύπτουσα μονοστρωματική εξαγωνική συμπυκνωμένη συστοιχία των νανοσφαιρών πολυστυρενίου μετατρέπεται σε μη συμπυκνωμένες συστοιχίες μέσω εγχάραξης (etching) με πλάσμα οξυγόνου. Οι εγχαραγμένες νανοσφαίρες πολυστυρενίου λειτουργούν έπειτα σαν μάσκα για την βαθιά εγχάραξη μέσω ενεργών ιόντων του πυριτίου χρησιμοποιώντας την διαδικασία "Bosch". Το τελευταίο βήμα στην κατασκευή των μικρο-κωνικών ακίδων πυριτίου είναι η διαμόρφωση μιας πιο λείας και αιχμηρής μορφολογίας χρησιμοποιώντας ένα συνδυασμό θερμικής οξείδωσης και υγρής εγχάραξης.

Οι συστοιχίες αυτές μικρο-κωνικών ακίδων πυριτίου, ταξινομήθηκαν σε τρεις κατηγορίες, με βάση το ύψος των ακίδων, εμφανίζοντας μια ποικιλία αρχιτεκτονικών (Πίνακας 4.2) και χρησιμοποιήθηκαν μαζί με επίπεδο πυρίτιο σε in vitro κυτταρικές καλλιέργειες χρησιμοποιώντας σαν μοντέλο την κυτταρική σειρά HEK293 (εμβρυονικά ανθρώπινα νεφρικά κύτταρα). Έπειτα από την λειτουργικοποίηση της επιφάνειας των συστοιχιών μικρο-κωνικών ακίδων με πλασμίδιο που έχει κωδικοποιημένη πράσινη φθορίζουσα πρωτεΐνη, πραγματοποιήθηκε η μεταφορά του πλασμιδίου με μηχανική διείσδυση χρησιμοποιώντας την φυγόκεντρο, με τις ακίδες στραμμένες προς τα κύτταρα (Μέθοδος Μεταφοράς 1). Ένα τέτοιο σύστημα μεταφοράς μπορεί να μας προσφέρει δύο κύρια πλεονεκτήματα: γρήγορη και παράλλη μεταφορά του πλασμιδίου σε μια μεγάλη ποσότητα κυττάρων. Πριν προχωρήσουμε στα πειράματα διαμόλυνσης των κυττάρων, εξετάσαμε την βιωσιμότητα αυτών κατά την διάρκεια της επαφής τους με τις μικρο-κωνικές ακίδες καθώς και την ύπαρξη ή όχι διείσδυσης αυτών στο κυτταρόπλασμα μέσω της κυτταρικής μεμβράνης με την βοήθεια FIB-SEM.

Τα πειράματα βιωσιμότητας των κυττάρων έδειξαν πως μια παρατεταμένη (για μερικές ώρες) επώαση της όλης προαναφερθείσας διάταξης οδηγεί σταδιακά στο θάνατο των κυττάρων και στις δύο περιπτώσεις. Τόσο στο ίχνος που αφήνουν οι μικρο-κωνικές ακίδες, μετά την αφαίρεσή τους, στα πηγάδια καλλιέργειας αλλά και στην ίδια την επιφάνεια των ακίδων. Αυτό πιθανά αποδίδεται στην έλλειψη οξυγόνου και θρεπτικών συστατικών που ήταν διαθέσιμα στα κύτταρα κατά την επαφή. Παρ'όλα αυτά όμως, μια σύντομη επώαση (το πολύ 30 λεπτών) αφήνει όλα τα κύτταρα ζωντανά.

Επιπλέον η παραμονή προσκολλημένων κυττάρων στην επιφάνεια των πηγαδιών καλλιέργειας, μας αφήνει το ενδεχόμενο να επιτύχουμε διαμόλυνση των κυττάρων και στα πηγάδια καλλιέργειας.

Όσον αφορά την απεικόνιση με FIB-SEM, οι εικόνες φθορισμού που πήραμε αποκάλυψαν την επιτυχή διείσδυση των μικρο-κωνκών ακίδων, όλων των χαρακτηριστικών, στο κυτταρόπλασμα μέσα σε 15 και 30 λεπτά επώασης αντίστοιχα. Αυτή είναι μια καλή αλλά όχι επαρκής ένδειξη πως θα έχουμε και διαμόλυνση των κυττάρων.

Τέλος, προχωρήσαμε σε πειράματα διαμόλυνσης των κυττάρων για να εξετάσουμε την αποτελεσματικότητα του συστήματος μεταφοράς μας. Για συγκριτικούς λόγους, πειράματα διαμόλυνσης των κυττάρων πραγματοποιήθηκαν με την χρήση και μιας επιπλέον μεθόδου (τα κύτταρα πάνω από τις μικρο-κωνικές ακίδες – Μέθοδος Μεταφοράς 2) ακολουθώντας ένα παρόμοιο πρωτόκολλο. Τα αποτελέσματά μας έδειξαν ότι είχαμε διαμόλυνση των κυττάρων με την χρήση και των δύο μεθόδων μεταφοράς. Τα διαμολυσμένα κύτταρα ανιχνεύθηκαν στην επιφάνεια των συστοιχιών από μικρο-κωνικές ακίδες και κυρίως σε εκείνες που αποτελούνταν από ταυτόχρονα υψηλότερες και αιχμηρότερες ακίδες. Παρ'όλα αυτά, κανένα διαμολυσμένο κύτταρο δεν ανιχνεύτηκε στα πηγάδια καλλιέργειας χρησιμοποιώντας την Μέθοδο Μεταφοράς 1 (μικρο-κωνικές ακίδες πάνω από τα κύτταρα) μέσα σε 20 λεπτά επώασης.

Συνοψίζοντας, σε αυτή την εργασία παρουσιάσαμε αρχικά μία καινοτόμο μέθοδο για την κατασκευή κάθετα ευθυγραμμισμένων συστοιχιών νανοσυρμάτων πυριτίου με κωνικό προφίλ χρησιμοποιώντας ένα συνδυασμό λιθογραφίας νανοσφαιρών και βαθιάς εγχράραξης με την χρήση ενεργών ιόντων. Σε δεύτερο στάδιο, χρησιμοποιήσαμε αυτές τις συστοιχίες νανοσυρμάτων πυριτίου σαν πλατφόρμα διαμόλυνσης (transfection) κυττάρων in vitro για την μεταφορά πλασμιδιακού DNA σε κύτταρα HEK293. Η μεταφορά του πλασμιδίου επιτυγχάνεται με μηχανική διείσδυση των νανοσυρμάτων μέσα στο κυτταρόπλασμα με την βοήθεια της φυγόκεντρου, χρησιμοποιώντας ένα πολύ σύντομο πρωτόκολλο. Προτείνουμε ότι ένα τέτοιο σύστημα μεταφοράς θα μπορούσε να είναι ένα μελλοντικό εργαλείο στην διευκόλυνση των πρακτικών της γονιδιακής θεραπείας.

Table of Contents

List of Abbreviations

C_4F_8: Octafluorocyclobutane

DNA: Deoxyribonucleic Acid

DRIE: Deep Reactive Ion Etcher

ECR: Electron Cyclotron Resonance

FDA: Fluorescein Diacetate

FIB-SEM: Focused Ion Beam-Scanning Electron Microscopy

GFP: Green Fluorescent Protein

H_2O_2: Hydrogen Peroxide

H_2SO_4: Sulfuric Acid

HF: Hydrogen Fluoride

HMDS: Hexamethyldisilazane

ICP: Inductively Coupled Plasma

L/UL chamber: Load/Unload chamber

MC: Micro-Conical

MCs: Microcones

mRNA: messenger RNA

NLD: Neutral Loop Discharge

NSL: Nanosphere Lithography

PDL: Poly-D-lysine

PECR: Partial Electron Cyclotron Resonance

PI: Propidium Iodide

PS: Polystyrene

PSNS: Polystyrene Nanospheres

RF: Radio Frequency

RNA: Ribonucleic Acid

SEM: Scanning Electron Microscopy

SF_6: Sulfur Hexafluoride

SiNWs: Silicon Nanowires

siRNA: small interfering RNA

VA-SiNWs: Vertically Aligned-Silicon Nanowires

VLS growth: Vapor-Liquid-Solid growth

List of Figures

List of Tables

1. General Overview

1.1 The ‘Book of Life’

In humans genetic information, also known as our genome, can be described as the ‘Book of Life’. This book is structured as follows:

- It has two volumes. One volume of the book is inherited from the mother and the other from the father
- Both volumes contain 23 chapters each, equivalent to the 23 pairs of chromosomes in human body cells that contain genetic information
- The 23 chapters (chromosomes) are made up of a number of recipe pages (coding DNA or genes) and in-between (non-coding) pages of DNA
- Some of the chapters contain many pages while others only have a few. Some chromosomes are large and contain many thousands of genes and non-coding DNA while others are much smaller
- Genes are sections of DNA that code for the proteins our body needs to function
- In-between (non-coding) sections of DNA have various jobs, not all of which we understand
- Careful examination of the words within genes show that all the words are made up of three letters (triplets) such as AGT, GGT, ACT, CAA etc.
- There are four letters used in the genetic book; A, T, C and G. Each letter stands for a nucleotide base: **A** for Adenine, **T** for Thymine, **C** for Cytosine and **G** for Guanine.

Just as reading the words on the page of a book allows an understanding of the author’s message, the body is able to read the triplets in genes to make the protein needed for our cells to work. Our cells don’t need all the instructions all the time. Pages of our genetic book can be closed and then reopened when needed. Each type of cell can have different parts of the genetic book opened or shut because different cells do different jobs in our body. Which genes are turned on or off can be influenced by our diet, chemical exposure, exercise, ageing and messages from other genes in the body (3).

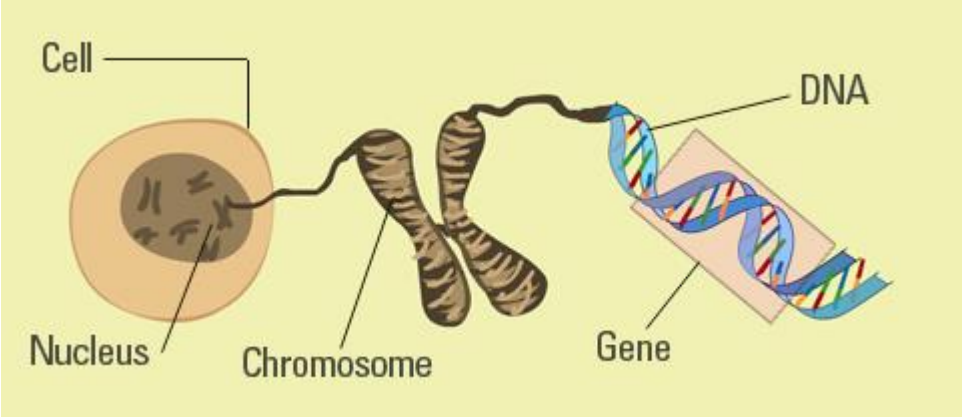

Figure 1.1: Schematic representation of a gene (4).

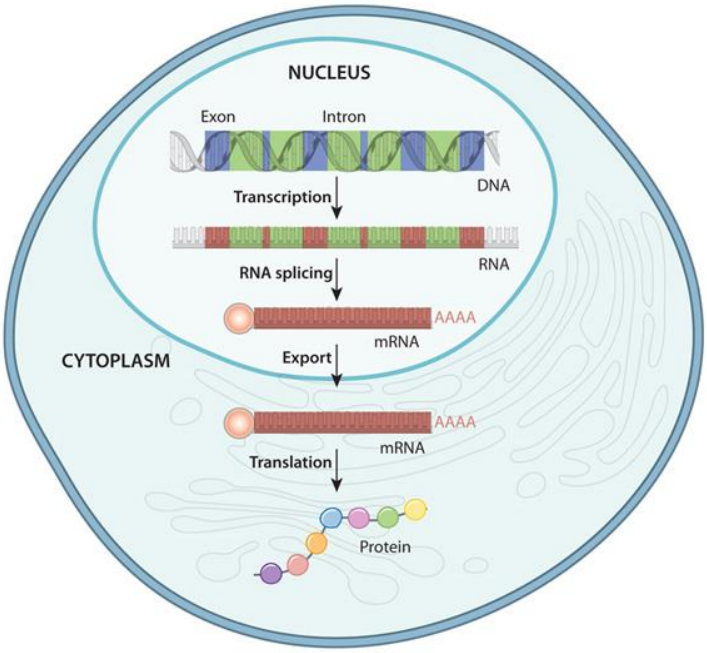

Figure 1.2: Schematic illustration of the flow of information from DNA to protein in a eukaryote.
First, both coding and non-coding regions of DNA are transcribed into mRNA. Some regions are removed (introns) during initial mRNA processing. The remaining exons are then spliced together, and the spliced mRNA molecule (red) is prepared for export out of the nucleus through addition of an endcap (sphere) and a polyA tail. Once in the cytoplasm, the mRNA can be used to construct a protein (5).

1.2 DNA variations

We all have small variations in our genetic code. That is why we are all unique. Even identical twins have some variations in their DNA by the time they are born. Because we inherit our genes from our parents, members of the same family share their DNA including its variations. These variations include: changes in the sequence of letters in the gene message, missing of nucleotide base/s (A, G, T or C) or insertion of base/s.

Variations in the code can occur during our life for a variety of reasons including exposure to radiation, certain chemicals or by chance. Ageing, for example, is a common cause of genetic variation. Throughout our lives, our cells are continually being replaced. Some variations in the genetic information do not seem to make any difference to the function of our cells. These types of DNA variations are quite common. Other DNA variations can be associated with an increased risk of health condition, for example diabetes or cancer. Some DNA variations can mean the gene instruction is incorrected so a faulty protein is made or the control switch is changed. A variation in a gene that creates a fault is called a pathogenic variant or mutation. A DNA mutation can cause a problem for one cell type but not another, since not all cells use all of the possible proteins.

When a DNA change causes a faulty protein in cells that need that protein, it usually results in disease symptoms that can sometimes be recognized as a genetic condition. Since we have two copies of each gene, if one copy has a mutation and the other copy is working, then we may not develop any problems. We are all born with DNA mutations and sometimes these can be beneficial or cause no problem. When a gene variation is present in egg or sperm cells, it can be passed on to children. In other cases, a new gene variation can arise in an egg or sperm cell. This is called a de novo change.

The person arising from that egg or sperm cell will be the first in the family to have the DNA change, which may then be passed down to his or her children and future generations (3).

About 4000 diseases have been traced to gene disorders (1). Cystic fibrosis and Huntington's disease, for example, are considered as single-gene disorders, which involve mutations in the DNA sequences of single cells. As a result, the protein that the gene codes for is either altered or missing. Down syndrome, from the other hand, is a result of an extra copy of a specific chromosome. Finally, Alzheimer's disease and some types of cancer, such as breast and ovarian cancer, are multifunctional disorders, which involve variations in multiple genes, often coupled with environmental causes (6).

1.3 Gene therapy and its recent advances

Gene therapy has long fascinated scientists, clinicians and the general public because of its potential to treat a disease at its genetic roots. This is achieved by counteracting or replacing a malfunctioning gene within the cells adversely affected by the condition.

As simple as the concept sounds, the hurdles to put it into practice are daunting. Gene transfer must overcome complex cellular and tissue barriers to deliver new genetic information into the target cell to drive proficient expression of a therapeutic molecule without disrupting essential regulatory mechanisms. The gene-corrected cells must be present in large enough quantities to reverse the condition, escape immunological recognition and survive in the long term, or be able to transmit the modification to their progeny to sustain the benefit.

Several gene-therapy trials have been performed in the past two decades for inherited diseases, cancer and chronic infections, but only a few reported clear clinical benefits and in some, individuals experienced severe adverse events related to the vectors. Overall, concern and scepticism rose over further deployment of these strategies. But these attitudes are radically changing. A number of phase I/II gene-therapy clinical trials have reported remarkable evidence of efficacy and safety for the treatment of various severe inherited diseases of the blood, immune and nervous system, including primary immunodeficiencies, leukodystrophies, thalassaemia, haemophilia and retinal dystrophy, as well as cancers such as B-cell malignancies. Behind these advances lie improved vector designs that enable the safe delivery of therapeutic genes to specific cells. Technologies for editing genes and correcting inherited mutations, the engagement of stem cells to regenerate tissues and the effective exploitation of powerful immune responses to fight cancer are also contributing to the revitalization of gene therapy (7).

1.4 Transfection

Transfection is a procedure that introduces foreign nucleic acids into cells to produce genetically modified cells. The introduced genetic materials (DNAs and RNAs) exist in cells either stably or transiently depending on the nature of the genetic materials. For stable transfection, introduced genetic materials that usually have a marker gene for selection (transgenes) are integrated into the host genome and sustain transgene expression even after host cells replicate (Fig. 1.3 A). In contrast with stably transfected genes, transiently transfected genes are only expressed for a limited period of time and are not integrated into the genome (Fig. 1.3 B). Transiently transfected genetic materials can be lost by environmental factors and cell division, so the choice of stable or transient transfection depends on the objective of the experiment (8).

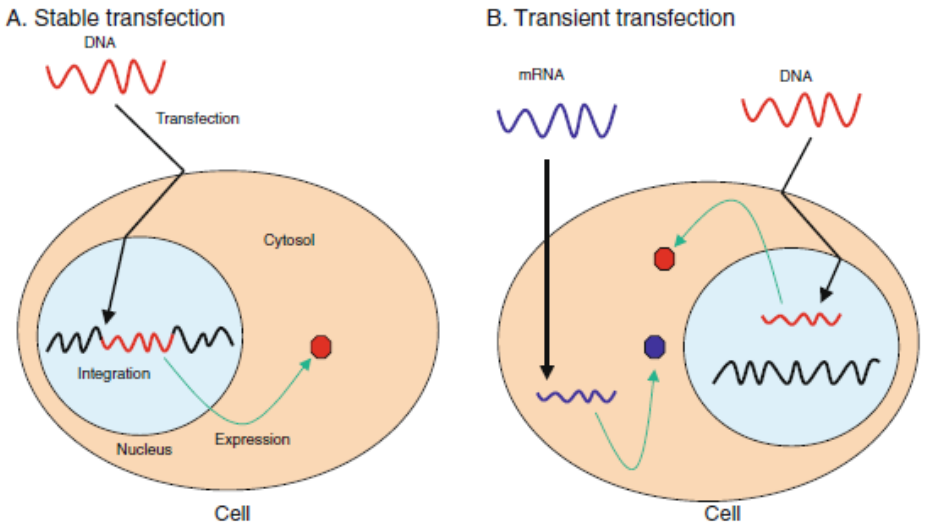

Figure 1.3: Schematic diagrams of two different transfections. (A) Stable transfection. Foreign DNA (red wave) is delivered to nucleus by passage through the cell and nuclear membranes. Foreign DNA is integrated into the host genome (black wave) and expressed sustainably. (B) Transient transfection. Foreign DNA is delivered into the nucleus but is not integrated into the genome. Foreign mRNA (blue wave) is also delivered into the cytosol, where it is translated. Hexagons are expressed proteins from transfected nucleic acids. Black arrows indicate delivery of foreign nucleic acids (8).

1.5 Gene delivery methods

The ideal vector for gene delivery would have at least the following characteristics: (i) specificity for the targeted cells, (ii) resistance to metabolic degradation and/or attack by the immune system, (iii) safety, i.e., minimal side effects and (iv) an ability to express, in an appropriately regulated fashion, the therapeutic gene for as long as required (9).

Generally, the methods of gene delivery can be divided into two categories: viral and non-viral delivery.

1.5.1 Viral delivery

Virus-mediated DNA transduction is a common gene delivery technology. Viruses represent highly evolved natural vectors for the transfer of foreign genetic information into cells (10). Virus-mediated transfection is highly efficient and it is easy to achieve sustainable transgene expression in vivo owing to the viral nature of integration into the host genome. Retroviruses and adenoviruses are the most commonly used vectors and have already been tested in clinical trials (9).

The major drawbacks of virus-mediated transfection are immunogenicity and cytotoxicity. Introduction of a viral vector may cause an inflammatory reaction and an insertional mutation, because viral vectors integrate into the host genome randomly, which may disrupt tumor suppressor genes, activate oncogenes, or interrupt essential genes (11). Another disadvantage of this method is that a virus package has limited space for a foreign gene to keep infectivity (8). For these reasons, alternative research has focused on non-viral gene delivery methods, which could potentially overcome most of the limitations (12).

1.5.2 Non-viral delivery

Non-viral transfection include mechanical methods (microinjection, gene gun), physical methods (electroporation, sonoporation, laser irradiation), magnetic field enhanced transfection or magnetofection and chemical methods (9).

1.5.2.1 Mechanical methods

Microinjection

Microinjection is the most direct method to introduce DNA into cells, either into the cytoplasm or into the nucleus (13). This is a microsurgical procedure that is conducted on a single cell, using a glass needle (i.e., a fine, glass, microcapillary pipette), a precision positioning device (a micromanipulator) to control the movement of the micropipette, and a microinjector. Extrusion of fluid containing the genetic material through the micropipette uses hydrostatic pressure. Injections are typically carried out under direct visual control, using a microscope. The small tip diameters of these micropipettes, combined with the high precision of the micromanipulator, allow for accurate and precise DNA delivery.

Conceptually, microinjection is the simplest gene delivery method. However, it is difficult to apply. It is a laborious procedure; only one cell at a time can be injected, typically allowing for only a few hundred cells to be transfected per experiment (14). Therefore, microinjection, at its current technological level, is impractical for most, if not all, in vivo gene delivery applications (9).

Gene gun

The idea behind gene-mediated particle bombardment (or use of the so-called gene gun) is to move naked DNA plasmid into target cells on an accelerated particle carrier (15). Biolistic (a contraction of biological and ballistic) delivery utilizes heavy metal particles propelled at a sufficient velocity into the target cell. Acceleration is achieved by a high-voltage electric spark, or a helium discharge (16). The particles must be non-toxic, non-reactive, and smaller than the diameter of the target cell (most commonly 1-1.5μm). Naked DNA can be precipitated onto these microparticles, and is then gradually released within the cell post-bombardment. In the original method, a gunpowder acceleration system was used to propel DNA-coated tungsten particles, which penetrated the plasma membrane and ultimately resulted in gene expression. Different types of devices have been developed since and gold beads are usually employed.

The efficiency of this delivery technique depends on several parameters, such as the loading of DNA onto the particles, the particle size, and the timing of delivery (17). In addition, the final distribution of DNA-coated beads is influenced by the fine tuning of the acceleration imparted by the gene gun (18). Optimal responses are dependent on the number of DNA-coated beads delivered, and on the degree to which the particles are coated with plasmid (9).

1.5.2.2 Physical methods

Electroporation

A common physical tool to introduce DNA into cells is an electric field. This technique termed electroporation or electropermeabilization, exposes the cell membrane to high-intensity electrical pulses that can cause transient and localized destabilization of the barrier (19). During this perturbation, the cell membrane becomes highly permeable to exogenous molecules, such as DNA, present in the surrounding medium. Permeabilization requires that the externally applied electric field surpasses a critical, threshold value. For a cell suspension, electroporation requires on the order of 1 V, although the absolute potential depends upon the pulse width, composition of membrane, etc (20). The transient increase in permeability is believed to result from the creation of electric field-induced pores (hence, the term electroporation). However, the precise mechanism, by which these pores are

created and subsequently resolve remains the subject of much debate and further study. Equally the mechanism of DNA uptake via the putative pores remains a subject of investigation. Using freeze-fracture electron microscopy, the size of these membrane openings in red blood cells was shown to be between 20 and 120nm (9).

The efficiency of this method is influenced by several physical (especially, pulse duration and electric field strength) and biological (including DNA concentration and conformation, cell size) factors. It follows that the exact conditions for optimal electroporation must be determined for each cell type. Equally, it has been proposed that different electroporation conditions are required for molecules of different sizes. The instrumentation required for electroporation consists of a pulse generator and an "applicator" which includes the electrodes. The three-dimensional geometry of the electrodes determines the strength, homogeneity, orientation and shape of the electric field, as well as the current flow and the total energy transferred to the target tissue during electroporation (21-23).

Sonoporation

Sonoporation enhances cell permeability via the application of ultrasound. Ultrasound covers a wide range of frequencies and wave-forms, but attention has been principally focused on sonoporation using sinusoidal probes at megahertz frequencies. It has been thought that acoustic cavitation is the most probable mechanism involved in sonoporation. Cavitation causes mechanical perturbation and collapse of active bubbles, and the associated energy release can permeabilize adjacent cell membranes (24). Like electroporation, sonoporation is thought to induce the transient formation of small pores in the cell membrane allowing for the direct transfer of genetic material into cells and several types have been successfully transfected in vitro.

Optimization of ultrasound-mediated gene transfer depends upon several factors, including transducer frequency, acoustic pressure, pulse duration, and exposure duration. Additional factors are also important, such as the ultrasound contrast agent concentration and its formulation. Both diagnostic equipment and specific ultrasound devices have been used for sonoporation (25). The latter comprises of a piezoelectric transducer, which can be air-backed, focused or not, together with a generator and amplifier. This type of system permits enhancement of transfection with subtle modifications in the range of physical settings possible.

Laser-mediated transfection

Laser-mediated transfection (also known as optoporation or phototransfection) uses a pulse laser to irradiate a cell membrane to form a transient pore (26). When the laser induces a pore in the membrane the nucleic acids in the medium are transferred into cell because of the osmotic difference between the medium and the cytosol. The laser methods enables one to observe the transfecting cell and to make pores at any location on the cell. This method can be applied to very small cells, because it uses a laser, but it requires an expensive laser-microscope system. Finally, transfection efficiency depends on several parameters, including energy level, the number of pulses, and the pulse duration (9).

1.5.2.3 Magnetofection

Magnetofection is a new method to enhance the introduction of gene vectors into cells. The idea is to associate magnetic nanoparticles with DNA and either its transfection reagent or its virus vector (27). The magnetic nanoparticles are made of iron oxide, which is biodegradable, with a polymer coating (28). Their association with the gene vectors is achieved by salt-induced colloidal aggregation. The magnetic particles are then concentrated preferentially into the target cells by the influence of an external magnetic field. This technology allows delivery of the genetic material to the target cell surface and may even promote uptake, in that it has been demonstrated that the field can cause extravasation of the magnetic particles into the surrounding tissue (that is, the magnetic field may "pull" the magnetic particle across the plasma membrane and into the cell) (29). DNA is then released into the cytoplasm, with the hope that the magnetic particles will not influence cellular function. Note that magnetofection is a method that enhances standard transfection procedures using viral or non-viral vectors (and much more rarely with naked DNA); that is, the magnetic field per se is ineffective unless DNA vector is complexed to a magnetic particle. Nevertheless, decent transfection efficiencies, with rapid kinetics, have been reported (9).

1.5.2.4 Chemical methods

Chemical methods are based on cationic lipids (lipoplexes) or cationic polymers (polyplexes) (+ charged) that complex electrostatically with DNA/RNA molecules (- charged). These positively charged nucleic acid/chemical complexes are attracted to the negatively charged cell membrane. The transfection efficiency of the chemical methods depends largely on factors such as the nucleic acid/chemical complex ratio, solution pH, and cell membrane characteristics and is often inferior to virus-mediated methods (10). However, these methods have benefits, including relatively low cytotoxicity, no mutagenesis and no size limitation on the packaged nucleic acid (12).

1.5.3 Summary

All gene delivery methods described above have both positive and negative features, in terms of efficiency and practicality, and it is unlikely that a single approach will be universally ideal for all DNA delivery applications. For instance, in quiescent (non-dividing) cells including primary immune cells, especially, none of these traditional approaches has proved to be effective (12). Thus, the development of new methods for the effective delivery of plasmids and small interfering RNA (siRNA) into diverse cell types, with high yields, has the potential to transform gene therapy and underpin functional genomics studies. In this context, nanomaterials such as SiNWs, nanostraws, hollow nanoneedle and carbon nanofibers have been explored for gene delivery in a process termed "impalefection" (12).

1.6 Nanostructured materials

The unprecedented ability to control and characterize materials and structures on the nanometer scale has led to a rapid development of a plethora of nanostructured materials, including nanoparticles, nanowires, nanorods, nanocapsules, nanofibers, nanotubes, nanocomposites, nanostructured surfaces and thin solid films with nanoscale thickness. In many cases, the properties of such nanostructured materials can be very different from those of corresponding bulk materials, and desirable novel electrical, mechanical, chemical, optical, magnetic, thermal, and biological properties may be obtained. Among many other properties, nanostructured materials have the increased ability to **cross biological barriers**, which are inaccessible to larger materials or be specifically functionalized to bind to specific biological targets, such as ligands, proteins, antigens or cell types (e.g. tumor cells).

Nanostructured materials are fabricated and controlled by a powerful range of nanotechnology tools and techniques – advanced synthetic methods, supramolecular chemistry, surface science, nanolithography, new or improved analytical techniques and high-performance computer simulations. Analytical tools, such as atomic force microscopy (AFM), scanning tunneling microscopy (STM) and near-field scanning optical microscopy, have provided revolutionary improvements in our ability to visualize structures and events all the way down to the molecular and atomic scale. High-performance computer simulations based on advanced mathematical and physical modelling are at present a necessary tool in the development, design, and understanding of nanostructured materials.

Synthetic methods, supramolecular chemistry and surface science are considered bottom-up approaches of nanofabrication since they involve building up nanostructures materials from nano- or sub-nano-scale entities (namely, atoms or molecules), in much the same way that nature does. With advancements in synthetic methods, nanostructured materials can be synthesized with precisely controlled morphologies, sizes and seemingly limitless chemical functional groups. Remarkable progress in the field of supramolecular chemistry has enabled the design of molecular components to interact favorably with each other in such a way that they can self-assemble, through noncovalent interactions, into larger, well-defined entities on the nanoscale with tailored properties (30). The development of synthetic methods and supramolecular chemistry has permitted the access to carbon-based nanoparticles such as fullerenes and metallic (e.g. Au, Ag, Pt), semiconducting (e.g. CdSe, CdS, ZnS, GaAs), magnetic (e.g. Fe_3O_4), polymeric and hybrid (e.g. core-shell) nanoparticles. These bottom-up techniques have also allowed achieving other morphologies such as nanowires, nanorods, nanocapsules, nanofibers and nanotubes. Among the different nanotubes, carbon nanotubes (CNTs), which were discovered in 1991, have received much attention due to their unique physical/mechanical, electronic, chemical, optical and other properties (30).

Advances in surface science now permit the fabrication of nanoscale molecular-assembly structures onto a variety of substrate surfaces using techniques such as Langmuir-Blodgett films (LBFs), self-assembled monolayers (SAMs) and two-dimensional supramolecular assemblies. Among these three techniques, SAMs are the most widely used for surface functionalization. SAMs are formed via adsorption of molecules from solution or gas phase, creating two-dimensional quasi-ordered molecular assemblies on conducting, semiconducting or insulating surfaces with a wide range of terminal functionalities (e.g. carboxylic acid, amine, nitro, hydroxyl and methyl groups).

In contrast to the bottom-up technologies mentioned above, one can fabricate nanostructured materials via etching away bulk material to achieve the required smaller structural architectures. This process type is regarded as the top-down approach and it is generally achieved by nanolithography. The nanolithographic processes could be linked to sculpting a block of stone to obtain the required

image. Many lithographic techniques of different complexity, efficiency, areal scale, and cost have been utilized for patterning surfaces with nanometer resolution. These techniques include novel nanolithography techniques such as nanoimprint lithography, colloidal lithography, soft lithography and dip-pen lithography, as well as conventional techniques such as electron-beam lithography and photolithography. Photolithography or electron-beam lithography (EBL) uses UV light or electrons to irradiate a sensitive polymer layer (called resist) to form nanopatterns on the resist that are subsequently transferred to the substrate material, often by etching. While EBL and photolithography are able to generate features with extremely high resolution (e.g. sub-5 nm and sub-20 nm for EBL and ArF double exposure immersion photolithography, respectively), these techniques have their limitations in terms of materials that can be patterned and the high costs of investment in equipment (31).

Novel nanolithography-based techniques have emerged that enable limitations associated with conventional lithography techniques to be overcome (32). Soft lithography, which includes techniques such as contact printing, replica molding and embossing, is a very useful alternative because it has been developed specifically for making large-scale nanostructures with a low-cost, flexible processing capability. Soft lithography is characterized by the use of a patterned elastomer as the stamp, mold or mask to generate structures with feature sizes as small as 30 nm (30, 33). The drawback of soft lithography is that it still requires the assistance of conventional lithographic techniques to design the masks or masters. In an attempt to address this challenge, an increasing amount of attention has been paid to the use of two-dimensional arrays of nanospheres as masks for etching or templates for deposition. This technique for sub-10 nm patterning has been termed **nanosphere lithography (NSL)** or colloidal lithography and its application is most suitable under situations in which a periodic arrangement of the nanostructures is required.

These enabling bottom-up and top-down technologies, in addition to advanced analytical techniques and high-performance computer simulations, are driving the integration of nanotechnology in cell biology (30).

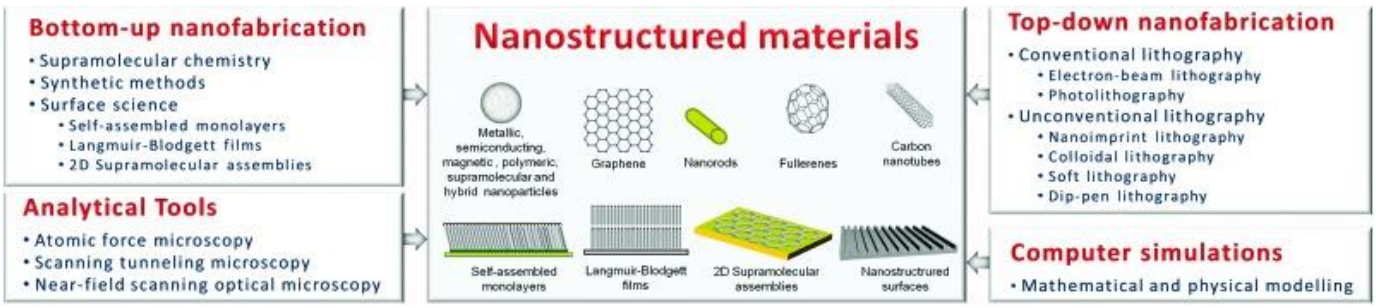

Figure 1.4: Schematic representation of examples of nanostructured materials, which can be fabricated and controlled by a powerful range of nanotechnology tools and techniques – bottom-up and top-down nanofabrication technologies, new or improved analytical techniques and high-performance computer simulations (30).

1.6.1 Silicon nanowires (SiNWs)

Methods for Si-NW fabrication: Numerous methods have been developed to fabricate SiNWs, including vapour–liquid–solid (VLS) growth, solution-based growth, reactive ion etching and electrochemical etching or MACE (12).

The vapor-liquid-solid (VLS) mechanism (Fig. 1.5), is the most commonly used mechanism for NW synthesis. The VLS approach relies on the deposition of metallic nanoparticle catalysts of defined diameter on a substrate. The substrate is heated in a tube furnace above the eutectic temperature of the relevant metal-semiconductor system in the presence of the semiconductor reactant vapor-phase source. According to this mechanism, an anisotropic growth is promoted by the presence of a liquid alloy-solid interface (Fig. 1.5 (a) & (b)). Based on the binary-phase diagram, the semiconductor and the metal catalyst, for example Si (from the decomposition of SiH_4) and Au respectively, will form a liquid alloy when the temperature is higher than the eutectic point of 363°C (Fig. 1.5 (c)) . The liquid surface has a large accommodation coefficient and is therefore a preferred site of deposition for incoming Si vapor. After the liquid alloy becomes supersaturated with Si, SiNW growth occurs by precipitation at the solid-liquid interface, because the growth temperature is higher than the eutectic point, but lower than the melting point of the nanowire material (12).

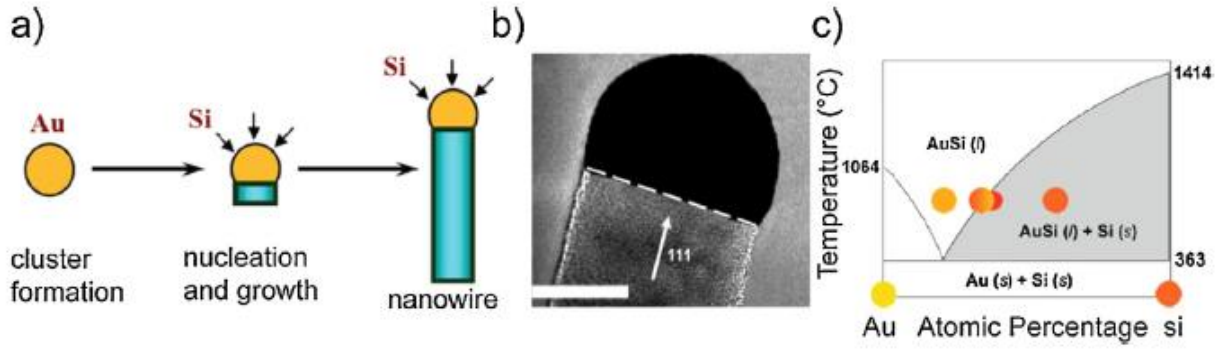

Figure 1.5: Schematic illustration of the VLS growth of SiNWs : (a) liquid droplet of Au-Si alloy first forms above the eutectic temperature (363°C) of Au and Si. The continued feed of Si in the vapor phase into the liquid alloy causes super-saturation of the liquid alloy, resulting in nucleation and directional NW growth. (b) HRTEM image shows a liquid droplet of Au-Si alloy on top of a SiNW. Scale bar: 20 nm. (c) The thermodynamics of VLS growth for binary-phase Au and Si (12).

However, the VLS approach has a limited ability to produce a vertical array of nanowires and requires the use of hazardous silane gases at high temperatures (34).

1.6.1.1 Vertically aligned silicon nanowires (VA-SiNWs)

Unlike horizontal nanowire elements, which lie within the substrate plane, vertically aligned nanowires are oriented perpendicular to the substrate (12). VA-NW arrays have been the subject of increasing interest, due to their potential to create **smart and functional NW-cell interfaces** (35-37).

1.6.1.1.1 VA-SiNWs as a biointerface

Vertically aligned silicon nanowire (VA-SiNW) arrays are an emerging platform applicable across several life science contexts, including biosensors and cell scaffolds (38). VA-SiNW arrays allow access to the internal structures of a cell without inducing toxicity, and can transport genes or other

bioactive molecules into it (39). This delivery technology, known as transfection, is extraordinarily efficient compared with conventional techniques that were mentioned above (Section 1.5.2).

NW-mediated transfection is not only compatible with continued cell viability, adhesion and proliferation, it bypasses the limitations inherent to endocytotic uptake mechanisms and directly transport exogenous materials into the cell interior (35). NW-mediated transfection is a form of mechanical transfection that is attributed to an "impaling mechanism", in which penetration by vertically aligned NW is driven predominantly by cell adhesion to the substrate and initiated soon after the application of cells to the NW array. Attempts to enhance the intracellular access process have been carried out by applying force to the NW-cell interface, by coating the NW with aminosilane and other cell adhesion promoting molecules, or by electroporation, as well as by adding membrane stabilizer molecules such as saponin to increase the odds of membrane penetration (38).

In 2010, Shalek et al. (39), reported on an experimental platform based on surface-modified VA-SiNWs that can deliver biomolecules into immortalized and primary mammalian cells. The method relied on the ability of the SiNWs to penetrate a cell's membrane and subsequently release surface-bound molecules directly into the cell's cytosol, thus allowing high efficient delivery of biomolecules without chemical modification or viral packaging. More recently, Elnathan et al. (34,38), examined the role of the geometrical characteristics of SiNW arrays, fabricated via NSL and tMACE techniques, in controlling cell behaviour and transfection efficiency of both human immortalised cell lines such as HEK (Human Embryonic Kidney) 293 cells and human primary cell types such as hDPSC (human Dental Pulp Stem Cells). They observed that the transfection efficiency strongly depends on NW height and varies greatly between cell types. For the majority of the tested cell types, medium heights (1.2-3.5 μm), small diameters (<400 nm), and densities between 0.6 and 1 NW μm^{-2} were associated to high transfection efficiency. In addition, there was direct evidence that cells exhibiting high transfection efficiency were impaled by SiNW arrays without the application of any external force. In another recent study, Chiappini et al. (40), demonstrated that a tunable array of biodegradable silicon nanoneedles (SiNWs with a tapered profile), fabricated by metal assisted chemical etching and reactive ion etching, can access the cytosol to co-deliver DNA and siRNA to HeLa cells with an efficiency greater than 90%. The nanoinjection, in this case, was enhanced by the use of centrifugation force.

1.7 Fabrication of VA-SiNW arrays with tapered profile via deep reactive ion etching

1.7.1 Convective assembly deposition

Convective assembly is a particle monolayer coating technique that combines fluid evaporation, particle transport via fluid flow, and associated meniscus motion to rapidly and controllably deposit a diverse range of microspheres and cells into thin (<10 μm) highly uniform films. In convective assembly, the particle or cell assembly process begins at the periphery of an evaporating fluid film when the film's height becomes thinner than the diameter of the suspended particles. The meniscus formed around these particles include strong, long-range capillary forces that pull neighboring particles together into two-dimensional nuclei. The particle clusters travel with the liquid flux from the bulk suspension to the substrate-air-liquid contact line at the drying front as the fluid evaporates, resulting in the formation of closely packed arrays and subsequent propagation of the coating area.

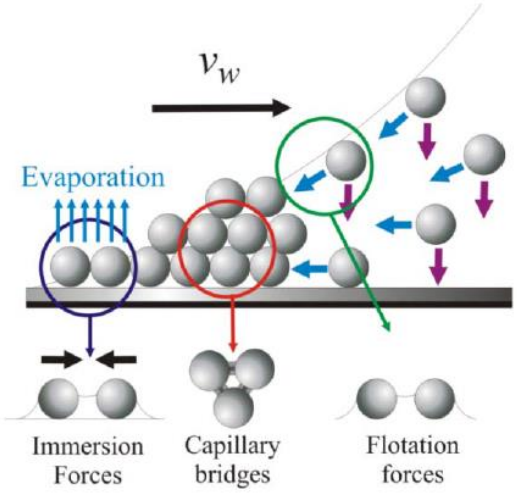

Figure 1.6: Schematic illustration of the convective assembly process. Blue and purple arrows denote particle convention and sedimentation in meniscus, respectively (41).

The coating growth rate is related to the fluid evaporation rate and particle volume fraction by the equation:

$$v_c = \frac{\beta j_e l \varphi}{h(1-\varepsilon)(1-\varphi)}$$

where β is a particle-particle interaction parameters; j_e is the evaporation rate; l is the drying length; φ is the volume fraction of the particles in suspension; h is the height of the deposited coating; and ε is coating porosity. Values of β vary between 0 and 1 and depend on particle-particle and particle substrate interactions; for low volume fraction and electrostatically stable particles, β≈1. Once v_c is determined, the length of the thin film where deposition occurs by convention can be calculated using a material flux balance:

$$L_{film} = \frac{v_w d_{cell} (1-\varepsilon)(1-c_i)}{\beta j_e c_i}$$

where v_w is the deposition rate and equal to v_c at steady state; and c_i is the concentration of the bulk suspension at that particular time (41).

1.7.2 Deep Reactive Ion Etching

Amongst top-down methods, deep reactive ion etching (DRIE) is regarded as a powerful method to fabricate vertical silicon structures or pillars (42). It is a plasma based dry etching technique. Dry etching is the preffered pattern transfer method since it offers a tunability of the etching profile, whereas the profile is usually not tunable for wet etching, with a curved profile resulted from an isotropic etching being the most typical. For majority applications, a completely anisotropic etching is desired since the resulted vertical profile retains the critical dimension of the mask and enables the etching of high aspect ratio structures. However, for some applications, a tapered profile is beneficial (43).

1.7.2.1 Bosch process

The Bosch, or time domain multiplex (TDM), process is a two step plasma process which alternates between passivation and etching through C_4F_8 and SF_6 gases respectively (44). It was patented by Robert Bosch GmbH and licensed by several companies including STS, Alcatel, Oxford instruments, and Unaxis.

The process starts with the etch step, where SF_6 is used to form plasma that is rich in free fluorine radicals, which react with the silicon to produce SiF_4, which is gaseous and pumped out of the system by the vacuum pump. This etch is isotropic and will only be allowed to etch for a limited depth, which is usually less than one micron. It is followed by the deposition step, which uses C_4F_8 (a cyclic fluorocarbon) to form the plasma. The C_4F_8 breaks apart into highly excited fragments that react one with another on the exposed silicon surface and build up a more or less strongly cross-linked layer of a Teflon-like polymer, which is deposited on the surface of the wafer. Although fluorocarbon film is deposited on all the surface of the substrate, it is used for sidewall passivation. At the beginning of the next etch step, the fluorocarbon polymer is removed from the horizontal surfaces of the substrate by ion bombardment. Ions created in the bulk plasma are accelerated across the sheath, gain energy and used to remove polymer. Increasing ion energy in the vertical direction results in a much higher rate of removal of fluorocarbon polymer on horizontal surfaces than that on vertical surfaces. After polymer removal the horizontal silicon surface is exposed to reactive fluorine-based species. The silicon at the base of the trench is etched chemically during this period, whilst the vertical surfaces remain protected by the fluorocarbon polymer layer. By switching back and forth between etch and deposition plasmas the silicon is etched in an anisotropic fashion to the desired etch depth (45).

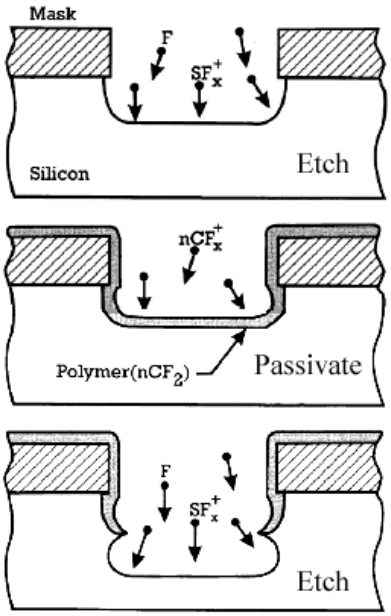

Figure 1.7: Schematic illustration of the Bosch process (46).

As cycles go on, the micromachining proceeds via a series of "bites" into the silicon, each on the order of 0.5μm – 5μm deep. These are usually called **"scalloping"** or **"ripple"**. For nanostructure etching, however, scalloping can become a serious problem. As feature size and scallop size become comparable, the process conditions have to be adjusted to minimize the ripple, in order to ensure smooth sidewalls at the nanoscale. This can be achieved by optimizing source power, bias power, gas flow rate, flow cycle time, substrate temperature and chamber pressure (42).

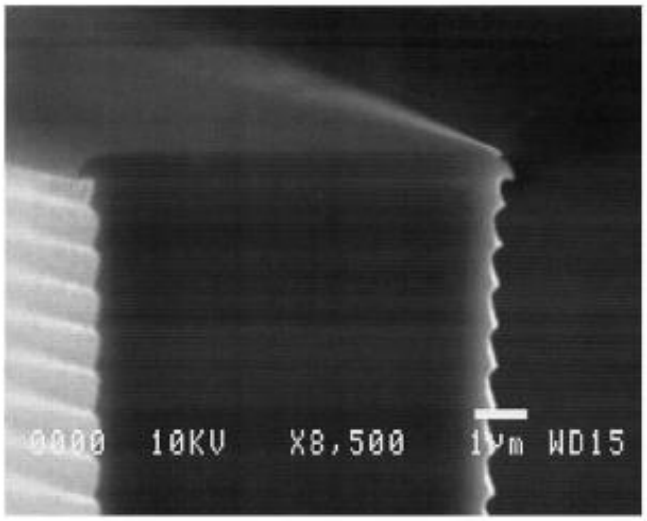

Figure 1.8: SEM micrograph of a typical scalloping pattern (42).

1.7.2.1.1 Etch chemistry

In the Bosch process, the deposition and etch steps are performed separately. During the deposition step, plasma breaks apart the strained cyclic hydrocarbon C_4F_8 into highly excited fragments. The individual fragments react one with another on the exposed surface and build up a more or less strongly cross-linked layer of polymer. This is called **plasma polymerization**. Although many neutral and ionic species are produced, the highest fluxes of species at the surface during deposition have been measured to be CF_2 and C_2F_4.
The general chemical reactions are:

$$c\text{-}C_4F_8 + e^- \xrightarrow{\text{gas phase}} 2C_2F_4 \xrightarrow{\text{gas phase}} C, F, CF, CF_2, CF_3$$

$$CF_2, C_2F \xrightarrow{\text{absorban \& polymerize at surface}} (CF)_x$$

In the etch step SF_6 is used. The etch step includes two mechanisms. One of them is removal of the horizontal component of the polymer, by accelerating the ions in the plasma to the wafer surface, with an applied RF bias between the plasma and the wafer chuck. After the removal of the polymer, silicon is isotropically etched using atomic fluorine generated from SF_6 plasma.
The main chemical reactions in the gas phase of the SF_6 etch are:

$$SF_6 + e^- \xrightarrow{k_1} SF_3 + 3F + e^-$$

$$SF_6 + e^- \xrightarrow{k_2} SF_2 + 4F + e^-$$

At the wafer surface, Si is etched by the following reaction:

$$F_{gas} \xrightarrow{k_3} F_{ads}$$

$$Si_{solid} + 4F_{ads} \longrightarrow (SiF_4)_{gas}$$

Since ion fluxes at the wafer surface are relatively low compared to the F flux, SiF_6 is a primarily chemical etch producing an isotropic profile. Using continuity equations at the surface, an analytical expression for the etch rate can be obtained as follows.

$$\frac{\partial SF_6}{\partial t} = \frac{F_{SF_6}}{V} - \frac{SC_{SF_6}}{V} - k_1 \mathrm{n} C_{SF_6} - k_2 n C_{SF_6} = 0$$

$$\frac{\partial F}{\partial t} = \frac{SC_F}{V} + 3k_1 n C_{SF_6} + 4k_2 n C_{SF_6} = 0$$

Although there are many other reactions in the plasma, it has been reported that the one producing SF_3 accounts for about 2/3 and that producing SF_2 accounts for 1/3 of the released etching species F. Solving for gas phase concentration of SF_6 and F:

$$C_{SF_6} = \frac{\frac{F_{SF_6}}{V}}{\frac{S}{V} + k_1 n + k_2 n}$$

$$C_F = \frac{V}{S}[3k_1n + 4k_2n]C_{SF_6} = \frac{V}{S}[3k_1n + 4k_2n] \frac{\frac{F_{SF_6}}{V}}{\frac{S}{V} + k_1n + k_2n}$$

Therefore, the etch rate at the surface can be expressed as:

$$\text{Etch Rate} = \frac{\Omega_{Si}}{4} k_3 C_F = \frac{\Omega_{Si}}{4} k_3 \frac{V}{S}[3k_1n + 4k_2n] \frac{\frac{F_{SF_6}}{V}}{\frac{S}{V} + k_1n + k_2n}$$

In spite of the rounded profiles, F chemistry is preferential to other etch chemistries due to the high volatility of SiF_4, the Si etch product. This is necessary for deep features, as the presence of less volatile etch products in small features sizes can inhibit etch rate.

The preferential etching of the bottom of the trench compared to its sidewalls can be modeled in several ways. Some literature suggests that the polymer is selectively deposited in the vertical sidewalls rather than on horizontal features as part of the dep/etch process balance. This would create a very thin polymer film on the bottom of the trench as compared to the sidewalls. Other sources indicate that polymer deposition is uniform, and that there is a third "breakthrough" etch step through the polymer from the bottom of the trench exposing Si to subsequent processing by the mostly chemical SiF_6 etch mechanism (45).

1.7.2.1.2 Process parameters

There are several parameters, including step times, gas flows and process pressure, that affect the process in different ways. Some of them are presented briefly in the following sections.

Step times

Step times are the individual etch and passivation times cycling during the process. They have a large influence on the profile and the etch rate. If the ratio of the etch and passivation cycles is too large, then sidewalls will not be sufficiently protected and the etch will result in reentrant profiles. Contrarily, if the cycle ratio is too small then it leads to excess passivation on the base of the trench. Moreover, if the deposition content of the etch step is too large then this can lead to the etch stopping altogether. Generally the larger the step time for the etch step, the larger the scallops or increased roughness on the sidewall. Increasing the switching frequency of the plasma gases decreases the scallops' size and reduces the roughness of the sidewalls by decreasing the isotropic etch time at the bottom of the trench before the next passivation step protects the sidewall. The optimum etch and passivation times and their ratio depend upon the application. For high aspect ratio structures, the duration must be short whilst for deep etches of large features etch time should be set to large value. It is important to realize that there is a fine balance between the step times (45).

Gas flow dependence

Increasing the SF_6 flow during the etch step generally, increases the etch rate of the process. After a threshold, increase in etch rate will depend on the applied power. In other words, for a particular flow of SF_6 there is a point at which more power is required to ionize the SF_6 gas, and if this power is not supplied then the additional gas will not be ionized into reactive species resulting no change in etch rate. In the same manner, thickness of the passivation layer will increase with increased C_4F_8 flow up to a certain limit (45).

Pressure dependence

The process pressure has a great impact on the overall etch results. Generally, higher pressures in the etch step lead to higher etch rates resulting from the increased number of fluorine radicals available. In addition, selectivity of the mask also increases with the increased process pressure. Increasing the pressure in the etch step, increases the availability of the free fluorine radicals for etching silicon chemically, resulting an increase in etch rate. Since increase in pressure also increases the collision ion/neutral scattering, ion energy and ion directionality will be reduced and this will reduce the etch rate of the mask. However, for high aspect ratio features this can cause a problem in terms of profile control. Processing high aspect ratio structures at high pressures causes the bowing and closing up towards the base of the trenches due to increased scattering of ions at higher pressures. Keeping the process pressure low results in better profile angle. However, this will also reduce the selectivity of the masking material as a consequence of the increased ion energy (45).

Electrode temperature

The passivation step strongly depends on the temperature of the substrate surface. During the process, the substrate is kept at a fixed temperature by cooling the chuck and temperature uniformity over the wafer is accomplished by helium flow at the back side of the wafer.
Increase in temperature, reduces the passivation rate, resulting in a decrease in the selectivity of the masking material (45).

1.7.2.2 Plasma generating systems

The requirements for DRIE processing plasma must include high density ions, electrons and radicals, excellent uniformity over a large diameter, low and controllable ion energies and negligible contamination from reactor sputtering at low pressures (45).

In conventional plasma etch systems, like RIE, plasma is typically generated by applying an RF electric field between two parallel plates. However, these systems cannot supply the plasma requirements of the DRIE processing. High plasma densities at low pressures have been achieved with electron cyclotron resonance (ECR) sources and magnetron systems. However, the presence of a strong magnetic field (850 G) leads to difficulties in achieving both good process uniformity and gate integrity (45).

Inductively Coupled Plasma (ICP) etching

One of the most commonly used method for generating high density plasma with a good uniformity is coupling electromagnetic energy from a coil surrounding the plasma chamber, called as inductively coupled plasma (ICP) (47).

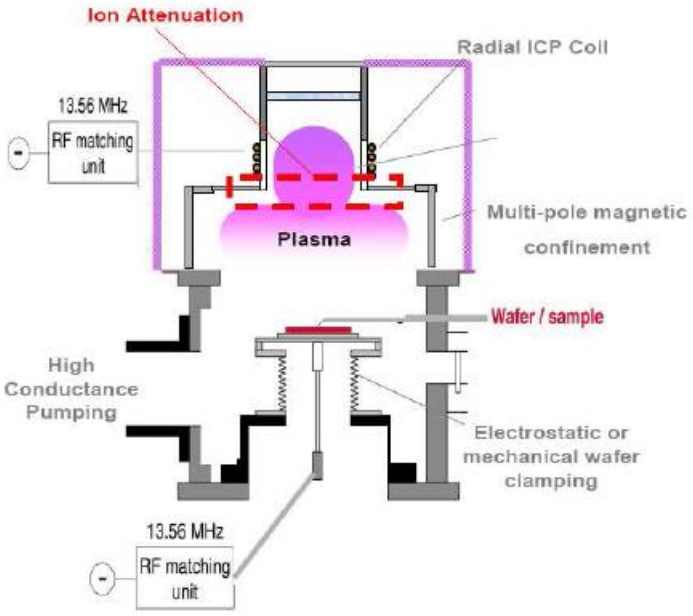

Figure 1.9: Schematic illustration of a typical ICP chamber (45).

RF coil surrounding the chamber generates a magnetic field inside the chamber. Secondly, the plasma will act as the secondary coil in a transformer. Since this RF magnetic flux density is time varying, it will induce a solenoidal electric field, according to Faraday's law ($\nabla x E = -\frac{\partial B}{\partial t}$). This induced electric field accelerates electrons and ions thereby causes collisions resulting more ions and electrons. Fig. 1.10 shows the sketch of a helical ICP coil chamber.

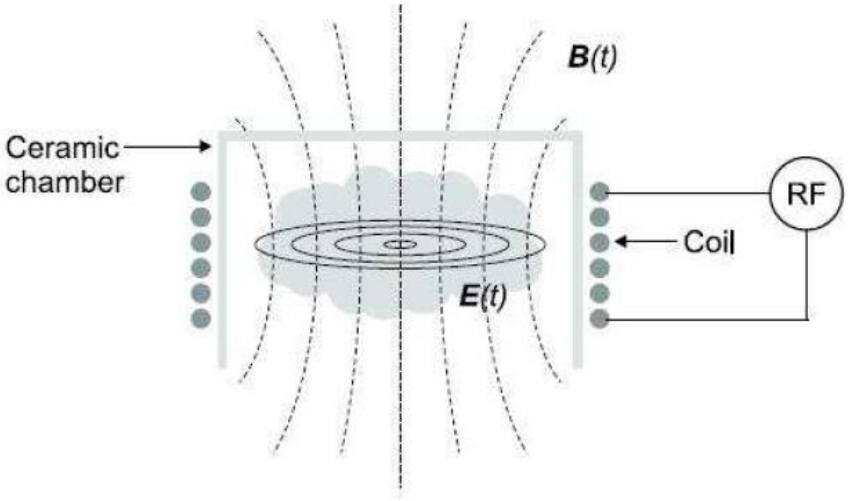

Figure 1.10: Sketch of a helical ICP coil chamber. The axial magnetic field induces an azimuthal electric field, which accelerates the charged particles (45).

Electrons and ions in the plasma will be accelerated with the presence of an induced electric field. Since the electron mass is much lighter than the ions', electrons will acquire a larger speed, and as a

result they will leave the plasma. Therefore the plasma will become electrically positive compared to the surrounding. Then the ions in the plasma will be accelerated towards the chamber walls. An independent RF bias between plasma and wafer chuck can be used for ion bombardment of the wafer by increasing the energy of the ions. Using RF frequencies prevents excessive charging of insulating substrates and enhances the efficiency of the ionization processes.

For capacitively coupled plasmas, the plasma efficiency is inversely proportional to the applied RF power since the plasma density is proportional to only the square root of the plasma power for the desired conditions where the sheath impedance dominates. The efficiency of inductive plasmas, on the other hand, is high in the density region desired for single wafer plasma processing. The inductive coupling method allows producing a dense plasma with an electron density around 10^{12} cm^{-3}. With the increasing density of the plasma, etch rate also increases, since the supply of the radicals is the limiting factor in the etch process.

Keeping the chamber pressure at low values, prevents the increased scattering, thus the directionality of the ion bombardment is maintained. With the combination of high density plasma and control on the ion bombardment high etch rates with high mask selectivities can be achieved (45).

Magnetic Neutral Loop Discharge (NLD) plasma

A neutral loop discharge (NLD) is a plasma generated along a closed magnetic neutral line (i.e. a loop along which the extremelly applied static magnetic field vanishes) by a radio frequency (RF) electric field. Such a magnetic field configuration may be formed by a system illustrated in Fig. 1.11 , where a magnetic neutral loop is formed between the two magnetizing coils on which currents flow in the same direction. If the magnetic neutral loop is placed in evacuated space with some filling gases and an RF field generated by an external loop antenna, a plasma is produced in torus-shaped region centreed around the magnetic neutral loop. NLD plasmas tend to have high plasma densities with relatively low electron temperatures and can be produced even at low gas pressures (48).With such unique characteristics for low-temperature plasmas, NLDs have been found especially suitable as plasma sources for some specific plasma processing applications where good directionality and high fluxes of ion bombardment at substrate surfaces are required (49).

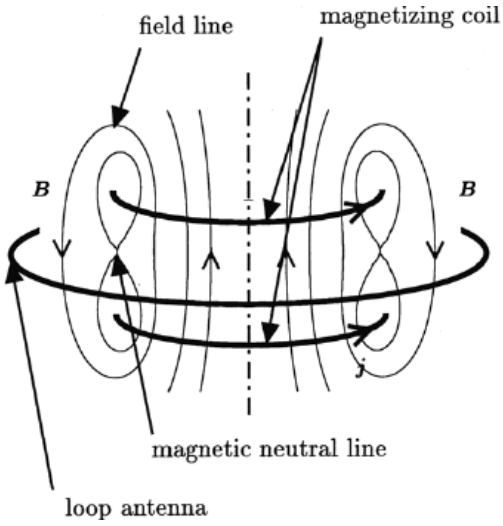

Figure 1.11: An example of magnetic configuration with a null field line (magnetic neutral loop) (49).

Electrons produced in such a plasma move under the influence of Lorenz forces exerted by the static magnetic field. In the presence of an RF electric field together with the magnetic field whose electron cyclotron frequency equals the RF frequency at some locations, electrons passing through the (narrow) region of resonant magnetic field tend to gain kinetic energy efficiently from the RF electric field. If spatial variation of magnetic field at the resonance region is larger than the typical size of electron motion (e.g. cyclotron radius), then the complete electron cyclotron resonance (ECR) may not occur. Nevertheless, electrons passing through the region still gain some energy from the RF field, which we call partial electron cyclotron resonance (PECR).

As a plasma source, an NLD plasma has two important advantages. One is the high ionization rates due to both efficient coupling with externally applied RF fields (i.e. PECR) and good electron confinement by the cusped magentic field. With such properties, a high-density, low-electron-temperature plasma can be generated in an NLD system at low gas pressures (e.g. less than 0.1 Pa). The other is its spatial and temporal controllability of magnetic field configuration, which allows optimization of plasma configuration during processing.

For plasma position control, vertically aligned three magnetizing coils, as depicted in Fig. 1.12, may be used. When currents flow in the top and bottom coils in the same direction, a circular magnetic neutral loop is formed between the two magnetizing coils, as in Fig. 1.11. With an additional current flowing in the opposite direction in the middle coil, the diameter of the formed neutral loop can be reduced and it may be positioned inside the reaction chamber, as shown in Fig. 1.12. By varying the current in the middle coil, one can vary the position of magnetic neutral loop to achieve optimal plasma configuration. When an RF electric field is applied in the azimuthal direction, a doughnut-shaped NLD plasma is produced along the magnetic neutral loop. Since the magnetic field vanishes at the neutral loop and increases as one moves away from it, the strength of magnetic field equals that for ECR at some distance from the neutral loop. The extent of the NLD plasma seems to be limited roughly in the torus region spanned by the magnetic neutral loop and ECR magnetic field.

Finally, compared with the equivalent ICP plasma, an NLD plasma can absorb RF power more efficiently and the absorbed energy is deposited in a doughnut-shaped region along the magnetic neutral loop, where efficient ionization takes place even at low gass pressures (49).

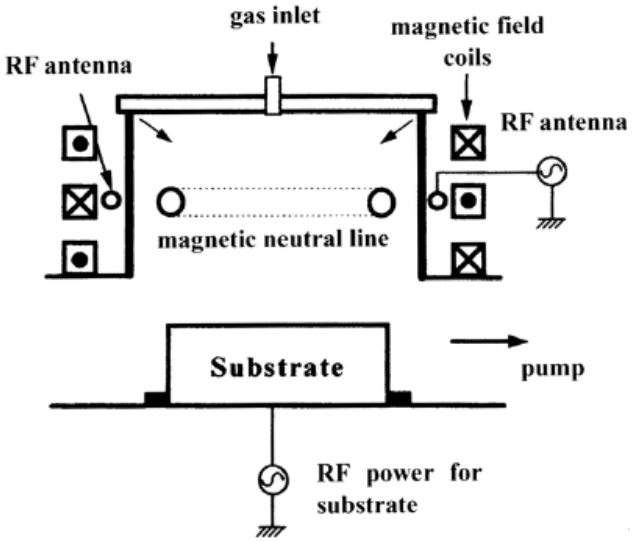

Figure 1.12: A schematic view of an NLD system with three magnetic coils (49).

2. The aim of the present Master thesis and the approach to the problem

2.1 Aim

The overarching aim of the present study was to develop a new technique in order to perform non-viral gene transfection in vitro. The technique is based on the fabrication of high aspect ratio vertically aligned silicon nanowire (VA-SiNW) arrays for efficiently introducing genes into living cells, with minimal impact on the cell's viability and function.

Using a combination of nanosphere lithography and Deep Reactive Ion Etching, arrays of VA-SiNWs with a tapered profile, called "Si MC tips", were fabricated, exhibiting different geometrical characteristics (such as height and tip diameter). These Si MC tips together with flat Si wafers have been then applied to in vitro cell cultures. The model cell line used was human embryonic kidney (HEK293) cells.

2.2 Approach

The approach that we followed consists of the following steps: The first step is the fabrication of the Si MC tips via DRIE of silicon using polystyrene microspheres as a mask. Following this, Si MC tips are loaded with GFP (Green Fluorescent Protein)-plasmid; a small DNA molecule which is labeled with GFP and acts as a reporter for successful transfection. The next step is the delivery of the plasmid into the cells by mechanical penetration using centrifugation force. This is performed first by applying the Si MC tip arrays onto the cells, facing towards them, and then by spinning of the whole setup using a centrifuge. After centrifugation and incubation of the Si MC tips with the cells for a specific period of time, Si MC tip arrays are removed from the well plate and we are probing cell transfection in both cases. At the footprint that the Si MC tips left on the well plate and on the Si MC tips themselves. A delivery system like this ideally exhibits two main advantages. It can offer us **parallel delivery** of plasmid to a huge amount of cells in a **short time**.

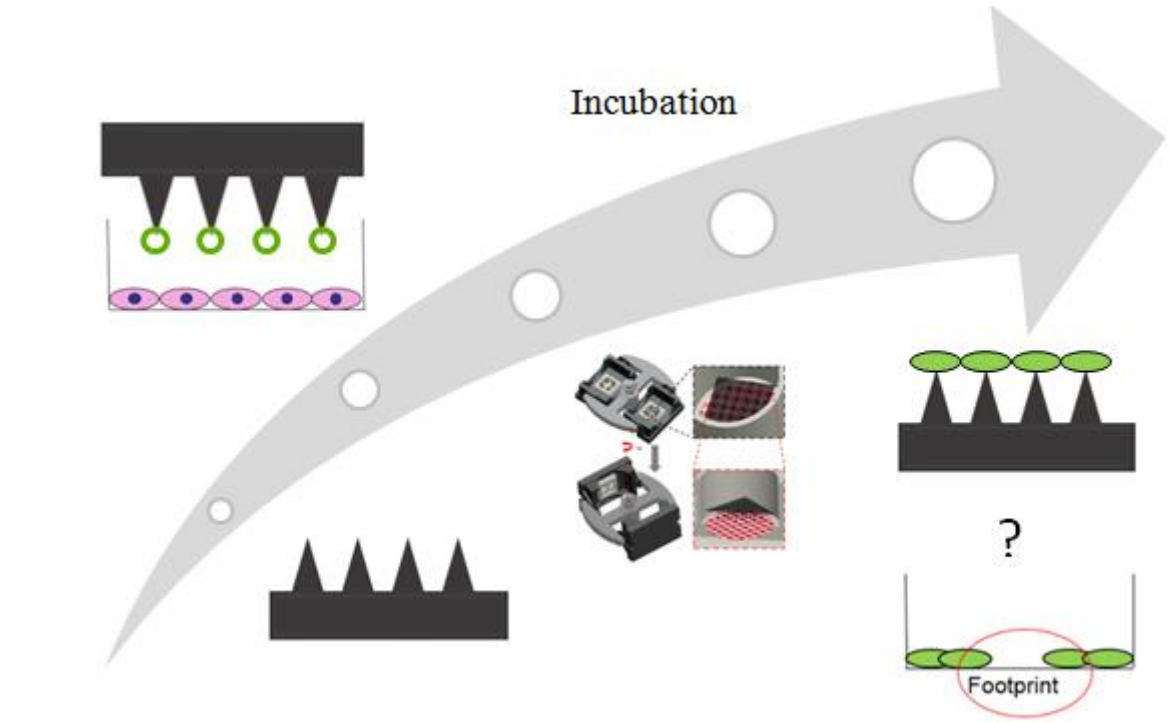

Figure 2.1: Schematic illustration of our approach to the problem.

3. Experimental Part: Materials & Methods

3.1 Chemicals and Materials

All chemicals were obtained from commercial sources and used without further purification. Sulfuric acid (H_2SO_4, 95-97%) and hydrofluoric acid (HF, 48%) were purchased from Scharlau Chemie (Chem-Supply Pty. Ltd Australian representation). Hydrogen peroxide (H_2O_2, 30%) was from Merck (Australia). Poly-D-lysine hydrobromide for cell culture (P7280), propidium iodide and fetal bovine serum (FBS) were all obtained from Sigma-Aldrich (Australia). P-type silicon wafers, 3-6 Ω cm, <100> were purchased from Silicon Quest (USA). Polybead microspheres solutions (4.5μm - #17135, 2.5% w/v) were purchased from Polysciences, Inc. (USA). The gWiz high-expression enhanced green fluorescent protein vector (gWiz eGFP) was purchased from Aldevron (USA). Fluorescein diacetate (FDA), 100X L-glutamine-penicillin-streptomycin supplement Opti-MEM medium and Hoechst 33342 fluorescent stains were obtained from Life Technologies.

3.2 Si MC tips

3.2.1 Fabrication technique

Flat silicon wafers (3", P - Boron, 3-6 Ωcm, <100>) were cut equally into 4 pieces and dipped into boiling Piranha solution (70% H_2SO_4:H_2O_2 v/v) for 1 h to remove organic contaminants. This was followed by washing with MilliQ water, ethanol, acetone and drying under a N_2 jet. Finally, samples were treated with O_2 plasma in an RF power system at 50W and at an O_2 flow rate of 15 cm^3 min^{-1}.

Hexagonal close-packed PSNS monolayers were then deposited over ~5 cm^2 of silicon wafer by convective assembly. The apparatus included a mounted microscope slide that was used as a blade for the PSNS depositions, 50 mm motorized translation stage (MTS50-Z8), a digital camera, and a TMC 66 series csp vibration isolation system. The blade was adjusted to leave a small space between the bottom edge of the blade and the Si substrate. Then ~24μl of PSNS suspension was injected into the space between the blade and the sample using a microneedle, forming a meniscus between the pinned substrate and the bottom edge of the blade. This resulted in a continuous contact line of PSNS suspension on the Si substrate. To deposit PSNS in a uniform monolayer, operating parameters such stage velocity and PS suspension concentration were adjusted. To monitor the uniformity of the assembly, the process was observed with a digital camera throughout.

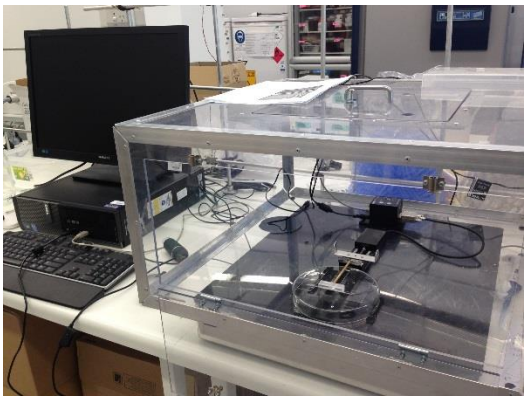

Figure 3.1: The convective assembly setup, located at the Future Industries Institute of University of South Australia (50).

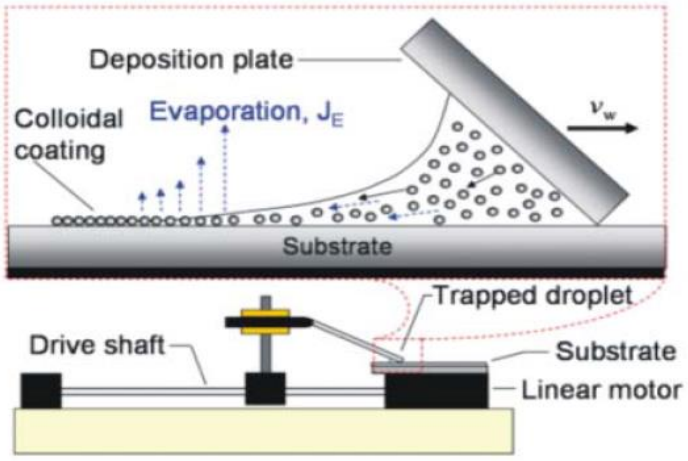

Figure 3.2: Schematic illustration of the convective assembly setup (41).

Samples prepared by convective assembly were first mounted, using thermal paste, on a 4" silicon wafer (dummy wafer) and then inserted into the Deep Reactive Ion Etcher (DRIE – ULVAC NLD570); a dry etching system equipped with a magnetic Neutral Loop Discharge (NLD) plasma source (Section 1.7.2.2).

This specific system has the ability to operate in two modes; silicon and glass etching. It consists of two separate chambers; a transfer and an etching chamber (Fig. 3.3 (a)). The transfer chamber, also known as Load/Unload (L/UL) chamber, is used for inserting/removing the samples in/from the system. It also prevents the repeated venting and pump-down of the main, etching, chamber. The etching chamber is subsequently the chamber, where all the processes (such as oxygen plasma etching) take place. It has three electromagnetic coils and an RF antenna, which is concentrically located with the middle coil. (Fig. 3.3 (b)). The plasma intensity is confined to the plane of the middle coil and the diameter of the plasma is proportional to the electromagnetic current, fact that enables the etching process to provide an extremely high uniformity.

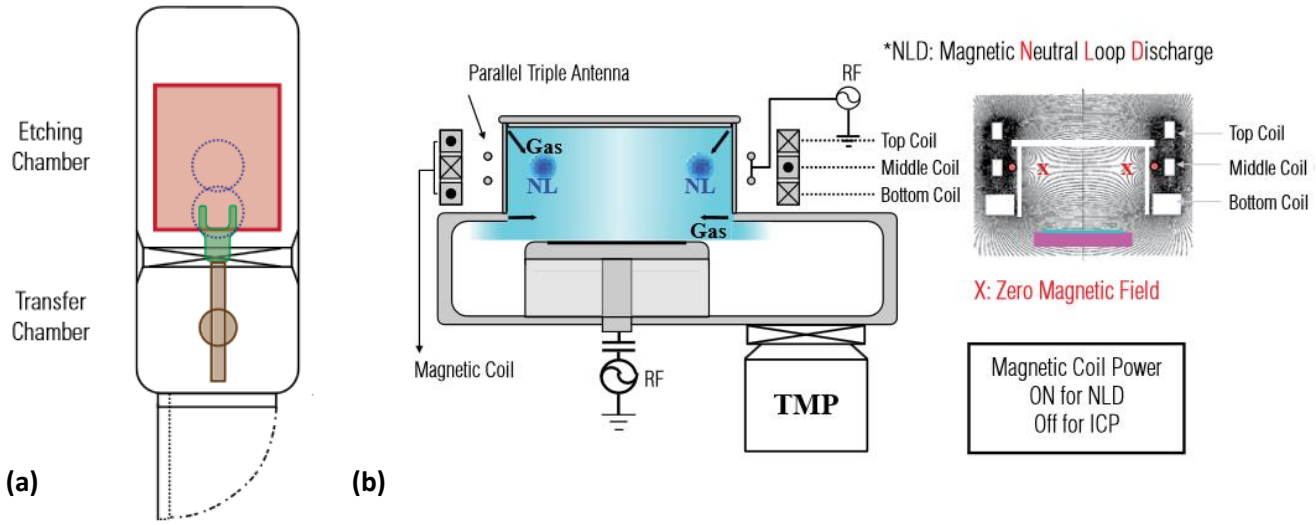

Figure 3.3: Schematic illustration of (a) a top view of the DRIE – ULVAC NLD570 and (b) the NLD system used (51). Abbreviations: TMP: Turbo Molecular Pump, NL: Neutral Loop

Figure 3.4: The DRIE – ULVAC NLD570 of ANFF SA node, located at the University of South Australia (52).

The close-packed PSNS were becoming non close-packed by O_2 plasma treatment. The O_2 plasma was performed according to a specific recipe. The recipe consists of three steps. The plasma is being created during the last step whereas the first two ones are used for stabilization of the O_2 flow.

Table 3.1: Example of an oxygen plasma recipe.
Abbreviations: APC: Automatic Pressure Control, PFC: Pressure Flow Control, AMC: Artificial Magnetic Conductor

Item	**Unit**	**Step 1**	**Step 2**	**Step 3**
APC Press Set	[Pa]	2	2	2
Trigger Press	[Pa]	2	0	0
PFC Press	[Pa]	500	0	500
PFC Flow Limit	[sccm]	0.3	0.3	0.3
MF C21 Flow Set (Ar)	[sccm]	0	0	0
MF C22 Flow Set (SF6)	[sccm]	0	0	0
MF C23 Flow Set (O2)	[sccm]	99	99	99
MF C24 Flow Set (C3F8)	[sccm]	0	0	0
MF C25 Flow Set (CF4)	[sccm]	0	0	0
MF C26 Flow Set (C4F8)	[sccm]	0	0	0
MF C28 Flow Set (H2)	[sccm]	0	0	0
Antenna RF Power Set	[W]	0	0	2000
Antenna AMC No.	[Pos]	1	1	1
Bias RF Power Set	[W]	0	0	25
Bias AMC No.	[Pos]	1	1	1
Magnet Top	[A]	30.6	30.6	30.6
Magnet Middle	[A]	52	52	52
Magnet Bottom	[A]	30.6	30.6	30.6
Process Time sec Set	[sec]	15	10	180
Bias V_{pp} Low Set	[V]	0	0	0
Bias V_{pp} High Set	[V]	0	0	0
Return Step No	[No]	0	0	0
Step Loop Count	[Times]	0	0	0
Loop Max Time Set	[sec]	12	12	12

Bias Vpp ≈ 90 V

Table 3.2: Explanation of the role of the parameters involved in both oxygen plasma and silicon etching recipes.

Parameter	Purpose
APC Pressure (Pa)	It controls the pressure in the etching chamber during etching/plasma discharge.
Trigger Pressure (Pa)	Oxygen's pressure that ignites the plasma
PFC Pressure (Pa)	Helium's pressure
PFC Flow Limit (sccm)	Helium's minimum flow
Antenna RF Power (W)	RF power applied to the gases
Bias RF Power (W)	RF power applied to the substrate
Bias AMC No. (Pos)	Position for reflective power (substrate)
Antenna AMC No. (Pos)	Position for reflective power (gas)
Magnet Top/Middle/Bottom (A)	Current in the Top/Middle/Bottom magnet (standard values)
Process Time (sec)	Duration of each step
Bias V_{pp} (V)	Voltage peak to peak applied to the substrate
Return Step No. (No)	Process returns to the specific step
Step Loop Count (Times)	Number of loops per step
Loop Max Time (sec)	Maximum duration of each loop

After a lot of optimization we concluded to the following values of the parameters: **99 sccm** for the O_2 flow, **2000 W** for the antenna RF power and **25 W** for the bias power. As far as the PFC flow limit is concerned, is selected to be quite low (**0.3 sccm**) in order for the process to be stopped in case there is not enough cooling of the substrate. Antenna AMC and bias AMC are switched to **position No.1** for zero reflective power. The value of the APC pressure was selected after running a test of the correlation between the APC pressure and the bias V_{pp}, keeping the antenna RF power constant. The test showed that the bias V_{pp} increases proportionally with the APC pressure. As we prefer the bias V_{pp} to be low (<100V), for less ion bombardment of the substrate, we concluded from the diagram (V_{pp} – APC) that **2 Pa** is the appropriate APC pressure value. Finally, as far as the process time is concerned, it was varied depending on the final height of the Si MC tips that we wanted to achieve. As mentioned before, O_2 plasma etching reduces the size of the PSNS, which subsequently affects the degree of silicon etching in the next step. The exact O_2 plasma etching recipes can be found on **Appendix A**.

The reduced size PSNS serve as a mask during the silicon etching. The process that was followed is the well-known "Bosch process'' (Section 1.7.2.1). It was performed according to a specific recipe (Table 3.3) consisting of three steps. The first step is used for the stabilization of the SF_6 plasma, which is used for silicon etching in the second step. Following that, C_4F_8 plasma is used for passivation layer

deposition. The process then returns to step 2, where sequential etching and passivation occurs for a specific number of loops. The number of loops is directly associated with the final height of the Si MC tips.

Table 3.3: Example of a silicon etching recipe.
Abbreviations: APC: Automatic Pressure Control, PFC: Pressure Flow Control, AMC: Artificial Magnetic Conductor

Item	Unit	Step 1	Step 2	Step 3
APC Press Set	[Pa]	1	0.67	0.67
Trigger Press	[Pa]	1	0	0
PFC Press	[Pa]	600	600	600
PFC Flow Limit	[sccm]	0.3	0.3	0.3
MF C21 Flow Set (Ar)	[sccm]	0	0	0
MF C22 Flow Set (SF6)	[sccm]	30	30	0
MF C23 Flow Set (O2)	[sccm]	0	0	0
MF C22 Flow Set (C3F8)	[sccm]	0	0	0
MF C22 Flow Set (CF4)	[sccm]	0	0	0
MF C22 Flow Set (C4F8)	[sccm]	0	0	25
MF C22 Flow Set (H2)	[sccm]	0	0	0
Antenna RF Power Set	[W]	1500	1500	750
Antenna AMC No.	[Pos]	1	1	1
Bias RF Power Set	[W]	30	30	10
Bias AMC No.	[Pos]	2	2	2
Magnet Top	[A]	30.6	30.6	30.6
Magnet Middle	[A]	52	52	52
Magnet Bottom	[A]	30.6	30.6	30.6
Process Time sec Set	[sec]	1	14	4
Bias Vpp Low Set	[V]	0	0	0
Bias Vpp High Set	[V]	0	0	0
Return Step No	[No]	0	0	2
Step Loop Count	[Times]	0	0	29
Loop Max Time Set	[sec]	0	0	0

Bias $V_{pp} \approx 90$ V

After a lot of optimization we concluded to the following values of the parameters: **30 sccm** and **25 sccm** for the SF_6 and C_4F_8 flow respectively and **1500/750 W** for the antenna RF power ratio. As far as the bias RF power ratio is concerned, is selected to be **30/10 W** in order to have the desired tapered profile. The PFC flow limit is selected to be again quite low (**0.3 sccm**) in order for the process to be stopped in case there is not enough cooling of the substrate. Antenna AMC and bias AMC are switched to **position No.1 and No.2** for zero and almost zero reflective power respectively. The value of the APC pressure was selected again after running a test of the correlation between the APC pressure and the bias V_{pp}, keeping the antenna RF power constant, following the same idea as in the oxygen plasma recipe above. The optimized value for the process time ratio is **14/4s**. Finally, the number of the loops varies, as it is associated to the final height of the Si MC tips that we want to achieve and limited by the time of the oxygen plasma treatment already performed. The exact silicon etching recipes can be found in combination with the oxygen plasma ones on **Appendix A**.

Once the whole process is finished, we are removing the sample first from the DRIE system and then from the "dummy" - holding wafer by cleaning carefully the backside of the sample with acetone. The DRIE system should be then cleaned thoroughly by running the "long oxygen cleaning" recipe. Generally, the amount of hours spent for the etching process must be equal to the amount of hours spent for oxygen plasma cleaning.

In order to achieve smoother and sharper tips all samples were subjected to the following post treatment. At first, silicon micro-conical tips were thermally oxidized at 1000^0C for 3 h in air environment within a box furnace. Following this, wet etching in 1:1 solution of HF:EtOH was carried out in a 15 ml standard Teflon container for 10 min at room temperature. Finally, samples were washed thoroughly with MilliQ water and dried under a N_2 jet.

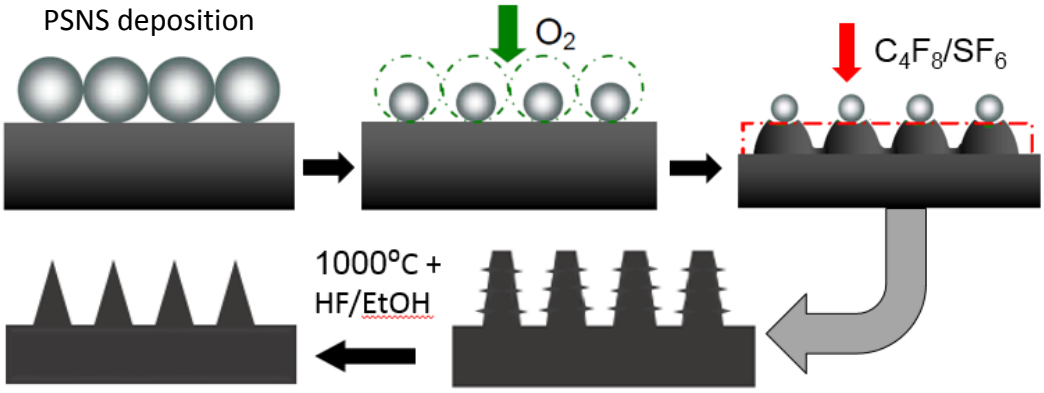

Figure 3.5: Schematic illustration of the fabrication technique of the silicon micro-conical tips.

3.2.2 Characterization of Si MC tips

The as-prepared silicon micro-conical tips were investigated regarding their morphological characteristics using Scanning Electron Microscopy (SEM).

3.2.2.1 Scanning Electron Microscopy (SEM)

3.2.2.1.1 Technique

Scanning Electron Microscope (SEM) is a type of microscope that uses an electron beam to illuminate the specimen and produce a magnified image. The beam of electrons is produced at the top of the microscope (electron gun), follows a vertical path through the column of the microscope, makes its way through electromagnetic lenses, which focus and directs the beam down towards the sample. The beam passes through pairs of scanning coils or pairs of deflector plates in the electron column, typically in the final lens, which deflect the beam in the x and y axes so that it scans over a rectangular area of the sample surface. The focused beam of high-energy electrons generates a variety of signals at the surface of solid specimens. The signals that derive from electron-sample interactions reveal information about the sample, including external morphology of surface topography, chemical composition and other properties such as electrical conductivity. The spatial resolution of SEM depends on the size of the electron spot, which in turn depends on both the wavelength of the electrons and the electron-optical system which produces the scanning beam. Depending on the instrument, the resolution ranges between 1 and 20 nm (53).

3.2.2.1.2 Experimental process

SEM was performed on a Carl Zeiss Microscopy Merlin with the GEMINI II column equipped with a field-emission gun operated at 2 kV. The secondary electron images were recorded with a parallel on-axis in-lens secondary electron detector.

3.2.2.1.3 Image analysis

SEM images were analyzed by an image processing algorithm (Image J, National Institutes of Health, Bethesda, MD, USA).

3.2.3 Surface modification of the Si MC tips

Before proceeding to cell experiments, silicon micro-conical tips were subjected to the following surface modifications. Thermal oxidation was carried out at 1000 ^{0}C for 3 h in air environment within a box furnace. The samples were then sterilized in 70% EtOH and were allowed to dry at room temperature in a laminar flow cabinet. Following this, the substrates were coated with poly-D-lysine (PDL) at concentration of 167 μg/ml and incubated at 4 ^{0}C for 4 h in order to allow **plasmid adsorption via electrostatic interactions** and promote cell adhesion. The unbound PDL was then washed with PBS away.

3.2.4 In vitro experiments with HEK 293 cells

3.2.4.1 HEK 293 cells

HEK293 is a cell line derived from human embryonic kidney cells grown in tissue culture. They are also known as HEK cells. This particular line was initiated by the transformation and culturing of normal HEK cells with sheared adenovirus 5 DNA. The transformation resulted in the incorporation of approximately 4.5 kilobases from the viral genome into human chromosome 19 of the HEK cells. The cell line was cultured by scientist Alex Van der Eb, in the early 1970s, at his lab at the University of Leiden in Holland, whereas the transformation was performed by Frank Graham, another scientist in Van der Eb's lab, who invented the calcium phosphate method for transfecting cells. The source of the cells was a healthy, aborted fetus. As far as the name is concerned, it was derived from the fact that it was Frank Graham's 293rd experiment.

HEK cells are popular for their ease of growth and transfection, making them a common cell culture in biological research. In addition, due to their high transfection efficiency, HEK cells are used to produce exogenous proteins or viruses for pharmaceutical and biomedical research purposes (54).

3.2.4.2 Cell culture

Human embryonic kidney cells (HEK293, ATCC CRL – 1573) were grown and maintained at 37^{o}C in a fully humidified atmosphere with 5% CO_2 in Dulbecco's modified Eagle's medium (DMEM) supplemented with 10% fetal bovine serum (FBS), 2 x 10^{-3} M L-glutamine U ml^{-1} penicillin and 100g/ml streptomycin. Medium was exchanged twice a week. The adherent cells were detached and harvested by using 0.05% trypsin/EDTA solution treatment. Serial passaging (1:3 split) at 70-80% confluence was performed.

3.2.4.3 Cell viability assay

Extensive cell viability experiments were carried out in order to ensure that cells remain alive during their contact with the silicon micro-conical tips.

3.2.4.3.1 Experimental process

HEK293 cells were seeded in a 24-well plate at density of 1 x 10^5 cells/ml in DMEM complete medium, which was followed by incubation at 37^0C in a fully humidified atmosphere with 5% CO_2 till cells were fully adhered to the wells. Arrays of silicon micro-conical tips were then placed to float on culture medium with the tips facing towards the cells and the whole setup was centrifuged at a speed of 7 g for 1 min. After centrifugation, an outline of the area of contact between the tips and the cells was drawn for each well. Following this, the well plate was incubated at 37 ^{0}C in a fully humidified atmosphere with 5% CO_2 for 5 h. The above process was repeated for incubation times of 3 h, 30 m and 3 m respectively.

The viability of the cells was assayed by **live-dead staining** using a final concentration of 15 µg/ml fluorescein diacetate (FDA) and 5 mM propidium iodide (PI) in PBS for 3 min at 37^0C. Samples were then removed from the wells and both samples and wells were first washed with PBS and then observed under an inverted Eclipse Ti-S fluorescence microscope (Nikon, Japan) using standard filters for FITC (fluorescein icocyanate, 495 nm excitation/517 nm emission) for FDA and TRITC (tetramethylrhodamine, 538 nm excitation/619 nm emission) for PI. Observations were conducted at three different locations on the surface of each sample at magnification of the 20x objective lens.

3.2.4.4 Cell transfection

3.2.4.4.1 Delivery methods

During our cell transfection experiments we used two different delivery methods as presented in Fig. 3.6 and 3.7.

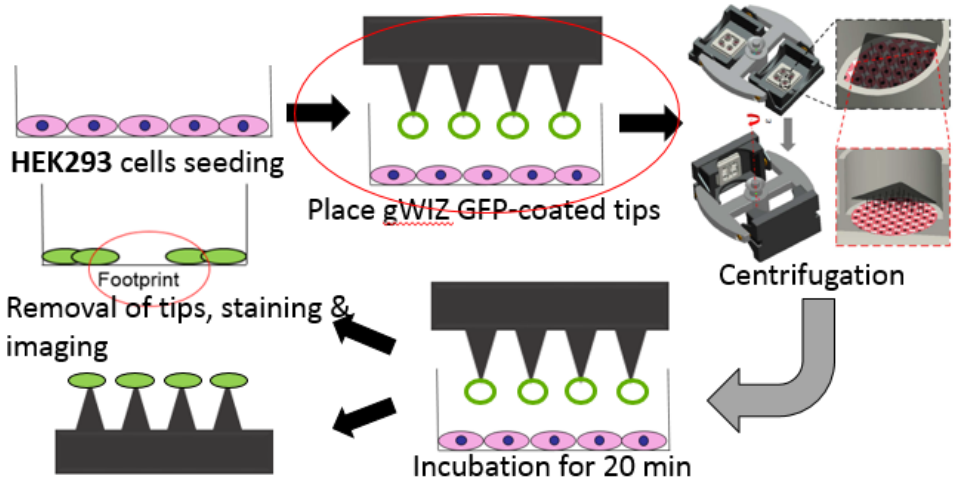

Figure 3.6: Delivery Method 1 – Si MC tips on top of the cells.

: Green Fluorescent Protein(GFP) – plasmid
: Non-transfected cells
: Transfected cells

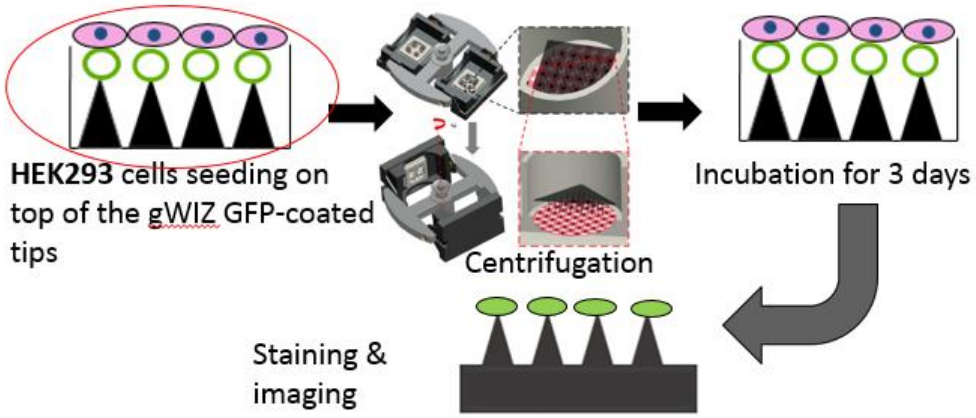

Figure 3.7: Delivery Method 2 – Si MC tips on the bottom.

: Green Fluorescent Protein(GFP) – plasmid
: Non-transfected cells
: Transfected cells

In the case of Delivery Method 1, after the incubation we are probing cell transfection in both cases. Firstly, at the footprint that the tips leave, after their removal, on the well plate and secondly on the tips themselves (Fig. 3.6).

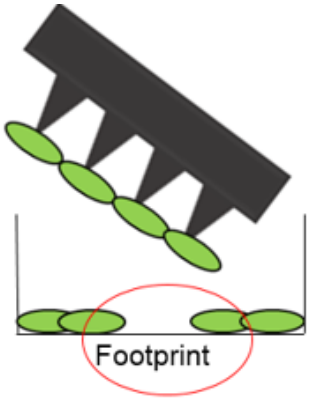

Figure 3.8: Schematic illustration of the footprint that the Si MC tips leave on the well plate after their removal using Delivery Method 1.

Delivery Method 1 - Experimental process

HEK293 cells were seeded in a 24-well plate at a density of 1 x 10^5 cells/ml in Opti-MEM medium, which was followed by incubation at 37 °C in a fully humidified atmosphere with 5% CO_2 till cells were fully adhered to the wells. To transfect gWIZ-GFP plasmid into the cells, the substrates were placed in a 24-well sterile format. Following this, gWIZ-GFP plasmid was diluted to 20 μg/ml in PBS and 100 μl of this solution was added per well on top of the substrates. The substrates were then incubated at 4 °C overnight and unbound plasmid was washed with PBS away. Subsequently, substrates were placed to float on culture medium with the tips facing towards cells and the whole setup was centrifuged at a speed of 7 g for 1 min. After centrifugation, an outline of the area of contact between the tips and the cells was drawn for each well. Following this, the well plate was incubated at 37 °C in a fully humidified atmosphere with 5% CO_2 for 20 min.

After the incubation, both substrates and wells were washed with PBS and then fixed in a solution of 4 % paraformaldehyde (PFA) in PBS (PH = 7.4) for 10 min, followed by permeabilization in PBS-0.25% Triton X-100 for 5 min at room temperature. After washing three times for 5 min each at room temperature in PBS, the nuclei were stained with Hoechst 33342 at a final concentration of 5 μg/ml for 15 min at room temperature. Results were evaluated with inverted Eclipse Ti-S fluorescence microscope (Nikon, Japan).

Delivery Method 2 – Experimental process

To transfect gWIZ-GFP plasmid into the cells, the substrates were placed in a 24-well sterile format. Following this, gWIZ-GFP plasmid was diluted to 20 μg/ml in PBS and 100 μl of this solution was added per well on top of the substrates. The substrates were then incubated at 4 °C overnight and unbound plasmid was washed with PBS away. HEK293 cells were seeded onto the substrates at a density of 1 x 10^5 cells/ml in Opti-MEM medium, which was followed by centrifugation at 7 g for 1 min. The well plate was then incubated at 37 °C in a fully humidified atmosphere with 5% CO_2 for 72 h. Opti-MEM was replaced by DMEM complete medium after 6 h of incubation.

Following the incubation, substrates were washed with PBS and then fixed in a solution of 4 % paraformaldehyde (PFA) in PBS (PH = 7.4) for 10 min, followed by permeabilization in PBS-0.25% Triton X-100 for 5 min at room temperature. After washing three times for 5 min each at room temperature in PBS, the nuclei were stained with Hoechst 33342 at a final concentration of 5 μg/ml for 15 min at room temperature. Results were evaluated with inverted Eclipse Ti-S fluorescence microscope (Nikon, Japan).

3.2.4.5 Characterization

3.2.4.5.1 FIB-SEM imaging

3.2.4.5.1.1 Technique

FIB-SEM is an alternative approach for 3D SEM imaging. The instruments used for this method have two beams: a scanning electron beam for imaging the sample and an ion beam that abrades material from the exposed surface of the specimen. While gallium is the material used most commonly in these instruments, other sources such as iridium or elemental gold are used occasionally. The use of two beams and the mechanism by which the FIB-SEM operates, require the sample's stage to be tilted so that both beams act on the sample at the same location.

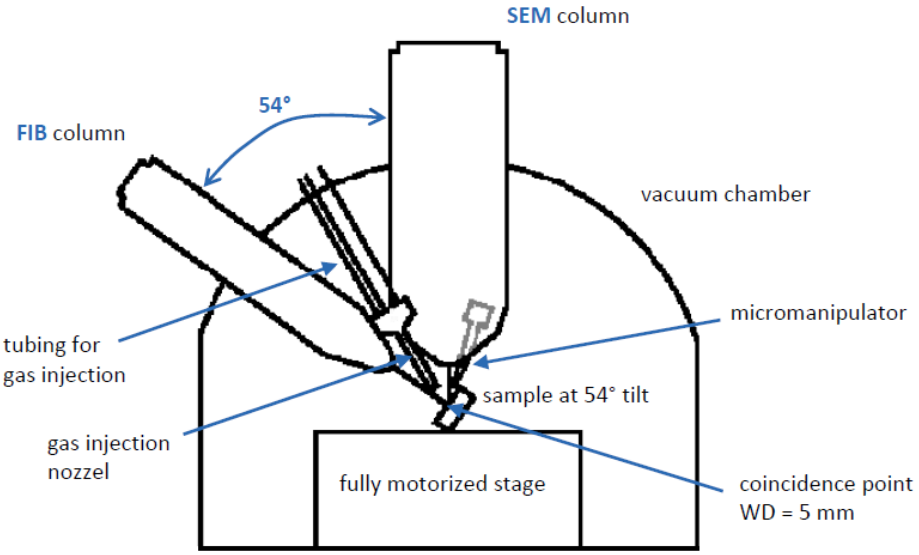

Figure 3.9: Schematic illustration of a FIB-SEM setup (55).

Once the object of interest is located, the stage is tilted (~ 54^0 in presently available instruments) and the beams are aligned to be incident at the same region of the specimen. The FIB is oriented directly above the block face and a pad of platinum is deposited on top of the imaging area (56).
The principle of deposition is Chemical Vapour Deposition (CVD). The precursor gases are sprayed on the surface by a fine needle (nozzle), where they adsorb. In a second step, the incending ion beam decomposes the adsorbed precursor gases. Then the volatile reaction products desorb from the surface and are removed through the vacuum system, while the desired reaction products remain fixed on the surface as a thin film (Fig. 3.10 (a)). The deposited material is not fully pure however, because organic contaminants as well as Ga^+ ions (from the ion beam) are inevitably included. The platinum pad provides a platform for a pattern of marks that can be used to keep track of the thickness of the ablation along the z axis, a process known as z-tracking. Moreover, it protects the top of the imaging area from being damaged (57).

After the protective pad is deposited, a 'trench' is milled using the FIB, which exposes the imaging area (56). The removal of sample material is achieved using high ion current beam. The result is typical sputtering of sample material, as illustrated schematically in Fig. 3.10 (b) (57). The sample face to be imaged by the electron beam in FIB-SEM is orthogonal on the top face of the block. This must be taken into account when orienting and trimming the sample prior to data collection, as the successive slices removed are from the interior, not the surface of the block.

FIB-SEM technology has been used to collect high resolution 3D data, on cells and tissues, primarily for smaller volumes at higher resolution (56).

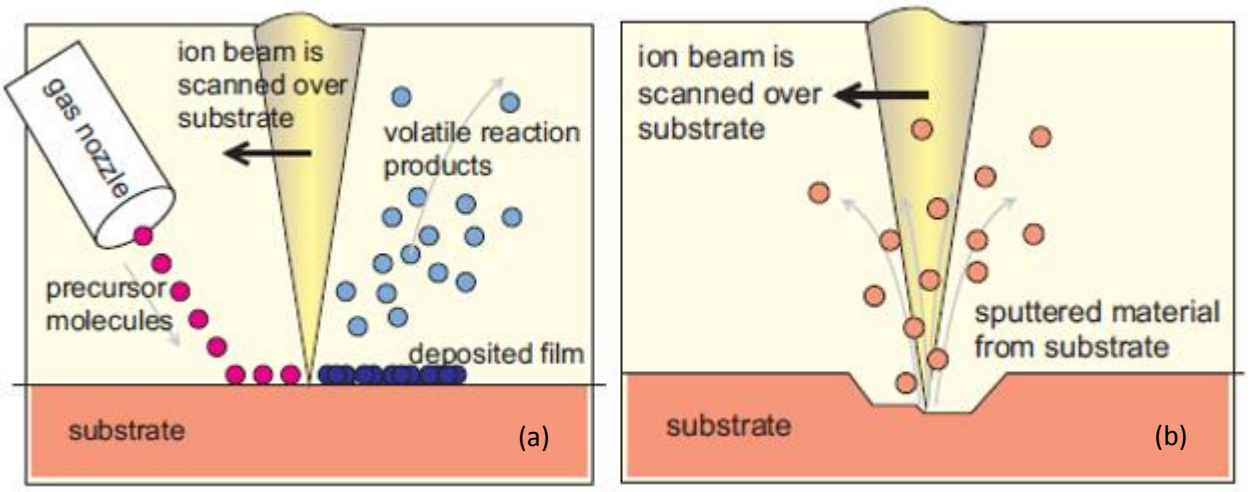

Figure 3.10: Schematic illustration of the principle of (a) deposition and (b) milling in a FIB-SEM (57).

3.2.4.5.1.2 Experimental process

The Helios Nanolab 600 dual beam FIB-SEM (FEI, North America NanoPort) was used to investigate the interaction between the silicon micro-conical tips and the cells.

The samples were prepared as follows. At first, samples were fixed with 4 % paraformaldehyde in PBS + 4 % sucrose (pH 7.2) solution for 30 min at room temperature, followed by washing twice in buffer (PBS + 4 % sucrose, pH 7.4) for 5 min each time. Following this, cells underwent post-fixation with 2 % osmium tetroxide (OsO_4) in water for 30 min at room temperature. After repeating the previous washing step with buffer, the cell specimens were gradually dehydrated by immersion tree times (for 10 min each time) in increasing concentrations of ethanol solutions (70%, 90% and 100%), which was followed by chemical drying with hexamethyldisilaxane (HMDS). For this purpose, cell specimen were dehydrated by immersion twice in 1:1 EtOH:HMDS and twice in 100% HMDS and allowed to dry in air. Finally, all substrates were mounted on SEM stubs. This was followed by 10 nm carbon coating with the help of a sputter coater to increase the conductivity of the specimen.

In FIB-SEM, 1-2 µm thick platinum was deposited at 30 kV with 0.46 nA current in the region of interest to protect it from ion-beam induced damage. Rough milling followed by polishing was carried out with decreasing current from 2.8 nA to 93 pA in several steps at 30 kV. Final polishing was carried out at 30 kV with 28 pA current.

3.2.4.5.2 SEM imaging

The morphology of the cells growing on the silicon micro-conical tips was analyzed by SEM.

3.2.4.5.2.1 Experimental process

All cell specimen underwent the same fixation and dehydration process as presented in paragraph 3.2.4.5.1.2. Substrates were then mounted on SEM stubs and sputter coated by 10 nm carbon in order to increase the conductivity of the specimen. SEM was performed on a Carl Zeiss Microscopy Merlin with the GEMINI II column equipped with a field-emission gun operated at 2 kV. The secondary electron images were recorded with a parallel on-axis in-lens secondary electron detector.

4. Results

4.1 Fabrication and characterization of Si MC tips

As mentioned before, the fabrication of the silicon micro-conical tips starts with the convective assembly deposition of PSNS (4.5 μm in diameter) monolayers over a piece of silicon wafer. Achieving uniform PSNS monolayers throughout the wafer is not so easy. Most of the times, we observe a combination of **monolayers**, **multilayers** and **holes** in the same piece (Fig. 4.1). This is depended on and can be adjusted by both stage velocity and PS suspension concentration.

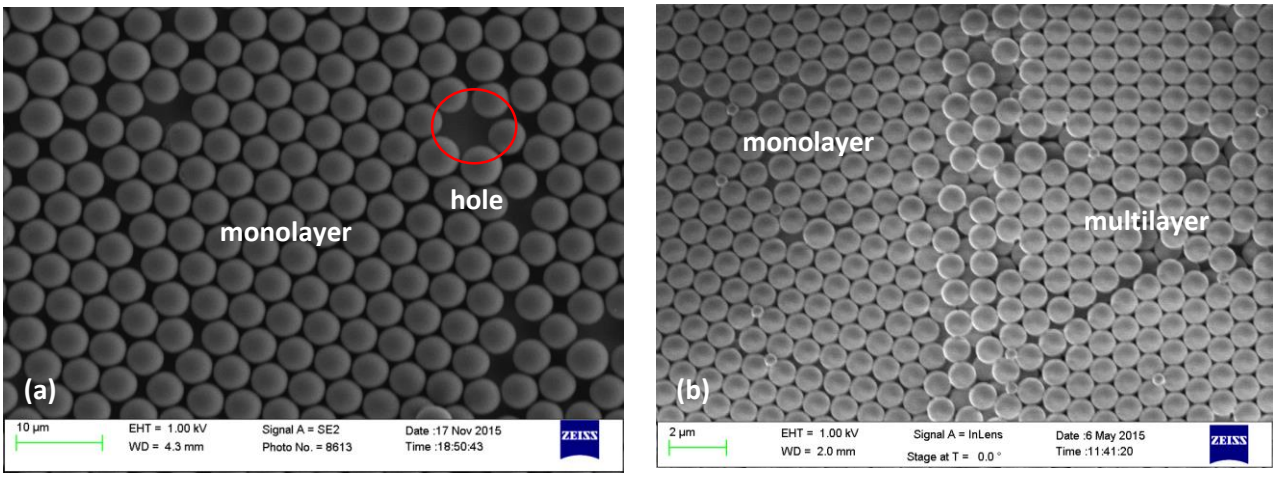

Figure 4.1 (a-b): Example of top view SEM images taken after convective assembly deposition of PSNS (4.5 μm in diameter).

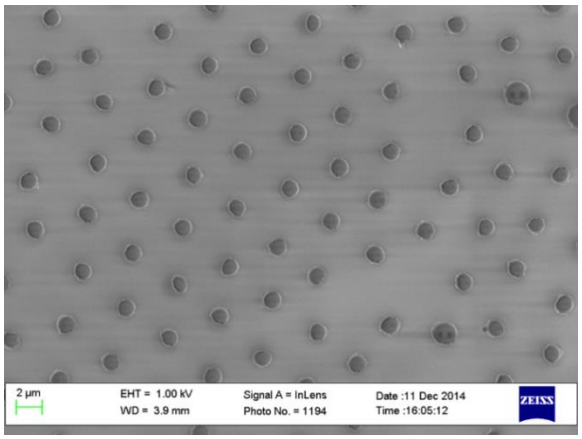

Figure 4.2: Example of a top view SEM image taken after 180 s of Oxygen Plasma processing of 4.5 μm PSNS. The diameter of the beads is reduced to around 1.2 μm.

The greater the oxygen plasma time, the smaller the size of the mask, fact that limits the number of loops during the silicon etching, which consequently leads to shorter tips. Here, we have to notice that there are a few variations in the initial size (diameter) of the PSNS (Fig. 4.1 (a)), which appear as defects in the later processing.

We achieved the fabrication of Si MC tip arrays with different characteristics such as height and tip diameter and a fixed density of 7 x 10^6 Si MC tip cm^{-2} by tuning the oxygen plasma time in correlation with the number of Si etching loops (Table 4.1). The detailed oxygen plasma and silicon etching recipes are presented on **Appendix A**. The Si MC tip arrays were classified in three different categories, regarding their height. The average characteristics of its category are presented in Table 4.2.

Table 4.1: A correlation between the oxygen plasma time, the number of loops during the silicon etching and the resulting Si MC tips' average height.

Oxygen Plasma Time (s)	# Loops during Si etching	Si MC Tips' Average Height (μm)
180	30	3
120	60	6
50	95	8

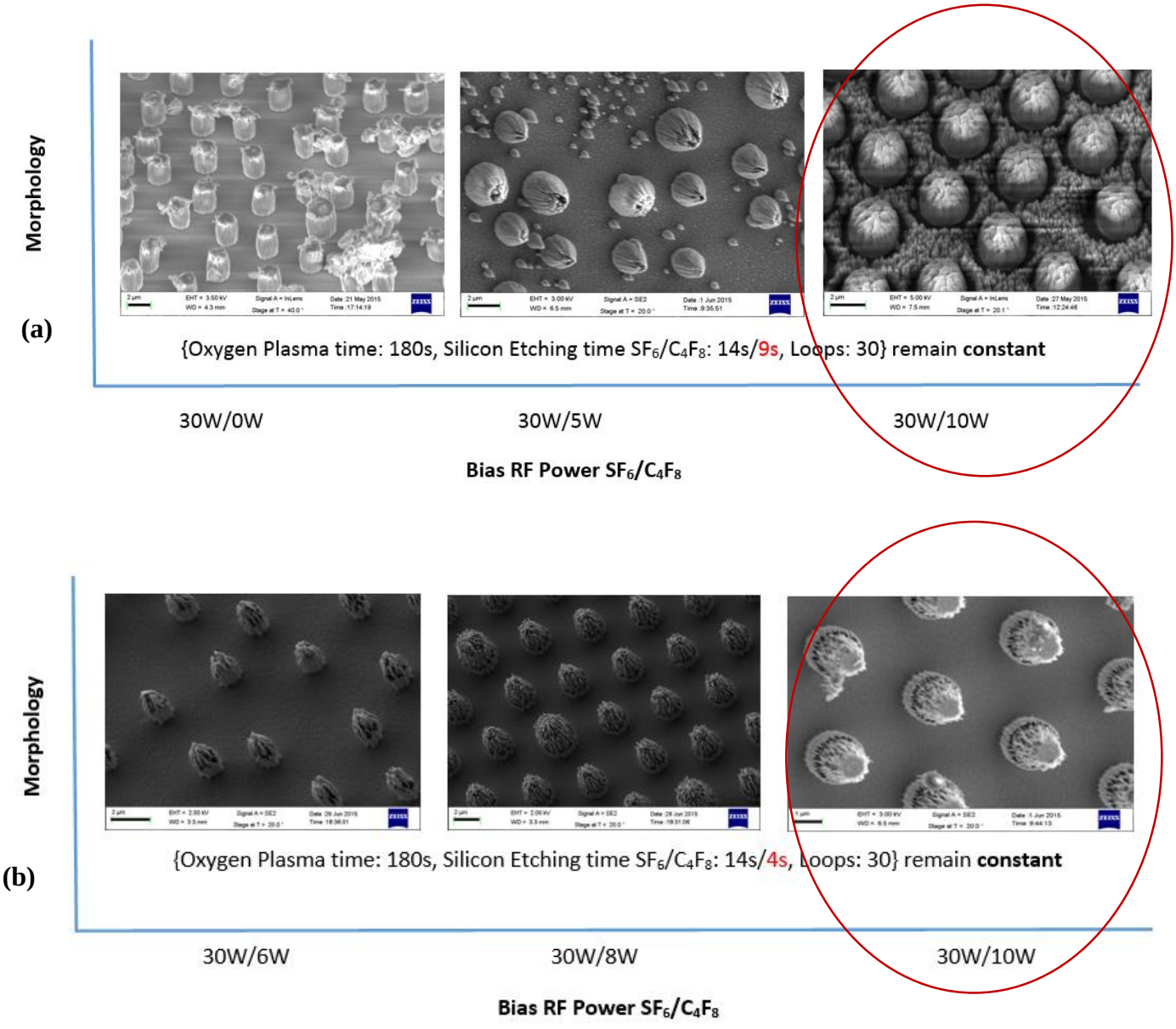

Figure 4.3 (a-b): Morphology diagrams, which present how the morphology of the Si MC tips changes by altering the bias RF power ratio, keeping the rest of the parameters constant.

The morphology diagrams presented in Fig. 4.3 are an example of the long optimization process that we followed in order to achieve the desired morphology of our Si NWs. By applying bias RF power to the passivation step together with the etching step, we started having a tapered profile, compared to the completely vertical one when zero power is applied to the passivation step. However, the roughness of the substrate indicates that we probably have to reduce the passivation step time. The reduction of the passivation step time from 9 to 4 s resulted in a more tapered profile of the NWs and a smooth substrate.

As we can see, the as-prepared Si MC tips are characterized by rough sidewalls and not so sharp tips. Sometimes, like in Fig. 4.4 (a), we can even notice the remaining part of the mask (bead). For this reason, all samples were subjected to a post treatment or "reshaping", which includes thermal oxidation and short wet etching in an HF-based solution. The result is these nice uniform arrays of Si MC tips as presented in Fig. 4.5 and 4.6.

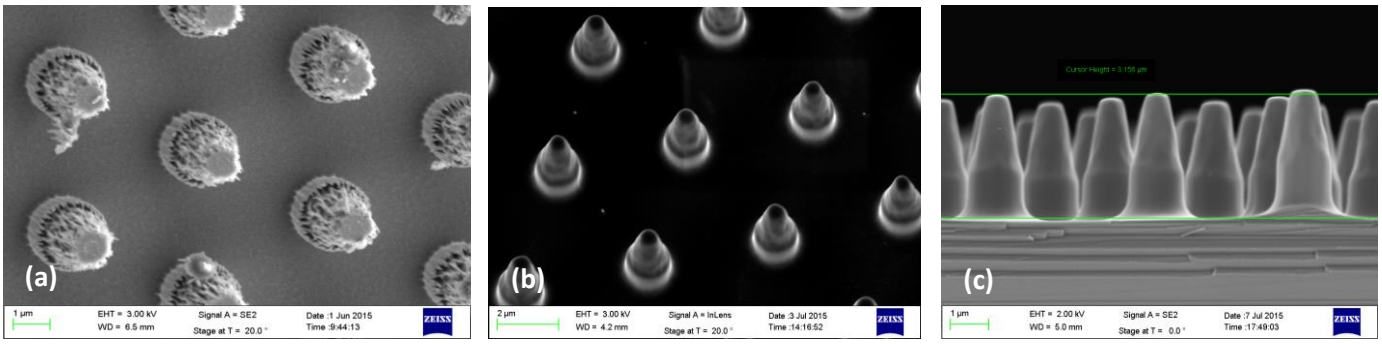

Figure 4.4 (a-c): Example of the "reshaping" of the Si MC tips via the post treatment of them after their removal from the DRIE. Tilted (20°) SEM image of (a) the as-prepared Si MC tips and (b) the same Si MC tips after post treatment. (c) Cross-sectional view of (b).

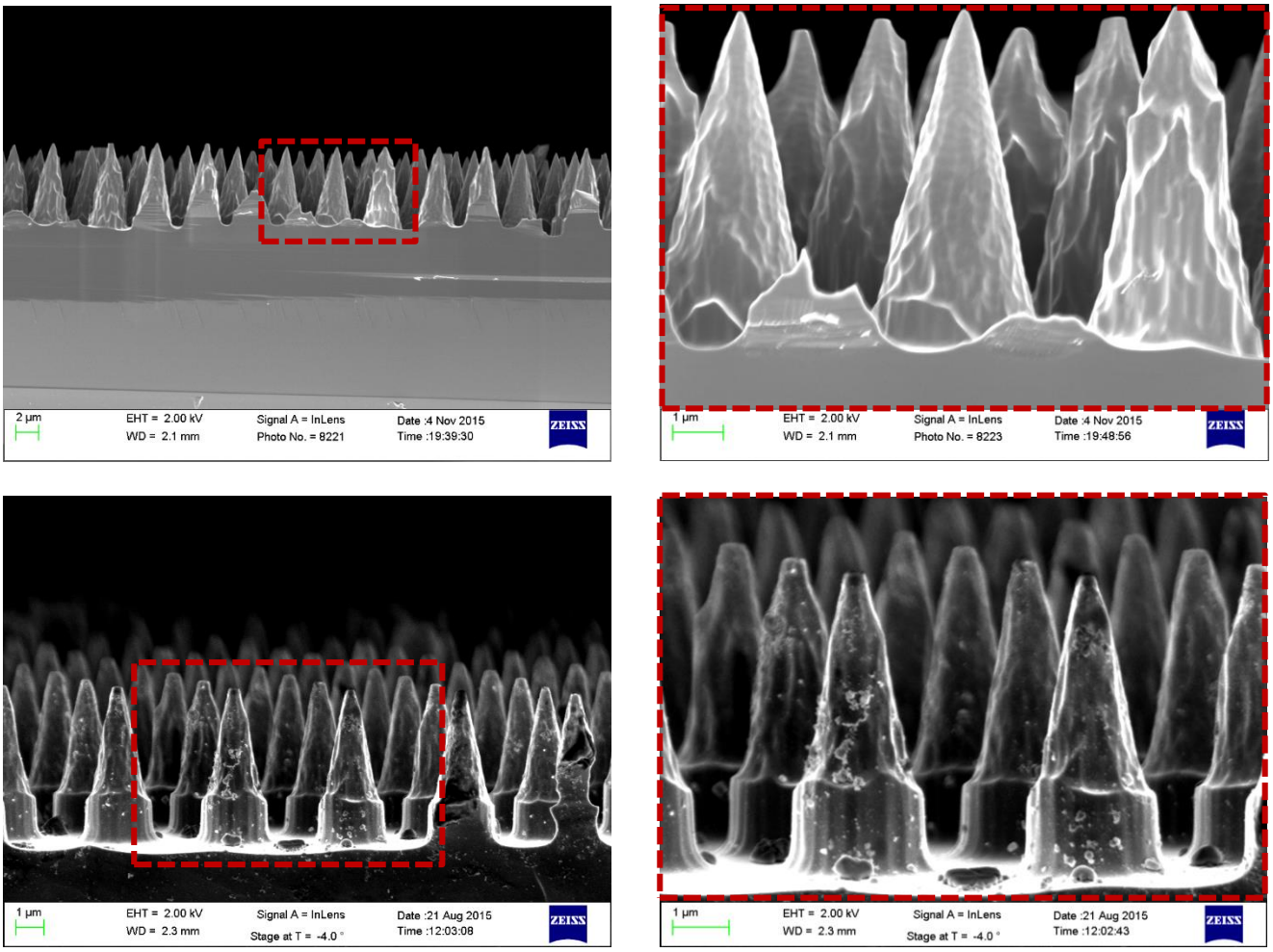

Figure 4.5: SEM images of Si MC tip arrays, with different characteristics, in a cross-sectional view.

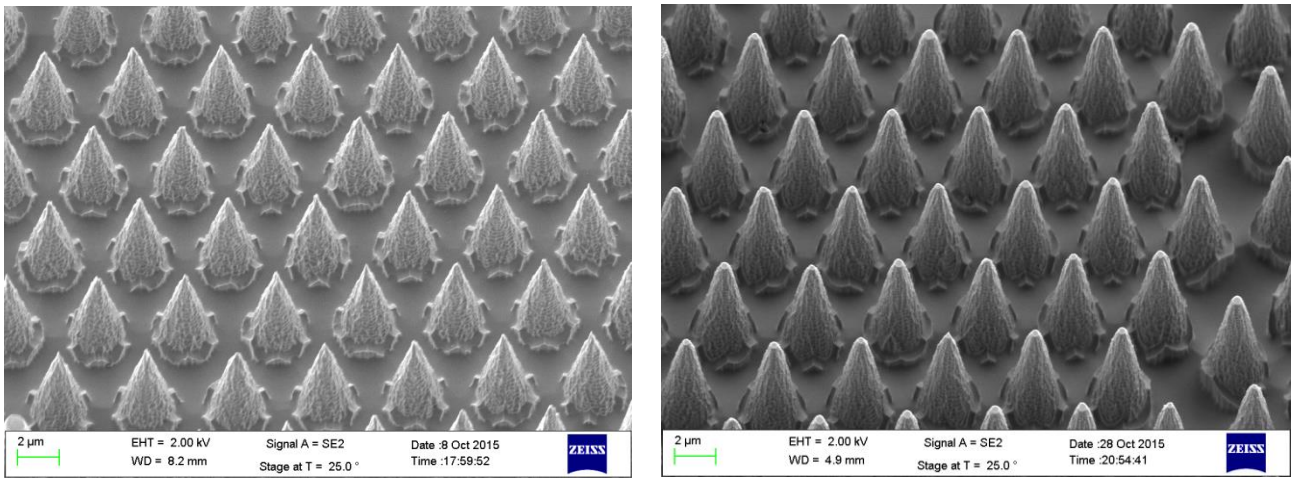

Figure 4.6: SEM images of Si MC tip arrays, with different characteristics, in a tilted (25°) view.

Table 4.2: Average geometrical characteristics of the different Si MC tips used in this study.

Si MC tips	Average Height ±STDEV (µm)	Average Tip Diam. ±STDEV (nm)	Average Aspect Ratio ±STDEV	Periodicity ±STDEV (µm)	Density ±STDEV Si MC tips /cm^2
low	2.96 ± 0.16	272 ± 48	4.11 ± 0.50	4.31 ± 0.10	7 ± 1 x 10^6
medium	5.62 ± 0.87	201 ± 113	4.52 ± 0.14	4.21 ± 0.45	7 ± 1 x 10^6
high	8.13 ± 0.75	200 ± 109	4.49± 0.11	4.22 ± 0.26	7 ± 1 x 10^6

4.2 In vitro experiments with HEK 293 cells

4.2.1 Interaction between HEK 293 cells and Si MC tips

At first, we wanted to see whether the Si MC tip arrays could support the growth of HEK 293 cells on top of them. The substrates (Si MC tip arrays) were placed on top of the cells, facing towards them (Delivery Method 1). The whole setup was then centrifuged and incubated for 6 h. The morphological analysis with SEM showed that HEK 293 cells were normally grown on all different types of Si MC tips (Fig. 4.7).

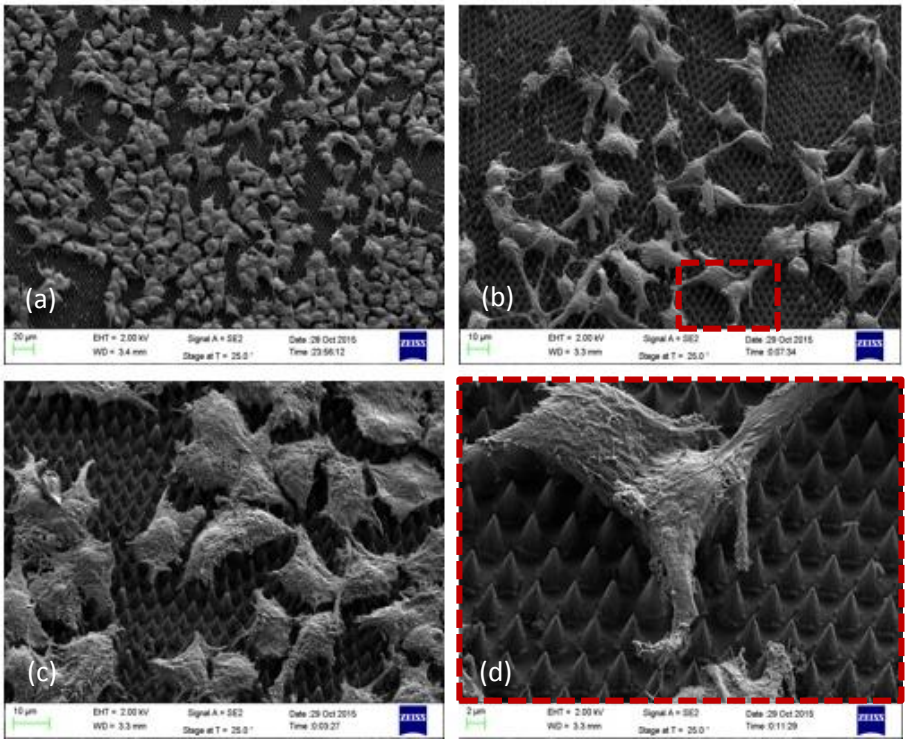

Figure 4.7: SEM images of HEK293 cells adhering to an array of Si MC tips of 7 x 10^6 MC tips cm^{-2} in density (with average tips' diameter of 130 nm and average heights of 7.8 μm) after centrifugation and 6 h of incubation with the tips facing towards them. Different tilted (25^0) views at magnification of (a) x 500, (b) x 1000 and (c) x 1800 respectively. (d) Zoomed-in image of (b) at magnification of x 4400.

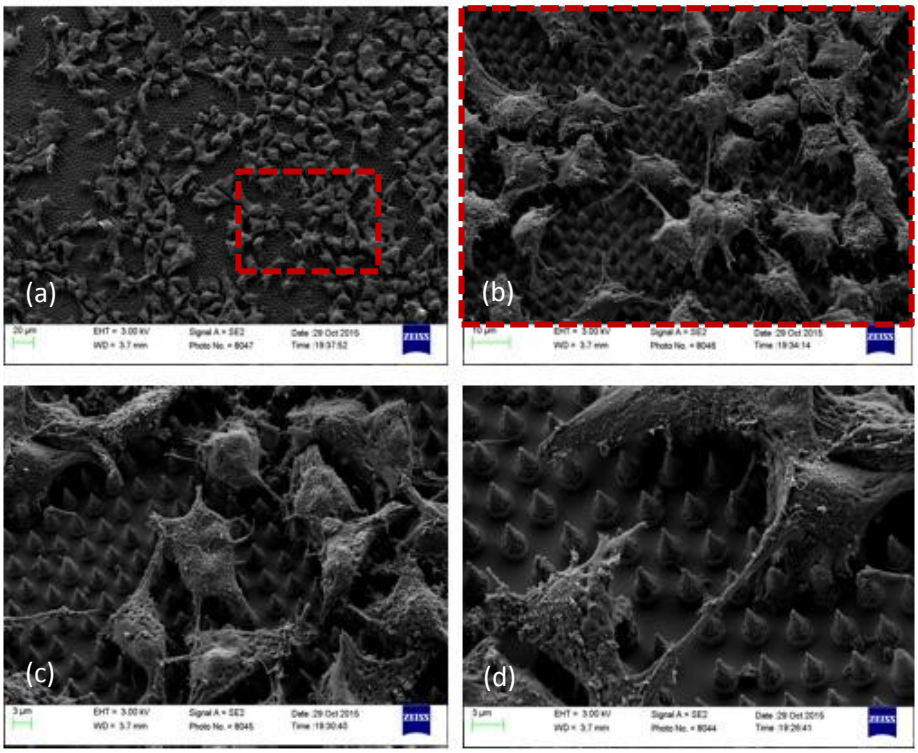

Figure 4.8: SEM images of HEK293 cells adhering to an array of silicon micro-conical tips of 7 x 10^6 MC tips cm^{-2} in density (with average tips' diameter of 190 nm and average heights of 6.3 µm) after centrifugation and 6 h of incubation with the tips facing towards them. Different tilt (25^0) views at magnification of (a) x 500, (c) x 3000 and (d) x 5000 respectively. (b) Zoomed-in image of (a) at magnification of x 1800.

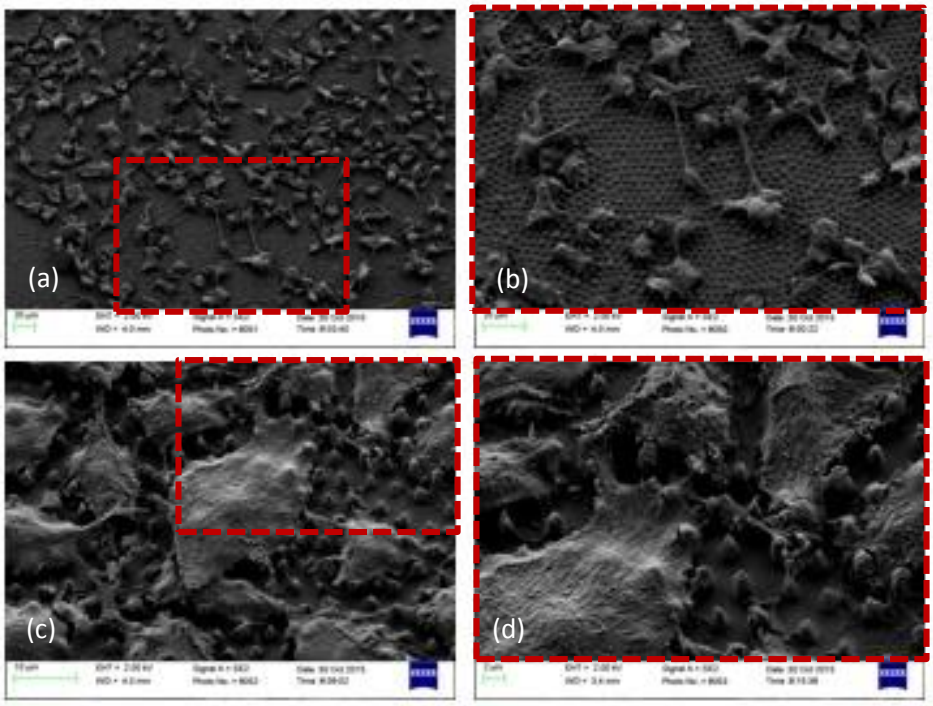

Figure 4.9: SEM images of HEK293 cells adhering to an array of silicon micro-conical tips of 7 x 10^6 MC tips cm^{-2} in density (with average tips' diameter of 630 nm and average heights of 3.2 µm) after centrifugation and 6 h of incubation with the tips facing towards them. Different tilt (25^0) views at magnification of (a) x 500 and (c) x 3000

respectively. (b) Zoomed-in image of (a) at magnification of x 1000 and (d) zoomed-in image of (c) at magnification of x 5000.

4.2.2 Cell viability as a function of incubation time

One of our first concerns was to ensure that the cells remain alive during their contact with the Si MC tips. For this reason, we ran several viability tests for different incubation times.
In the images below, the red color is an indicator of the dead cells, whereas the green indicates the cells that are still alive.

Long term viability results using **Delivery Method 1**:

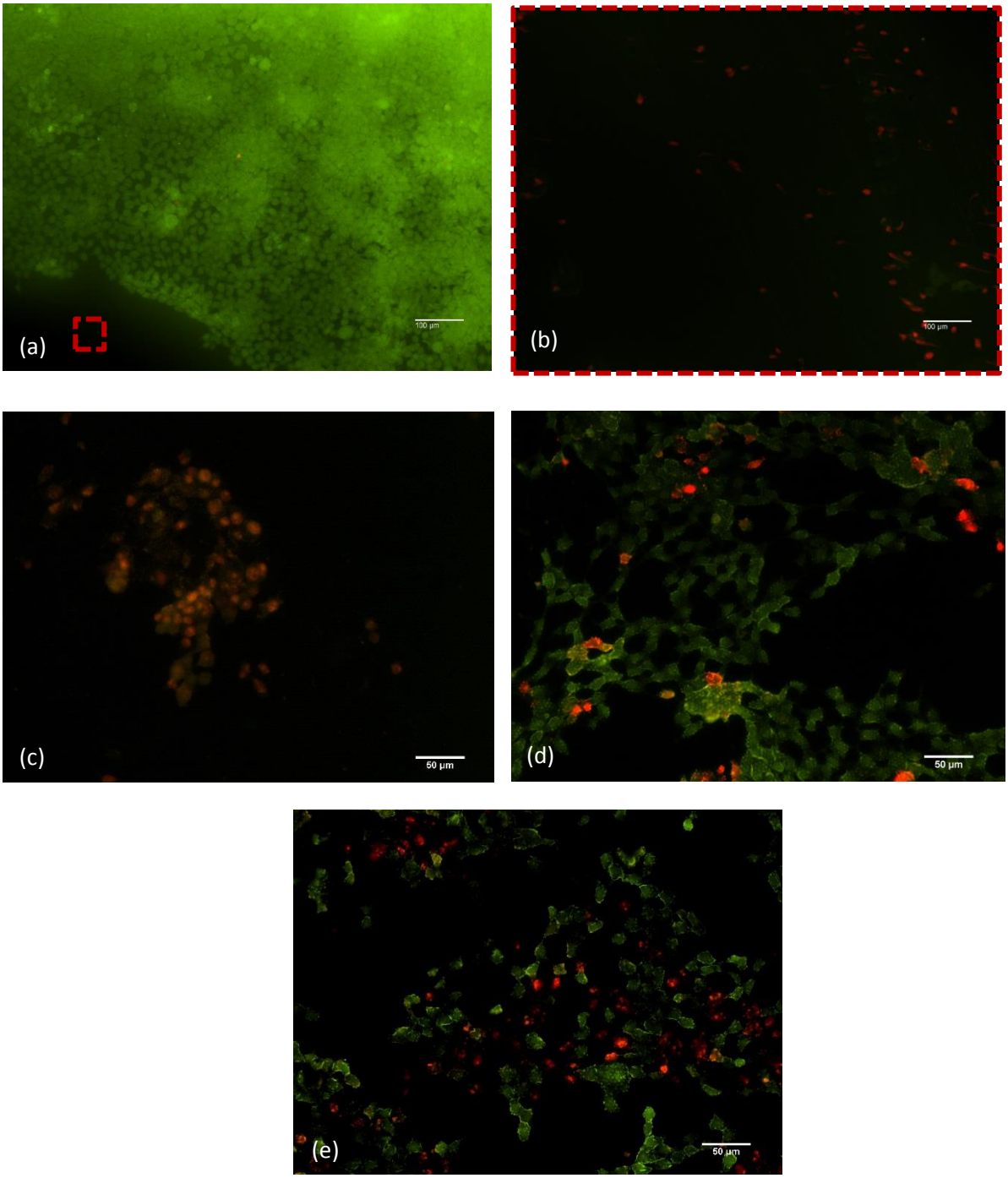

Figure 4.10: Fluorescent images taken after centrifugation and 5 h of incubation with the tips facing towards the cells, (a-b) from the well plate and (c-e) from the Si MC tips themselves. (a) Plethora of alive cells gathered at the sidewalls of the well plate and (b) remaining cells, that are mostly dead, at the footprint that the Si MC tips (with average tips' diameter of 115 nm and average heights of 9.4 μm) left on the well plate. (c) Image taken from the Si MC tips with the same characteristics as featured in (b). Image taken from Si MC tips with (d) average tips' diameter of 130 nm and average heights of 7.8 μm and (e) average tips' diameter of 1.6 μm (flat tips) and average heights of 5.4 μm.

After examining Fig. 4.10 (b) carefully, we can conclude that after 5 hours of incubation most of the cells were already dead at the footprint that the Si MC tips left on the well plate. In addition, the fluorescent images taken from the Si MC tips themselves, showed that cells started to become dead as well. A possible reason for that is the lack of oxygen and nutrition to the cells during their prolonged contact with the tips. On the contrary, the rest of the cells left on the well plate remained alive (Fig. 4.10 (a)). Considering these results, we decided that we have to reduce the incubation time in the next experiments.

Short term viability results using **Delivery Method 1**:

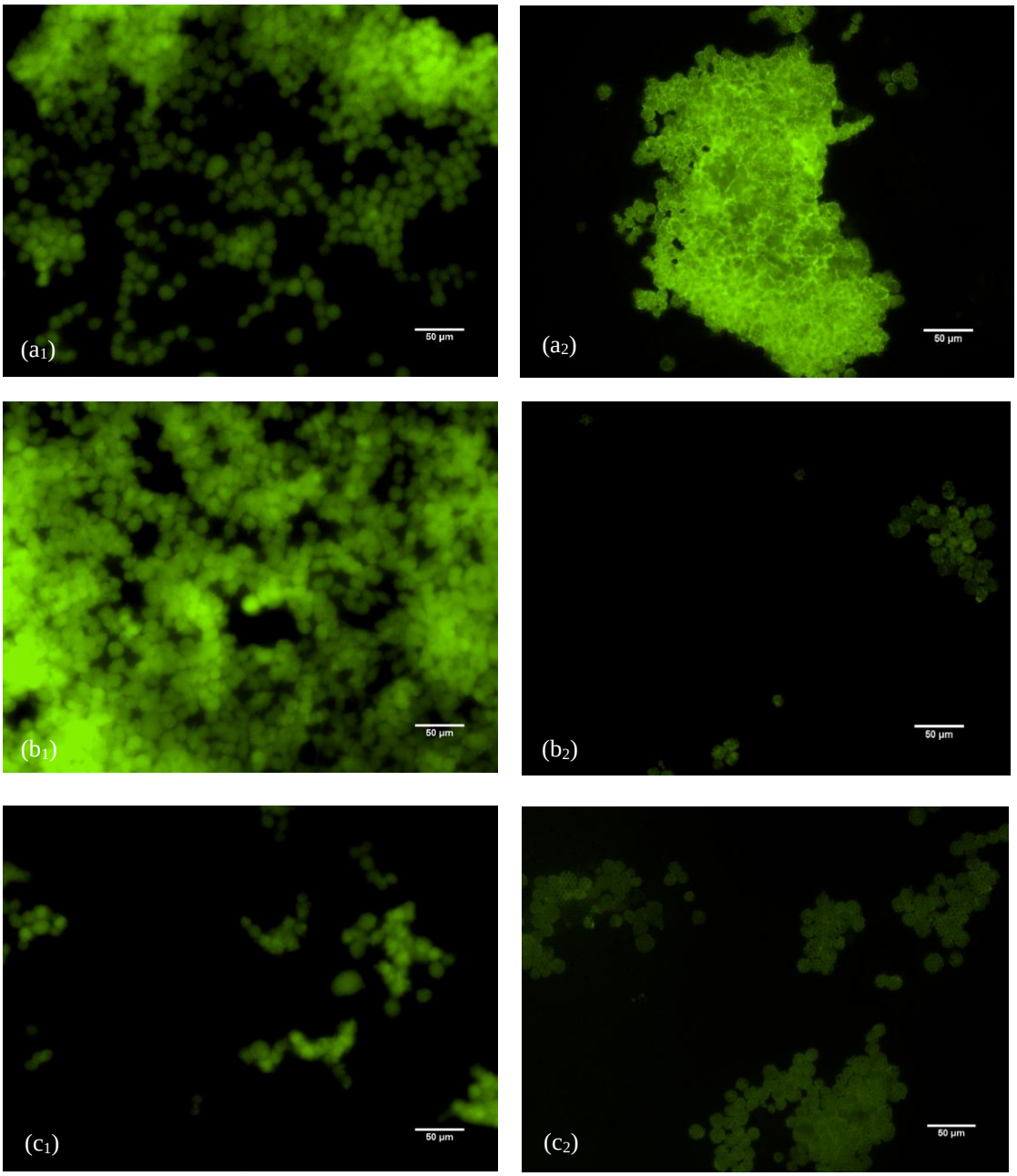

Figure 4.11: Fluorescent images taken after centrifugation and 3 m of incubation with the tips facing towards the cells, (a_1-c_1) from the well plate and (a_2-c_2) from the Si MC tips respectively. (a_2) average tips' diameter of 310 nm and average heights of 3.1 μm, (b_2) average tips' diameter of 320 nm and average heights of 6 μm and (c_2) average tips' diameter of 120 nm and average heights of 7.8 μm.

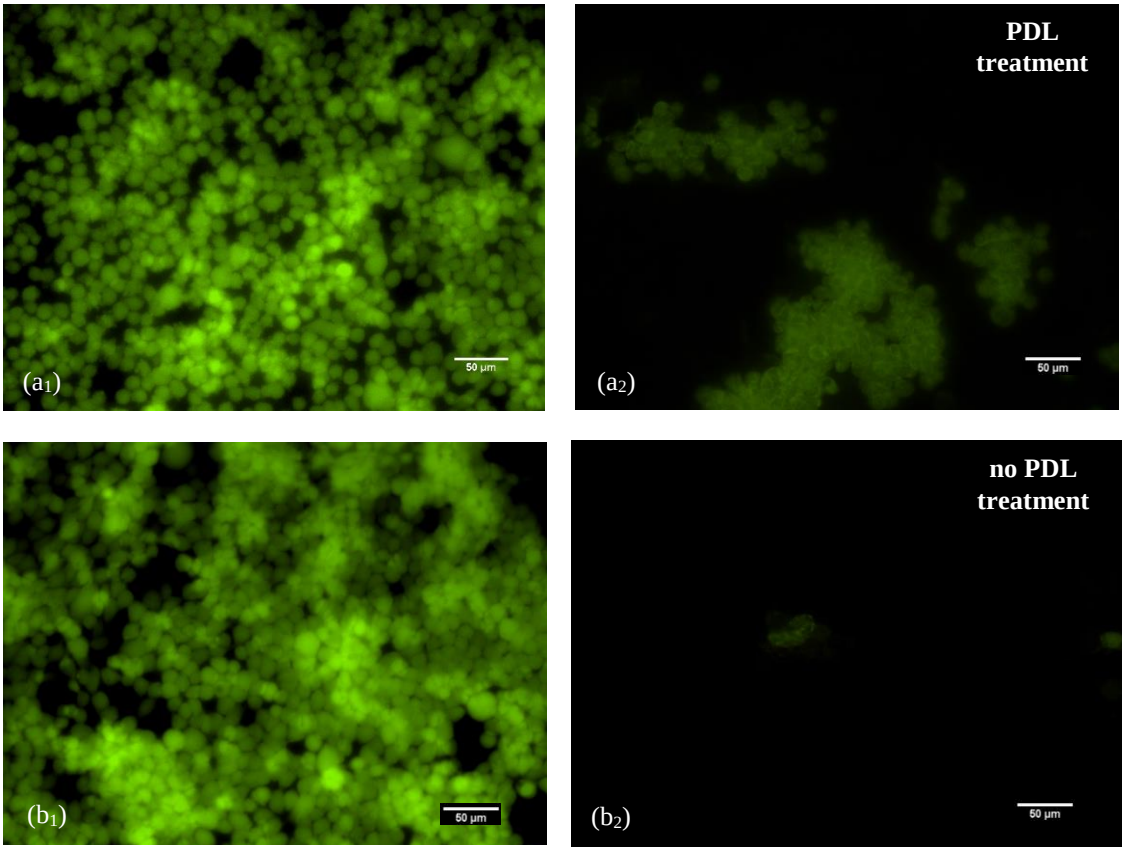

Figure 4.12: Fluorescent images taken after centrifugation and 3 m of incubation with the flat Si wafers (controls) facing towards the cells, (a_1-b_1) from the well plate and (a_2-b_2) from the flat Si wafers respectively.

As we can see from Fig. 4.11 all cells remained alive during their short-time contact with the Si MC tips, regardless their geometrical characteristics. Moreover, Fig. 4.12 (a_2) confirms that the coating of the substrates with PDL prior to cell culture (Section 3.2.3) enhances the cell adhesion.

Following this, we ran an additional experiment for 30 m of incubation this time.

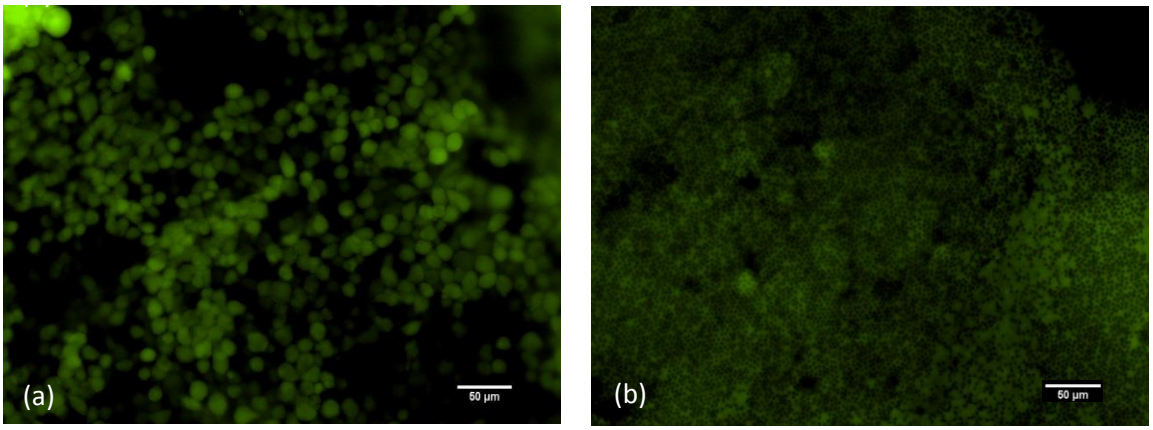

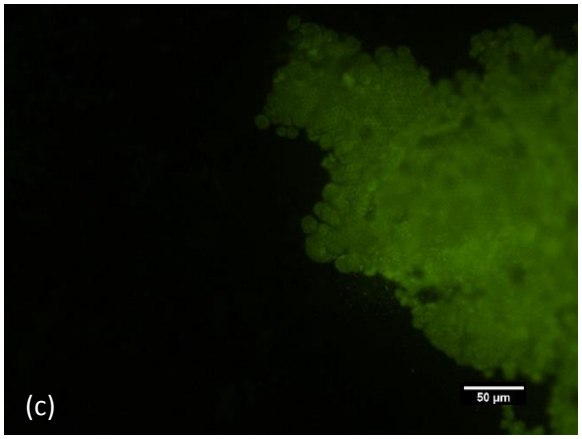

Figure 4.13: Fluorescent images taken after centrifugation and 30 m of incubation with the tips facing towards the cells, from the Si MC tips with (a) average tips' diameter of 310 nm and average heights of 3.1 µm, (b) average tips' diameter of 320 nm and average heights of 6 µm and (c) average tips' diameter of 320 nm and average heights of 9.2 µm.

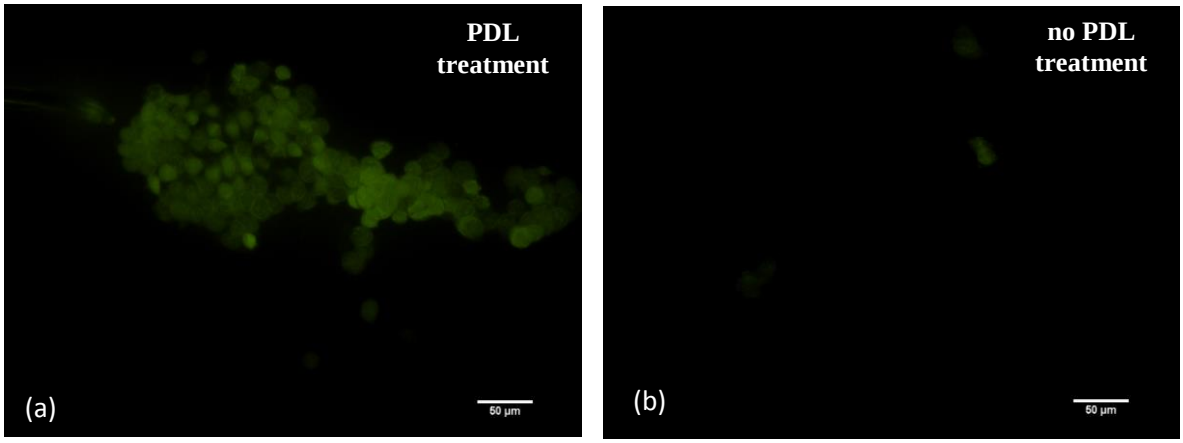

Figure 4.14: Fluorescent images taken after centrifugation and 30 m of incubation with the flat Si wafers (controls) facing towards the cells, from (a) a PDL treated flat Si wafer and (b) a non-PDL treated one.

We can clearly see that cells remained alive even after 30 m of contact with the Si MC tips. Individual Si MC tips appear as black dots under the HEK293 cells (Fig. 4.13 (b)). The reason why we did not take images from the footprint after 30 min of incubation is that the cells started already to become loose and detach from the well plate. It is important here to notice that according to our approach (Section 2.2), we are probing transfection not only at the Si MC tips but also at the footprint that the Si MC tips are leaving, after their removal, on the well plate. For this reason, we need to have a significant amount of cells left on the well plate.

In view of these results, we decided that our upcoming cell transfection experiments will be limited to 30 m of maximum incubation time.

4.2.3 Focused Ion Beam – SEM Imaging

Before proceeding to cell transfection studies, we used FIB-SEM in order to observe possible penetration of the Si MC tips through the cell membrane into the cytoplasm. The substrates (Si MC tip arrays) were placed once again on top of the cells, facing towards them (Delivery Method 1) and the whole setup was then centrifuged and incubated for two different times; 15 m and 30 m respectively.

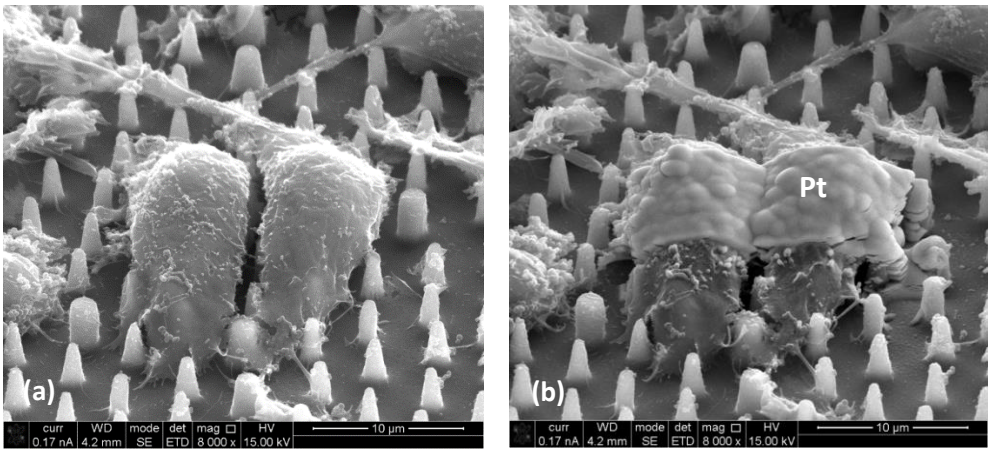

Figure 4.15: Tilted (52°) SEM image of (a) the interaction between two single HEK293 cells and Si MC tips (with average tips' diameter of 310 nm and average heights of 3.1 μm) after centrifugation and 15 m of incubation with the tips facing towards the cells and (b) platinum deposition on top of the two HEK 293 cells in order to protect them from the upcoming milling through the focused ion beam.

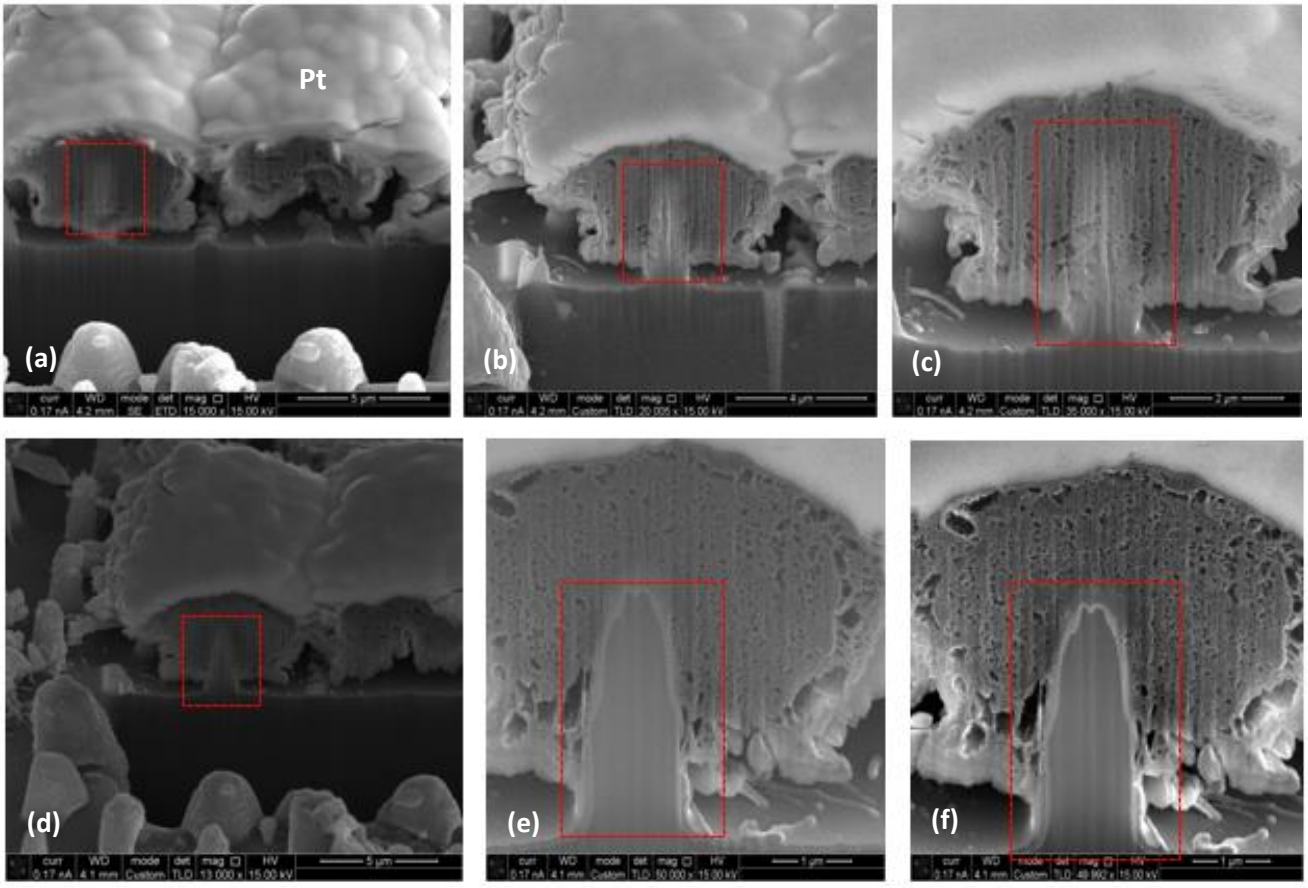

Figure 4.16 (a-f): FIB-SEM images of the sequential milling of the two HEK 293 cells of Fig. 4.15, revealing the full penetration of the Si MC tips into the cell's cytoplasm.

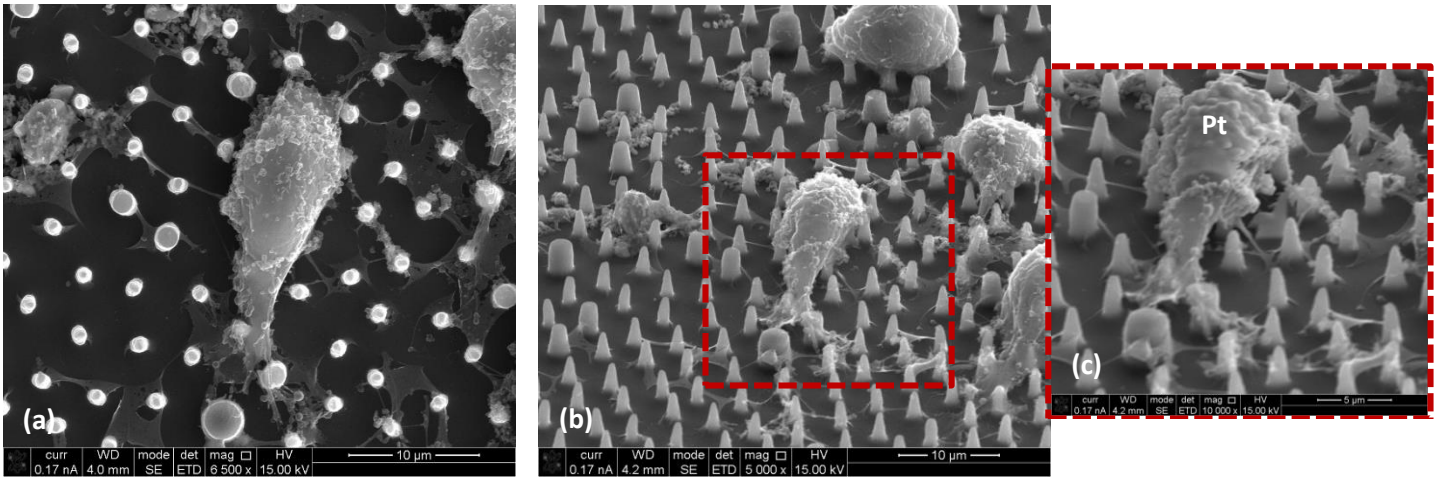

Figure 4.17: SEM image of the interaction between a single HEK 293 cell and Si MC tips (with average tips' diameter of 310 nm and average heights of 3.1 µm) after centrifugation and 30 min of incubation with the tips facing towards the cells in a (a) top and (b) tilted (52°) view. (c) Zoomed-in image of (b) after the platinum deposition.

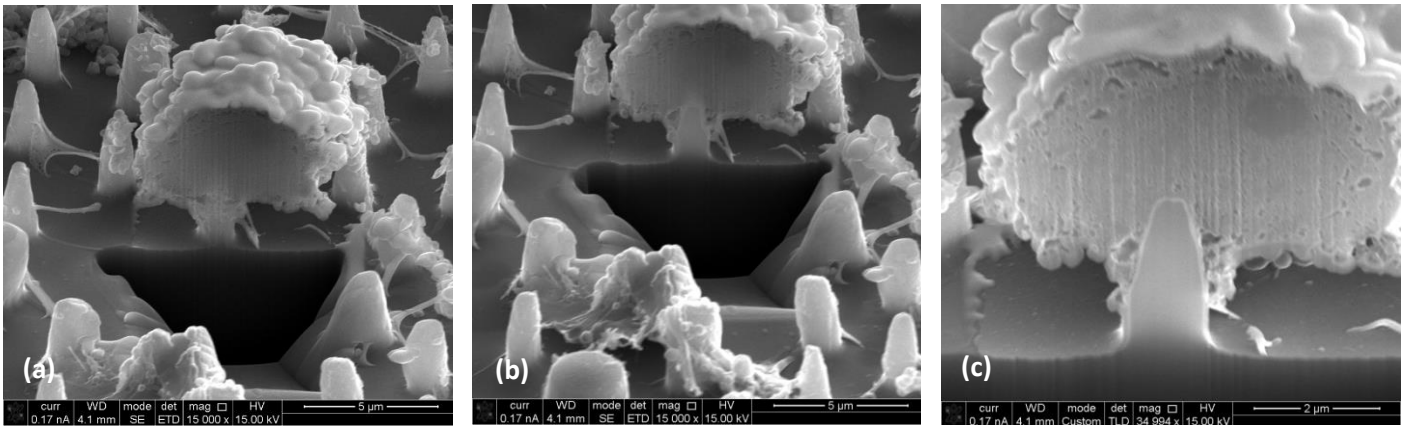

Figure 4.18 (a-c): FIB-SEM images of the sequential milling of the single HEK 293 cell of Fig. 4.17, revealing the penetration of the Si MC tips into the cell's cytoplasm.

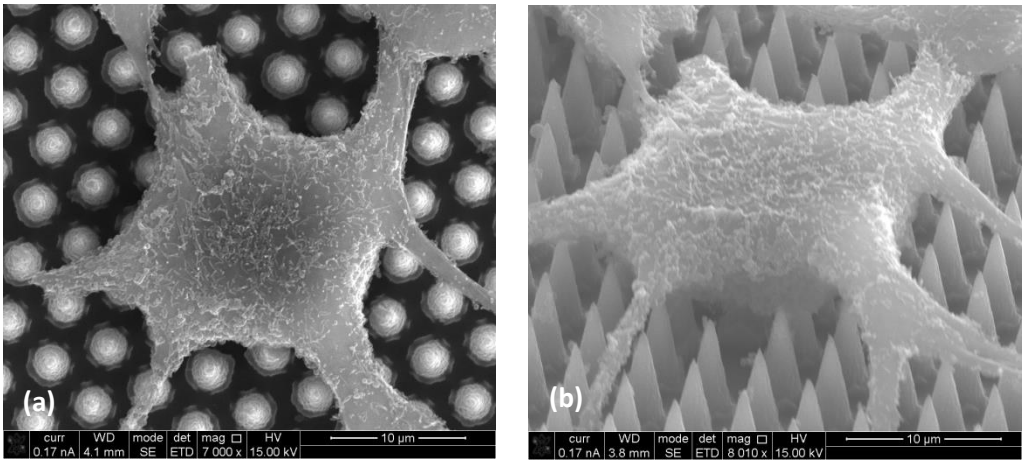

Figure 4.19: SEM image of the interaction between a single HEK 293 cell and Si MC tips (with average tips' diameter of 130 nm and average heights of 7.8 µm) after centrifugation and 30 min of incubation with the tips facing towards the cells in a (a) top and (b) tilted (52°) view.

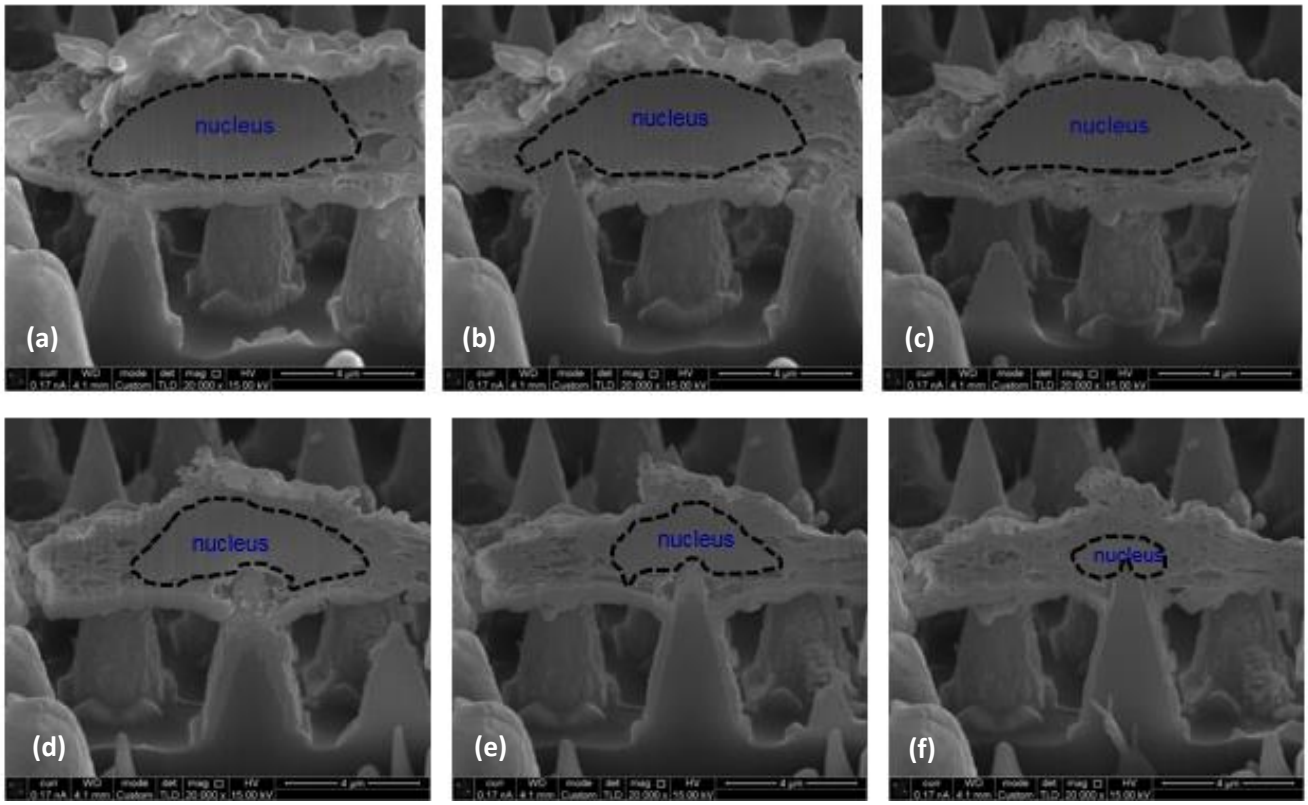

Figure 4.20 (a-f): FIB-SEM images of the sequential milling of the single HEK 293 cell of Fig. 4.19. Images (d-f) exhibit that the nucleus of the cell is being indented by the tip.

All the above FIB-SEM images are an indicator of the successful cytoplasm penetration of the Si MC tips within 30 m of maximum incubation time, which could probably give us transfection as well.

4.2.4 Cell transfection studies

After all the pre-work presented in the previous sections, we were ready to proceed to transfection studies and test the efficiency of our plasmid DNA delivery system.

It is important to notice, that all substrates and flat Si wafers (controls) used in this study were pretreated with PDL, in order to allow plasmid adsorption via electrostatic interactions and promote cell adhesion.

Representative fluorescent images from all the substrates used in the study are presented below. The green color is an indicator of the transfected cells (expression of the green fluorescent protein encoded in the reporter gene for successful plasmid DNA transfection), whereas the blue indicates the nucleus of the rest (non-transfected) cells.

Cell transfection results using **Delivery Method 1**:

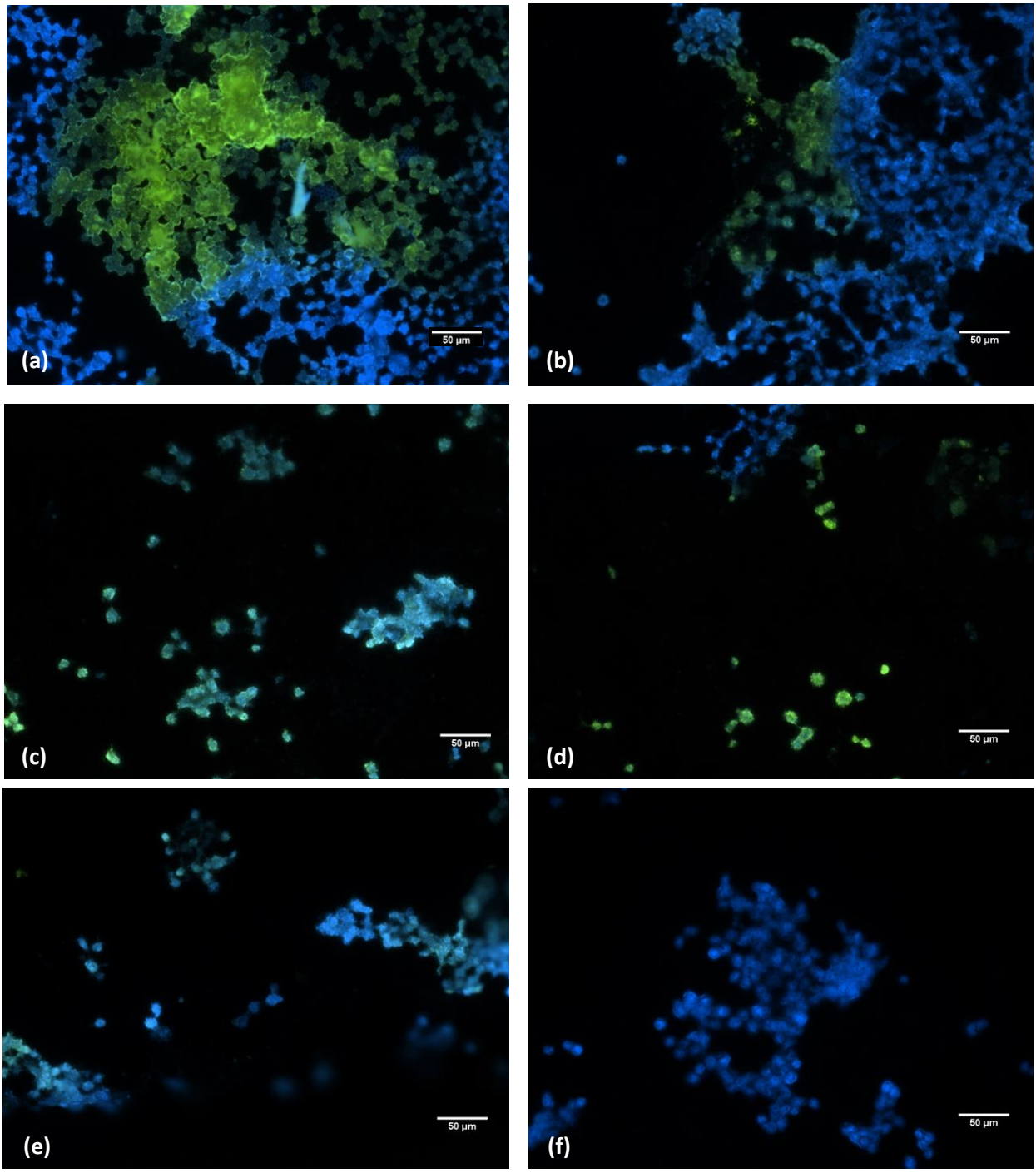

Figure 4.21: Fluorescent images taken after centrifugation and 20 m of incubation with the tips facing towards the cells, from the Si MC tips with (a) average tips' diameter of 130 nm and average heights of 7.8 μm, (b) average tips' diameter of 340 nm and average heights of 9.2 μm, (c) average tips' diameter of 93 nm and average heights of 4.6 μm, (d) average tips' diameter of 300 nm and average heights of 3 μm and (e) average tips' diameter of 220 nm and average heights of 2.8 μm. (f) Fluorescent image taken after centrifugation and **20 m of incubation**, from a flat Si wafer, used as a control.

After careful examination of the above images, we can notice a trend behind them. This is summarized in the following sentence "GFP is highly expressed in Si MC tip arrays comprising of high and pointed (<300 nm) tips in the same time ". As it was expected, the flat Si wafer, used as a control in our experiments, did not give us any transfection.

For comparative reasons, we additionally ran experiments using **Delivery Method 2**, where cells were placed on top of the substrates (Si MC tips); most common practice. This was followed by centrifugation and incubation for 3 d.

Cell transfection results using **Delivery Method 2**:

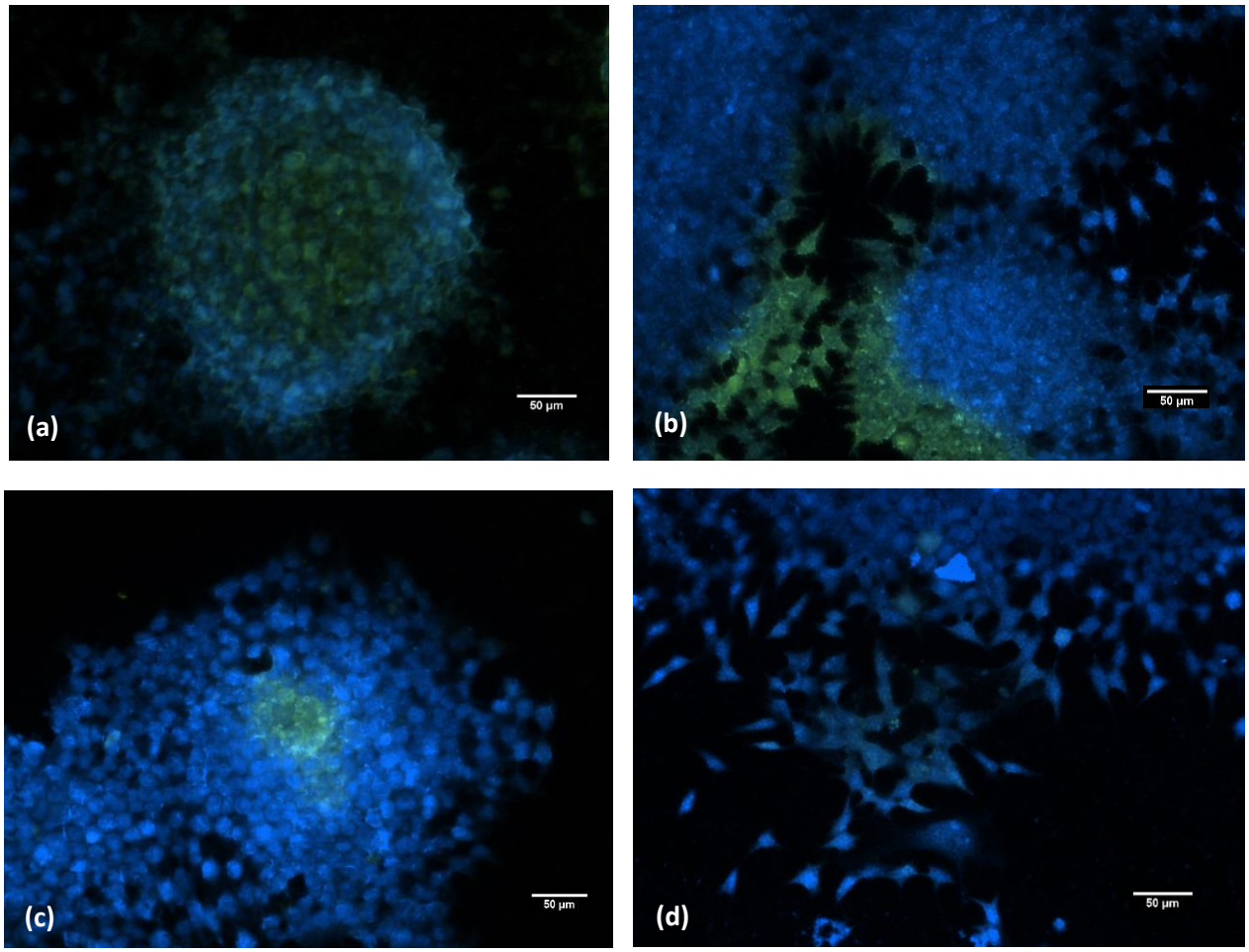

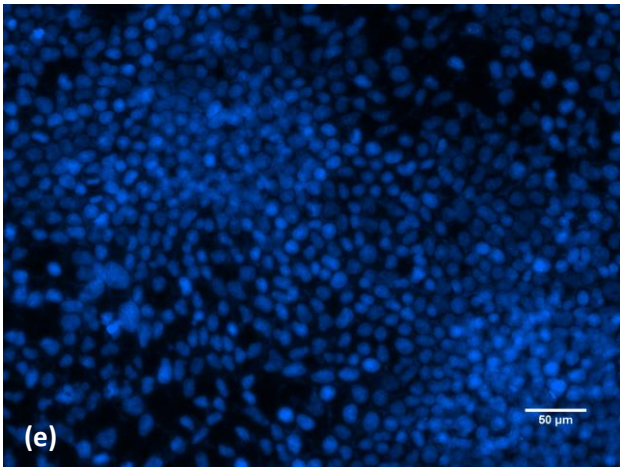

Figure 4.22: Fluorescent images taken after centrifugation and 3 d of incubation, with the cells facing towards the tips, from the Si MC tips with (a) average tips' diameter of 190 nm and average heights of 6.3 μm, (b) average tips' diameter of 93 nm and average heights of 4.6 μm, (c) average tips' diameter of 220 nm and average heights of 2.8 μm (d) average tips' diameter of 300 nm and average heights of 7.8 μm and (e) Fluorescent image taken after centrifugation and **3 d of incubation**, from a flat Si wafer, used as a control.

According to Fig. 4.22, the same trend, as featured in Fig. 4.21, is repeated. However, the two delivery methods exhibit quite a few differences. First of all, due to the prolonged incubation time used in Delivery Method 2, compared to the short-time one used in Delivery Method 1, there are much more cells attached to the substrates. In addition, the attached cells have grown onto the substrates and gradually changed their shape by developing filopodia protrusions. Most of the times, cells are gathered together forming nice clusters (Fig. 4.22 (a)). Another interesting thing to mention regarding the delivery method 2, is the areas where transfected cells were detected on the substrates. For example, when looking on Fig. 4.22(b) we can see that the transfected cells are located at the bottom of the substrate and plethora of non-transfected ones are grown on top of them. It seems that the non-transfected cells were grown in a later time, during the prolonged incubation, and they probably did not have any access to the Si MC tips in order to receive the plasmid and become transfected.

It is clear that both delivery methods are working. However, Delivery Method 1 is advantageous due to the short transfection protocol that it offers, fact of great importance in accordance with our initial approach (Section 2.2).

5. Discussion

The delivery of genes to mammalian cells using non-viral methods has become a very promising approach for gene therapy in the last few years (2). One of the current impediments of successful gene therapy is the inefficient delivery of the corrective nucleic acid code into target cells. New methods are required to deliver nucleic acid reagents into diverse cell types effectively and with high yields.

Achieving direct communication between vertically aligned silicon nanowire (VA-SiNW) arrays and mammalian cells, through the ability to engineer the architectures of VA-SiNW arrays and the surface chemistry, holds great opportunities to monitor and orchestrate gene delivery into mammalian cells.

In this study, we present the development of a novel delivery platform for in vitro non-viral cell transfection studies, comprising VA-SiNW arrays with a tapered profile, termed as "silicon micro-conical tips (Si MC tips)".

Development of VA-SiNW arrays with a tapered profile:

VA-SiNW arrays have been fabricated with a top-down fabrication approach, using a combination of nanosphere lithography (NSL) and Deep Reactive Ion Etching (DRIE) of silicon. The fabrication starts with self-assembly of a hexagonal close-packed (hcp) 2D array of polystyrene nanospheres (PSNS) over a large area of a Si wafer via convective assembly. The resulting hcp monolayer array is then converted into non-close-packed monolayer arrays using O_2 plasma etching. Following this, the etched PSNS serve as a lithographical mask for the DRIE of silicon using the “Bosch” process. The final step in the fabrication of the silicon micro-conical tip arrays includes the formation of a smoother and sharper morphology using a combination of thermal oxidation and wet etching in an HF-based solution.

After a lot of optimization, which included the variation of different process parameters, such as bias RF power ratio, number of loops etc., in order to achieve the desired morphology of our NWs, we successfully fabricated nice uniform arrays comprising of high aspect ratio Si MC tips. These arrays, which were classified in three different categories, regarding the height of the tips, exhibiting a range of architectures (Table 4.2). We observed that the key for successful fabrication lies in the right combination of the oxygen plasma and the silicon etching recipe. There is a strong correlation between the oxygen plasma time, the number of the loops during the silicon etching and the final height of the Si MC tips. This can be summarized in the following sentence: «The greater the oxygen plasma time, the smaller the size of the mask, fact that limits the number of loops during the silicon etching, which consequently leads to shorter tips». We finally concluded to three basic recipes (Appendix A) proceeding to small variations, when needed, due to temporary changes in the etch rate. Moreover, the areal density (D) as well as the periodicity (p) – $p = (1/D)^{1/2}$ – of the Si MC tips are determined by the initial diameter of the PSNS (4.5 μm in our case) and consequently remain, more or less, constant. Their optical properties have not been examined yet, however, we assume that as microstructures with a tapered sidewall profile, they could probably be useful in antireflection and light trapping applications in solar cells, light emitting diodes and photodetectors/imagers (43).

The aforementioned fabrication technique exhibits a lot of advantages. To begin with, nanosphere lithography (NLS) or colloidal lithography is a well-known, low-cost and high-throughput method (58) compared with the conventional lithographic techniques (e.g. e-beam lithography, photolithography) used for patterning. The main limitation of NSL is that, using convective assembly or any other conventional approach, typically close-packed arrays of particles are formed on the

substrate, where the interparticle separation is significantly smaller than the particle size. The interparticle distance can be increased by etching the deposited colloids, for example, in an oxygen plasma, like in our case. However, there are limitations in the shrinking ratio, before the morphology of the etched particles start to deviate uncontrollably from the spherical shape (34). Moreover, while NSL offers some control over geometry and position, the obtained arrangement of the NWs (after etching) shows only short-range periodicity due to the imperfect ordering of the nanospheres. Laser interference lithography (LIL), for example, easily yields patterns with perfect ordering of several cm^2 and can even produce faultless patterns over entire 300 mm wafers, if advanced techniques are used (59). In addition, DRIE, as a dry etching technique, offers the advantage of tunability of the etching profile, whereas the profile is usually not tunable for wet etching, with a curved profile resulted from an isotropic etching being the most typical (43). Moreover it eliminates the handling of dangerous acids and solvents and offers us high selectivity of the mask (60). However, it requires the use of specialized and consequently expensive equipment.

Microstructuring by ultra-short pulsed lasers is an alternative approach for the formation of arrays with high-aspect ratio microcones (MCs) on solid surfaces and particularly silicon (61). This method exploits a number of phenomena taking place under the action of intense pulsed laser irradiation of crystalline Si in the presence of a reactive gas, in order to induce morphological, structural and compositional modifications on its surface. The result is quasi-periodical conical structures of micrometer scale, decorated by nanometer scale protrusions (dual scale roughness). Apart from their unique morphology, these structures also exhibit improved optical, electronic and wetting response (62).

The ultrafast laser induced modification of materials is a single step process, in contrast to the one proposed by us above. One of its main advantages is the limited size of the affected volume. The combination of localized excitation and low threshold fluence can greatly reduce the extent of collateral damage to surrounding areas, so that the size of the affected material can be microscopic. As a consequence, ultrafast laser structuring techniques provide excellent control over micro- and submicron scales. Additional advantages include the high fabrication rate, noncontact interaction, applicability to many types of materials and reproducibility. Moreover, they allow the manufacture of structures with complex geometries, including 3D shapes or structures with varying wall shapes and etch depths, and various aspect ratios on the same substrate, which represents a great difficulty for planar clean-room techniques. Furthermore, lasers can be easily incorporated to computer-assisted fabrication systems for complex and customized 3D matrix structure design and manufacture (61). However, lasers are still considered as an expensive equipment, which is not always affordable by the laboratories.

VA-SiNW arrays as a novel delivery platform for non-viral cell transfection studies:

The above Si MC tips together with flat Si wafers have been applied to in vitro cell cultures using HEK293 cells as a model cell line. After functionalization of the Si MC tip arrays' surface with Green Fluorescent Protein (GFP)-plasmid, the delivery was performed by mechanical penetration using centrifugation force, with the Si MC tips facing towards the cells (Delivery Method 1). Before proceeding to cell transfection studies, we first examined the viability of the cells during their contact with the Si MC tips and secondly the existence or not of penetration through the cell membrane into the cytoplasm by FIB-SEM.

The viability studies demonstrated that a prolonged incubation (for a couple of hours) of the aforementioned setup, after centrifugation, leads to the death of the majority of the cells at the footprint that the Si MC tips leave on the well plate, once they are removed from it. In addition, the fluorescent images taken from the Si MC tips themselves presented that cells started to become dead as well. This is probably attributed to the lack of oxygen and nutrition available to the cells during the contact. However, a short incubation of maximum 30 m time leaves all the cells alive at both cases. At the footprint and at the Si MC tips themselves. Furthermore, there are still remaining cells attached on the well plate, fact that gives us the potential of achieving transfection on the well plate as well.

FIB-SEM image analysis revealed the successful cytoplasm penetration of the Si MC tips of all different characteristics within 15 m and 30 m incubation time respectively. This is a good but not an adequate indicator that we will have transfection as well.

Following this, we proceeded to transfection studies in order to test the efficacy of our plasmid DNA delivery system. For comparative reasons, cell transfection studies were performed employing an additional delivery method (cells on top of the Si MC tips – Delivery Method 2) and following a similar protocol. Our results showed that cell transfection was achieved using both delivery methods. Transfected cells were detected on the surface of the Si MC tip arrays and especially on those comprising of higher and pointed tips in the same time. However, no transfected cells were detected on the well plate using Delivery Method 1 (Si MC tips on top of the cells) within 20 m of incubation. As far as our controls (flat Si wafers) are concerned, they did not give us any transfection, thus highlighting the importance of the Si MC tips.

There are a lot of questions arising here. One of the things that we have to consider in order to explain these results in the whole, is the fact that most of the times there were some small defects in our samples. These include areas lacking in Si MC tips deriving from remaining holes during the convective assembly deposition of the PSNS. Areas like these, behave as our controls (flat Si wafer) and did not give us any transfection. The same thing happens in the case of remaining multilayers in our samples (Section 4.1). Another thing that we have to bear in mind is that although we pretreated all our samples with PDL, which is known to promote both the sorption of the plasmid via electrostatic interactions and the adhesion of the cells to the surface, we have not examined if our samples are coated uniformly with the plasmid after their washing with PBS. Thus, the evaluation of the coating is something that has to be definitely included to our future work as it will give us a better understanding of the results.

Another interesting thing to mention regarding Delivery Method 2, is the areas where transfection was detected on the substrates. The majority of the fluorescent images, present that the transfected cells are located at the bottom of the substrate and plethora of non-transfected ones are grown on top of them. It seems that the non-transfected cells were grown in a later time, during the prolonged incubation (3 d), and they probably did not have any access to the Si MC tips in order to receive the plasmid and become transfected.

Future work should definitely include the optimization of the experimental parameters in order to improve the transfection efficiency on the Si MC tips. For example, during our experiments, we kept the centrifuging speed constant to the minimum; 200 r.p.m. (7 g). According to another study (63), which was using a delivery system similar to ours, by increasing the centrifuging speed from 300 r.p.m. (12.8 g) to 500 r.p.m. (35.5 g), the cytosolic delivery efficiency of EthD-1 improved significantly from ~ 5 % to ~ 80 %, without causing much increase in the number of dead cells.

The great challenge, however, would be undoubtedly to try to culture the already transfected cells, once they are harvested by trypsinization from the Si MC tip arrays, for a long time e.g. 2-3 days in order to see if they can proliferate normally after their treatment with the Si MC tips. This was also the reason why we wanted to achieve transfection on the well plate in the first place. Unfortunately, we did not detect any transfected cells on the well plate within 20 m of incubation using Si MC tips of all different characteristics. Some other similar studies (63-64), instead of coating the NWs or nanoneedles with plasmid or any other desired molecule, propose the release of the molecules inside the culture medium. The principle, in this case, is **temporal deformation of the cell membrane** by the NWs. Depending on the size and geometry of the NWs, the cell membrane can be induced to be accessible to materials from the surrounding medium for a short period of time, and foreign materials can therefore directly diffuse into cell cytoplasm before the recovery of the membrane deformation. In particular, Wang et al. (63), demonstrated that this technique is applicable to deliver a broad range of molecules and materials, including small chemicals, antibodies, quantum dots (QDs), nanoparticles and DNAs, in a high throughput manner, when using a diamond nanoneedle array. Especially for delivering plasmid DNAs into neurons, the technique produces at least eightfold improvement in transfection efficiency with a dramatically shorter experimental protocol, when compared with the commonly used lipofection approach. Moreover, the nanoneedle-treated neuronal cells can be further maintained in long-term culture with proper cellular development and stable expression of GFP, and form functional synapses. In the same context, Paik et al. (64), using silicon nanoneedles with sharp nano-tips, exhibiting an areal density close to ours, demonstrated the uptake of molecular probes by up to 34 % of cells after nanoneedle treatment without causing significant death from cell membrane penetration. In this case, instead of centrifugation force, a known constant force (1.24 g· f, approximately 12 mN) was placed on top of the nanoneedle array for the control of the needle-cell interaction force.

Another interesting thing, which should be included to our future work, is to try to use this delivery system for different kind of cells, such as fibroblasts or even T lymphocyte cells. However, we have to consider that various types of cells require different NW array geometries for successful transfection. For instance, non-adherent immune cells require longer, thinner and denser NWs compared to the adherent ones (36).

Despite the future work needed, our proposed gene delivery system has a lot of advantages to offer. First of all, unlike previous methods using single nanoneedle to address individual cells with expensive equipment such as AFM, our system does not rely on any special equipment and is very straightforward with high throughput capability (63). Comparing the two delivery methods presented here, Delivery Method 1 is undoubtedly preferable due to the dramatically shorter experimental protocol that it offers, when compared with commonly used non-viral gene delivery methods.

6. References

1. http://www.ama-assn.org/ama/pub/physician-resources/medical-science/genetics-molecular-medicine/current-topics/gene-therapy.page

2. Towards safe, non-viral therapeutic gene expression in humans. Glover et al. : Nature Review Genetics, 2005

3. An Introduction to DNA, Genes and Chromosomes. : Centre for Genetics Education. http://www.genetics.edu.au/Publications-and-Resources/Genetics-Fact-Sheets/FactSheetDNAGenesChromosomes

4. http://www.eschooltoday.com/science/genetics/what-is-a-gene.html

5. http://www.nature.com/scitable/content/an-overview-of-the-flow-of-information-14711098

6. University of Utah, Health Sciences. http://learn.genetics.utah.edu/content/disorders/

7. Gene therapy returns to central stage. Naldini : Nature, 2015

8. Mammalian cell transfection: the present and the future. Kim et al. : Anal Bioanal Chem, 2010

9. Physical methods for gene transfer: Improving the kinetics of gene delivery into cells. Mehier-Humbert et al. : Advanced Drug Delivery Reviews, 2005

10. Viral vectors for gene therapy: the art of turning infectious agents into vehicles of therapeutics. Kay et al. : Nature Medicine, 2001

11. Transfection efficiency of cationic lipids with different hydrophobic domains in gene delivery. Zhi et al. : Bioconjugate Chem., 2010

12. Engineering vertically aligned semiconductor nanowire arrays for applications in the life sciences. Elnathan et al. : Nano Today, 2014

13. Microneedles for transdermal drug delivery. Prausnitz : Advanced Drug Delivery Reviews, 2004

14. Physical non-viral gene delivery methods for tissue engineering. Mellott et al. : Annals of Biomedical Engineering, 2013

15. Delivery of substances into cells and tissues using a particle bombardment process. Sanford et al. : Part. Sci. Technol., 1987

16. In vivo and in vitro gene transfer to mammalian somatic cells by particle bombardment. Yang et al. : Proc. Natl. Acad. Sci., 1990

17. In vivo particle mediated delivery of mRNA to mammalian tissues: ballistic and biologic effects. Sohn et al. : Wound Repair Regen., 2001

18. Intradermal ballistic delivery of micro-particles into excised human skin for pharmaceutical applications. Kendall et al. : J. Biomech., 2004

19. Electrotransfer as a non viral method of gene delivery. Favard et al. : Curr. Gene Ther., 2007

20. Study of mechanisms of electric field-induced DNA transfection. IV. Effects of DNA topology on cell uptake and transfection efficiency. Xie et al. : Biophys. J., 1992

21. Optimization of the transfection of human endothelial cells by electroporation. Schwachtgen et al. : Biotechniques, 1994

22. High-throughput transfection of differentiated primary neurons from rat frombrain. Marine et al. : J. Biomol. Screen., 2012

23. Optimization of a 96-well electroporation assay for postnatal rat CNS neurons suitable for cost effective medium-throughput screening of genes that promote neurite outgrowth. Hutson et al. : Front. Mol. Neurosci., 2011

24. Potential role of pulsed-high intensity focused ultrasound in gene therapy. Frenkel et al. : Future Oncol., 2006

25. Update on non-viral delivery methods for cancer therapy: possibilities of a drug delivery system with anticancer activities beyond delivery as a new therapeutic tool. Kaneda : Expert Opin. Drug Deliv., 2010

26. Targeted gene transfer in eucaryotic cells by dye-assisted laser optoporation. Palumbo et al. : J. Photochem. Photobiol. B., 1996

27. *Gene silencing mediated by magnetic lipospheres tagged with small interfering RNA. del Pino et al. : Nano Lett., 2010*

28. Insights into the mechanism of magnetofection using PEI-based magnetofectins for gene transfer. Huth et al. : J. Gene Med., 2004

29. Gene and cell therapy: Therapeutic mechanisms and strategies, 4th Edition. Nancy Smyth Templeton : CRC Press

30. Cellular nanotechnology: making biological interfaces smarter. Mendes : Chem. Soc. Rev., 2013.

31. In situ vaporization of very low molecular weight resists using 1/2 nm diameter electron beams. Isaacson et al. : J. Vac. Sci. Technol., 1981

32. Fully tunable silicon nanowires fabricated by soft nanoparticle templating. Elnathan et al. : Nano Lett., 2016

33. Soft lithography. Xia et al. : Annual Review of Materials Science, 1998

34. Versatile particle-based route to engineer vertically aligned silicon nanowire arrays and nanoscale pores. Elnathan et al. : ACS, Appl. Mater. Interfaces, 2015

35. Cell adhesion and spreading behavior on vertically aligned silicon nanowire arrays. Suijian Qi et al. : ACS, Appl. Mater. Interfaces, 2009

36. Interactions between semiconductor nanowires and living cells. Prinz : J. Phys.: Condens. Matter, 2015

37. Interfacing silicon nanowires with mammalian cells. Kim et al. : J. Am. Chem. Soc., 2007

38. Maximising transfection efficiency of vertically aligned silicon nanowires. Elnathan et al. : Advanced Functional Materials , 2015

39. Vertical silicon nanowires as a universal platform for delivering molecules into living cells. Shalek et al. :PNAS, 2010

40. Biodegradable silicon nanoneedles delivering nucleic acids intracellularly induce localized in vivo neovascularization. Chiappini et al. : Nature Materials, 2015

41. Engineering cellular photocomposite materials using convective assembly. Jenkins et al. : Materials, 2013

42. Deep reactive ion etching as a tool for nanostructure fabrication. Fu et al. : J. Vac. Sci. Technol. B , 2009

43. Fabrication of silicon nanostructures with large taper angle by reactive ion etching. Saffih et al.: J. Vac. Sci. Technol. B, 2014

44. Advances in deep silicon etch processing using Bosch process. Nozawa : J. Vac. Soc. Japan, 2010

45. Akin Aydemir. Master Thesis: Deep-trench RIE optimization for high performance MEMS microsensors. 2007

46. http://www.tf.uni-kiel.de/matwis/amat/semitech_en/kap_7/backbone/r7_2_2.html

47. High aspect ratio silicon etch : A review. Wu et al. : J. Appl. Phys., 2010

48. Etching technologies in NLD (magnetic Neutral Loop Discharge) plasma. Hayashi et al. : J. Vac. Soc. Japan, 2010

49. Magnetic neutral loop discharge (NLD) plasmas for surface processing. Uchida et al. : J. Phys. D: Appl. Phys., 2008

50. https://bionanotech.unisa.edu.au/?p=626

51. http://www.ulvac.com/userfiles/files/R%26D/13242_Ulvac%20Materials%20Brochure.pdf

52. http://www.anff.org.au/micro-and-nano-fabrication/sa-node/deep-reactive-ion-etcher-drie.html

53. Biomedical and biological applications of Scanning Electron Microscopy. Handbook of instrumental techniques. Cortadellas et al. : Scientific and Technological Centers of University of Barcelona, 2012

54. http://www.hek293.com/

55. Introduction to FIB-SEM, Basic Physics and Applications. Reuteler : Department of Materials - ETH

56. Encyclopedia of Cell Biology. Stahl et al. : Academic press, 2016

57. A review of focused ion beam applications in microsystem technology. Reyntjens et al. : J. Micromech. Microeng., 2001

58. The fabrication of high-aspect-ratio, size-tunable nanopore arrays by modified nanosphere lithography. Chen et al. : Nanotechnology, 2009

59. Sub-100 nm silicon nanowires by laser interference lithography and metal-assisted chemical etching. de Boor et al., : Nanotechnology, 2010

60. Fundamentals of Micromachining. Dry Etching lecture. Bruce K. Gale : University of Utah

61. Nanomaterials by ultrafast laser processing of surfaces. Stratakis : Sci Adv Mater, 2012

62. Making silicon hydrophobic: wettability control by two-length scale simultaneous patterning with femtosecond laser irradiation. Zorba et al., : Nanotechnology, 2006

63. Poking cells for efficient vector-free intracellular delivery. Wang et al., : Nature Communications, 2014

64. A highly dense nanoneedle array for intracellular gene delivery. Paik et al.,: Solid-State Sensors, Actuators and Microsystems Workshop - South Carolina, 2012

APPENDIX A

Basic recipes for the Deep Reactive Ion Etcher

Oxygen plasma recipe 1

Item	Unit	Step 1	Step 2	Step 3
APC Press Set	[Pa]	2	2	2
Trigger Press	[Pa]	2	0	0
PFC Press	[Pa]	500	0	500
PFC Flow Limit	[sccm]	0.3	0.3	0.3
MF C21 Flow Set (Ar)	[sccm]	0	0	0
MF C22 Flow Set (SF6)	[sccm]	0	0	0
MF C23 Flow Set (O2)	[sccm]	99	99	99
MF C24 Flow Set (C3F8)	[sccm]	0	0	0
MF C25 Flow Set (CF4)	[sccm]	0	0	0
MF C26 Flow Set (C4F8)	[sccm]	0	0	0
MF C28 Flow Set (H2)	[sccm]	0	0	0
Antenna RF Power Set	[W]	0	0	2000
Antenna AMC No.	[Pos]	1	1	1
Bias RF Power Set	[W]	0	0	25
Bias AMC No.	[Pos]	1	1	1
Magnet Top	[A]	30.6	30.6	30.6
Magnet Middle	[A]	52	52	52
Magnet Bottom	[A]	30.6	30.6	30.6
Process Time sec Set	[sec]	15	10	**180**
Bias Vpp Low Set	[V]	0	0	0
Bias Vpp High Set	[V]	0	0	0
Return Step No	[No]	0	0	0
Step Loop Count	[Times]	0	0	0
Loop Max Time Set	[sec]	12	12	12

Bias $V_{pp} \approx 90$ V

Silicon etching recipe 1

Item	Unit	Step 1	Step 2	Step 3
APC Press Set	[Pa]	1	0.67	0.67
Trigger Press	[Pa]	1	0	0
PFC Press	[Pa]	600	600	600
PFC Flow Limit	[sccm]	0.3	0.3	0.3
MF C21 Flow Set (Ar)	[sccm]	0	0	0
MF C22 Flow Set (SF6)	[sccm]	30	30	0
MF C23 Flow Set (O2)	[sccm]	0	0	0
MF C22 Flow Set (C3F8)	[sccm]	0	0	0
MF C22 Flow Set (CF4)	[sccm]	0	0	0
MF C22 Flow Set (C4F8)	[sccm]	0	0	25
MF C22 Flow Set (H2)	[sccm]	0	0	0
Antenna RF Power Set	[W]	1500	1500	750
Antenna AMC No.	[Pos]	1	1	1
Bias RF Power Set	[W]	30	30	10
Bias AMC No.	[Pos]	2	2	2
Magnet Top	[A]	30.6	30.6	30.6
Magnet Middle	[A]	52	52	52
Magnet Bottom	[A]	30.6	30.6	30.6
Process Time sec Set	[sec]	1	14	4
Bias Vpp Low Set	[V]	0	0	0
Bias Vpp High Set	[V]	0	0	0
Return Step No	[No]	0	0	2
Step Loop Count	[Times]	0	0	**29**
Loop Max Time Set	[sec]	0	0	0

Bias $V_{pp} \approx 90$ V

Oxygen plasma recipe 2

Item	Unit	Step 1	Step 2	Step 3
APC Press Set	[Pa]	2	2	2
Trigger Press	[Pa]	2	0	0
PFC Press	[Pa]	500	0	500
PFC Flow Limit	[sccm]	0.3	0.3	0.3
MF C21 Flow Set (Ar)	[sccm]	0	0	0
MF C22 Flow Set (SF6)	[sccm]	0	0	0
MF C23 Flow Set (O2)	[sccm]	99	99	99
MF C24 Flow Set (C3F8)	[sccm]	0	0	0
MF C25 Flow Set (CF4)	[sccm]	0	0	0
MF C26 Flow Set (C4F8)	[sccm]	0	0	0
MF C28 Flow Set (H2)	[sccm]	0	0	0
Antenna RF Power Set	[W]	0	0	2000
Antenna AMC No.	[Pos]	1	1	1
Bias RF Power Set	[W]	0	0	25
Bias AMC No.	[Pos]	1	1	1
Magnet Top	[A]	30.6	30.6	30.6
Magnet Middle	[A]	52	52	52
Magnet Bottom	[A]	30.6	30.6	30.6
Process Time sec Set	[sec]	15	10	**120**
Bias Vpp Low Set	[V]	0	0	0
Bias Vpp High Set	[V]	0	0	0
Return Step No	[No]	0	0	0
Step Loop Count	[Times]	0	0	0
Loop Max Time Set	[sec]	12	12	12

Bias $V_{pp} \approx 90$ V

Silicon etching recipe 2

Item	Unit	Step 1	Step 2	Step 3
APC Press Set	[Pa]	1	0.67	0.67
Trigger Press	[Pa]	1	0	0
PFC Press	[Pa]	600	600	600
PFC Flow Limit	[sccm]	0.3	0.3	0.3
MF C21 Flow Set (Ar)	[sccm]	0	0	0
MF C22 Flow Set (SF6)	[sccm]	30	30	0
MF C23 Flow Set (O2)	[sccm]	0	0	0
MF C22 Flow Set (C3F8)	[sccm]	0	0	0
MF C22 Flow Set (CF4)	[sccm]	0	0	0
MF C22 Flow Set (C4F8)	[sccm]	0	0	25
MF C22 Flow Set (H2)	[sccm]	0	0	0
Antenna RF Power Set	[W]	1500	1500	750
Antenna AMC No.	[Pos]	1	1	1
Bias RF Power Set	[W]	30	30	10
Bias AMC No.	[Pos]	2	2	2
Magnet Top	[A]	30.6	30.6	30.6
Magnet Middle	[A]	52	52	52
Magnet Bottom	[A]	30.6	30.6	30.6
Process Time sec Set	[sec]	1	14	4
Bias Vpp Low Set	[V]	0	0	0
Bias Vpp High Set	[V]	0	0	0
Return Step No	[No]	0	0	2
Step Loop Count	[Times]	0	0	**59**
Loop Max Time Set	[sec]	0	0	0

Bias $V_{pp} \approx 90$ V

Oxygen plasma recipe 3

Item	Unit	Step 1	Step 2	Step 3
APC Press Set	[Pa]	2	2	2
Trigger Press	[Pa]	2	0	0
PFC Press	[Pa]	500	0	500
PFC Flow Limit	[sccm]	0.3	0.3	0.3
MF C21 Flow Set (Ar)	[sccm]	0	0	0
MF C22 Flow Set (SF6)	[sccm]	0	0	0
MF C23 Flow Set (O2)	[sccm]	99	99	99
MF C24 Flow Set (C3F8)	[sccm]	0	0	0
MF C25 Flow Set (CF4)	[sccm]	0	0	0
MF C26 Flow Set (C4F8)	[sccm]	0	0	0
MF C28 Flow Set (H2)	[sccm]	0	0	0
Antenna RF Power Set	[W]	0	0	2000
Antenna AMC No.	[Pos]	1	1	1
Bias RF Power Set	[W]	0	0	25
Bias AMC No.	[Pos]	1	1	1
Magnet Top	[A]	30.6	30.6	30.6
Magnet Middle	[A]	52	52	52
Magnet Bottom	[A]	30.6	30.6	30.6
Process Time sec Set	[sec]	15	10	**50**
Bias Vpp Low Set	[V]	0	0	0
Bias Vpp High Set	[V]	0	0	0
Return Step No	[No]	0	0	0
Step Loop Count	[Times]	0	0	0
Loop Max Time Set	[sec]	12	12	12

Bias $V_{pp} \approx 90$ V

Silicon etching recipe 3

Item	Unit	Step 1	Step 2	Step 3
APC Press Set	[Pa]	1	0.67	0.67
Trigger Press	[Pa]	1	0	0
PFC Press	[Pa]	600	600	600
PFC Flow Limit	[sccm]	0.3	0.3	0.3
MF C21 Flow Set (Ar)	[sccm]	0	0	0
MF C22 Flow Set (SF6)	[sccm]	30	30	0
MF C23 Flow Set (O2)	[sccm]	0	0	0
MF C22 Flow Set (C3F8)	[sccm]	0	0	0
MF C22 Flow Set (CF4)	[sccm]	0	0	0
MF C22 Flow Set (C4F8)	[sccm]	0	0	25
MF C22 Flow Set (H2)	[sccm]	0	0	0
Antenna RF Power Set	[W]	1500	1500	750
Antenna AMC No.	[Pos]	1	1	1
Bias RF Power Set	[W]	30	30	10
Bias AMC No.	[Pos]	2	2	2
Magnet Top	[A]	30.6	30.6	30.6
Magnet Middle	[A]	52	52	52
Magnet Bottom	[A]	30.6	30.6	30.6
Process Time sec Set	[sec]	1	14	4
Bias Vpp Low Set	[V]	0	0	0
Bias Vpp High Set	[V]	0	0	0
Return Step No	[No]	0	0	2
Step Loop Count	[Times]	0	0	**94**
Loop Max Time Set	[sec]	0	0	0

Bias $V_{pp} \approx 90$ V